Surface Chemistry of TiO_2 Photocatalysts

Thesis by Steven Henry Szczepankiewicz

In Partial Fulfillment of the Requirements

for the Degree of

Doctor of Philosophy

California Institute of Technology

Pasadena, California

2001

(Defended March 12, 2001)

Non nobis, Domine, non nobis sed Nomine Tuo da gloriam.

Acknowledgements

I'd like to express my sincere gratitude to the many people responsible for guiding me to this point. Primarily, I would like to thank my research advisor, Michael Hoffmann, for providing me the opportunity to work with him, yet still allowing me tremendous freedom to develop my project. I am grateful for the trust he showed in allowing me to meet with professionals in the field. Thanks for being a great leader! Thanks also to the members of my Ph.D. committee: Nate Lewis, Bill Goddard, and Vince McKoy. Thanks also to Harry Gray for his constant guidance and encouragement throughout my years at Caltech.

I'd also like to thank John Moss for keeping my project moving in the lab, and for keeping me moving in the pool. I'd also like to thank Nathan Dalleska for serving as a sounding board for my ideas. Each proposal I presented to Nathan became more refined than the last because of his silent demand for excellence. Special thanks to A.J. Colussi for helping me to prioritize my goals without abandoning my curiousity. Thanks also to Bill Balcerski for reminding me that I'm almost "there," and for taking care of things when I was away.

I'd especially like to thank Tom Lloyd for helping me initiate my lab work, and for listening to my ideas from time to time as they developed, whether scientifically sound or otherwise.

Thanks to Todd Fuelberth, Kirk Hansen, Meredith Howard, Chris Treadway, and Todd Younkin for providing comfort and laughs in a seemingly foreign world, and for reminding me that there's more to life than just chemistry. Thanks to Fr. Brian Wilson, Fr. Andrew Mulcahey. Through your well-tailored guidance, I have developed as much in Spirit as I have in mind.

My family has been a constant motivating force. My parents helped me understand the importance of my work with the pride they took in it. I want to thank my daughter, Laura, for understanding why Daddy was working all the time, and for always being happy when I got home. Lastly, I'd like to thank my beautiful wife, Ainslie. You have made the greatest sacrifice to get me here today. Because of your unending support, you are responsible for this work as much as I am, but without the rewards at the end. Thank you for your constant strength.

Abstract

The surface chemistry of TiO_2 photocatalysts have been characterized by infrared spectroscopy, alcalimetric titrations, and photocatalytic reactivity. The fundamental processes governing electron transfer at the surface were investigated by inhibiting the photocatalytic reactions.

Free and trapped charge carriers in polycrystalline TiO_2 following bandgap irradiation are characterized by diffuse reflectance IR spectroscopy (DRIFTS). Irradiation of anatase *in vacuo* or in the presence of CD_3OD leads to decreased overall reflectance, to an absorbance at 3717 cm^{-1} (x), and to the decline of a 3647 cm^{-1} band. x persists for days in vacuum or dry O_2 and is only bleached by the action of $[O_2 + H_2O(g) + h\nu]$. It is assigned to a Ti(III)O-H vibration ensuing electron trapping at the acidic Ti(IV)OH centers that absorb at 3647 cm^{-1}. Irradiation under O_2 yields a band at 3683 cm^{-1} (Y) that corresponds to bound OH radicals. These last indefinitely *in vacuo*, but decay in a few hours under O_2. Since none of the above phenomena occur on defective TiO_{2-x} materials obtained by thermal annealing under vacuum, photochemical damage to actual catalysts involves concurrent surface reorganization. The presence of the 3717 cm^{-1} band is used to confirm this reorganization.

The decreased reflectivity is due to a spectrum-wide absorption signal proportional to $\lambda^{1.7}$ (λ = wavelength/μm), which indicates the presence of free conduction band electrons coupled with acoustic phonons in the lattice. Free electrons appear to

decay according to saturation kinetics. The fitted parameters indicate a limited number of reversible trapping states. The concentration of these states appears to be diminished by sequential UV treatments. A broad IR absorption peak centered at 3380 cm^{-1} is attributed to an electronic transition from an occupied surface electron trap 0.42 eV below the conduction band. The free carrier decay lifetime is lengthened as the samples are dehydrated.

Electric fields generated by photoexcited charge carriers in TiO_2 (anatase) produce Stark effect intensity and wavelength shifts for surface TiO-H stretching vibrations. Shallow electron-trapping states, observed as broad absorption bands above 3000 cm^{-1}, produce an apparently homogeneous electric field. Intensity changes and corresponding wavelength shifts for ν(TiO-H) are proportional to the magnitude and polarity of the electric field. O_2 is shown to reversibly abstract electrons from shallow trapping states. These results suggest that shallow electron traps are not associated with localized structures, but rather are delocalized across the TiO_2 surface.

The effect of poisoning the photocatayst is monitored during the oxidation of a phosphorous-containing organic substrate. The photoassisted oxidation of dimethyl-methyl-phosphonate (DMMP) over UV-irradiated TiO_2 is investigated as a simulant for warfare nerve agent detoxification. Adsorption uptake measurements are performed by MS analysis of a fine DMMP aerosol up and downstream of an adsorbant TiO_2 film. Photodesorption processes, gas phase intermediates and mineral products are quantified in situ by headspace GC-MS analysis of a static system. Non-volatile intermediates and

products are analyzed by HPLC analysis of both aqueous and organic extractions from the TiO2 film. Adsorbed intermediates are characterized and quantified in situ by DRIFTS of TiO_2 powders. Specific site binding of DMMP and catalyst poisoning are observed in the DRIFT spectra. A proposed mechanism suggests rapid detoxification of DMMP as a simulant, but extensive poisoning of the catalyst by the end products.

In a comparative investigation of titania surface chemistry, TiO_2 Q particles are synthesized and characterized by transmission electron microscopy, potentiometric titration, infrared analysis, and photocatalytic reactivity. TEM images show small individual particulates of anatase about 2 nm in diameter. Potentiometric titrations confirm the presence of a highly protonated gel layer on the surface of these particles. The infrared spectra indicate that this layer is amorphous. An autocatalytic enhancement of the photocatalysts during photooxidation of methyl orange suggests that reaction intermediates cause the collapse of the hydrated gel layer into a more active surface.

Two supplementary investigations are presented which confirm the previous results. MAS NMR data is presented which shows a paramagnetic influence from surface trapped electrons. The data also suggests localized trapping at a characteristic type of TiOH surface moiety. Theoretical calculations also confirm the band assignments presented in the previous chapters by reproducing the data with the predicted structural assignments.

Table of Contents

Chapter 1

Introduction

Among the various industrial applications for TiO_2 that exploit its unique combination of physical, chemical, spectroscopic, photochemical, and electrochemical properties, the greatest market is in the paint industry as a pigment.[1] In addition to its photo-optical properties, TiO_2 is cheap, easy to synthesize, stable, non-toxic, and environmentally benign. However, its photochemical reactivity can destroy the polymer binder in paint when exposed to direct sunlight, causing the paint to "chalk" as the white TiO_2 particles break free of the polymer. Passivating the pigment against such photoactivity usually requires "capping" the particles with an inert layer such as SiO_2 or Al_2O_3. The chemical interaction of the passivating layer with the active TiO_2 surface states must be optimized to minimize the photoactivity of the hybrid pigment.

In contrast, the ability of photoativated TiO_2 to oxidize organic molecules near its surface has been used to decontaminate polluted water and air.[2] The photoactivity arises from charge carriers that segregate in the bulk of the semiconductor with bandgap excitation and migrate to the surface where they initiate redox reactions. The large positive potential of the valence band hole, +3.0 V, is strong enough to initiate oxidation reactions at the surface such as the formation of hydroxyl radicals from adsorbed hydroxide ions. Proposed mechanisms for the UV sensitized TiO_2 photo-oxidation of organic substrates implicate both direct VB hole oxidation and hydroxyl radical mediated oxidation. The formation of a hydroxyl radical at the surface can be considered "trapping" the hole, which causes the VB hole to relax to a lower potential, but also fixes it at the surface, allowing it to react with the target substrate.

The trapping reactions that occur with the conduction band electron are influential in determining the photonic conversion efficiency. While the VB hole is powerful enough to initiate oxidation in either the free or trapped state, CB electrons can relax in trapping states below the reduction potential of the intended electron scavenger. Moreover, the mass of the CB electron is too large to allow significant diffusion directly from the conduction band, so it must be trapped in order to initiate a heterogeneous reduction. The electron trapping states with a potential negative enough to initiate O_2 reduction are defined as shallow trap states, and the rest are considered deep trap states. The potential energy diagram for these processes is shown in Figure 1.

Electrons are promoted from the valence band to the conduction band by UV excitation.[3] Both the electron and the corresponding hole rapidly relax to the band edges through phonon coupling. The charge carriers in TiO_2 can not directly recombine in the bulk since any transition between the band edges is forbidden. They eventually encounter the surface where they can escape the lattice or become trapped. Once either is trapped, the electron and hole are available for interfacial transfer, but are also subject to annihilation, which removes the oxidizing power of the VB holes and dissipates the energy as heat. The occupation of deep electron traps inevitably leads to annihilation with a VB hole since the electron does not have enough driving force to promote interfacial charge transfer to O_2.

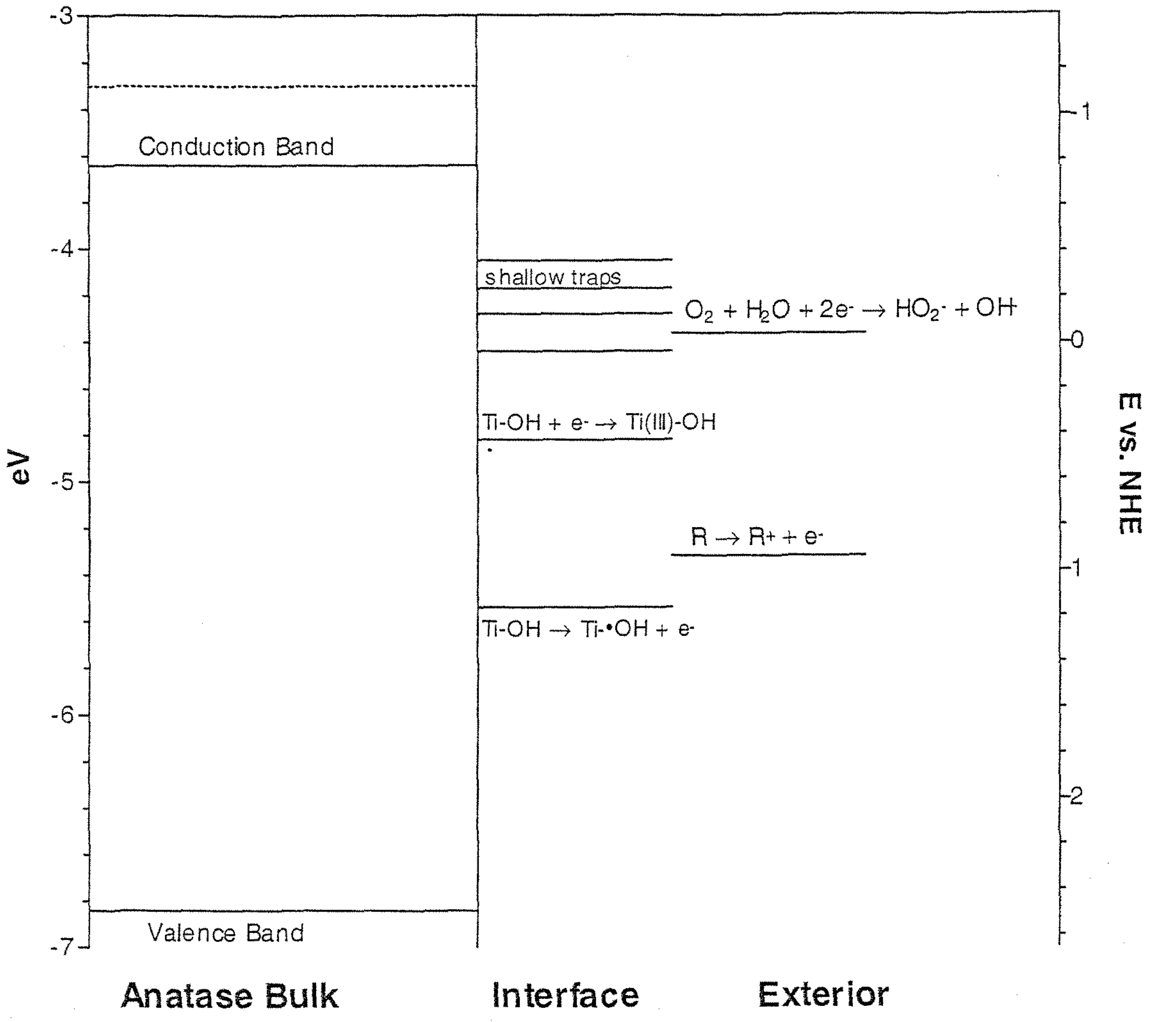

Figure 1: The quantitative potential energy levels responsible for the photoactivity of anatase TiO_2.

Under operational photocatalytic conditions, formation of carriers and interfacial charge transfer happen simultaneously, so trap state occupation is determined by the concentration of available carriers in the bulk. At high concentrations, electrons are annihilated from all traps by mobile holes and the annihilation kinetics limit the efficiency of interfacial electron transfer to a square root dependence on light flux. At low free carrier concentrations under low photon absorption conditions, the shallowly trapped electrons have enough time to transfer across the surface before annihilation, but the deeply trapped electrons remain indefinitely before being subject to annihilation. The partitioning of electrons between shallow and deep traps is evident in the sub-unit efficiency observed at extremely low photon fluxes.[4] This imposes a maximum photonic conversion efficiency for any particular photocatalyst, which is determined by the availability of deep electron traps.

The efficiency limitations caused by surface deactivation of photogenerated electrons is evident from studies performed on TiO_2 Q particles.[5] Q particles are extremely small microcrystallites, which exhibit a size quantization effect that increases the bandgap energy. In addition, the small crystallite size increases the available reactive surface area. Despite these physical advantages, the general photocatalytic efficiency of Q particles has never been demonstrated to exceed that of their larger, bulk-like counterparts. It is likely that the chemical deactivation of electrons at the surface limits the total efficiency, regardless of the internal semiconductor properties. A recent study using isotopically labeled $^{18}O_2$ during photocatalysis that initially yields ^{16}O-containing products[6] shows that the interfacial electron-transfer reactions are governed by more than purely thermodynamic factors.

Since electrons must be trapped in order to initiate interfacial reductions, and trapping depresses the electrons' reduction potential, the occupation of electron traps determines which reduction processes may proceed. This has implications for TiO_2 pigments, photocatalysts, photocell electrodes, and high temperature catalysts. The purpose of the research presented in this thesis is to elucidate the nature of the electron traps to open the possibility of understanding and eventually controlling them at the molecular level.

This thesis is organized into eight chapters, each of which may be read independently. This first chapter outlines the motivation for the research. The second chapter is an infrared spectroscopic investigation of hole trapping, deep electron trapping, and photoinitiated surface reconstruction at the particle-vacuum interface. The third chapter explores the kinetics of electron trapping and trap saturation in the presence of free conduction band electrons. The fourth chapter examines the Stark effect on the infrared vibrations to characterize the physical nature of shallow electron traps. The fifth chapter applies the discoveries from the preceding chapters to elucidate empirical observations during actual photocatalytic reactions. The sixth chapter presents the quantitative determination of hydroxide ion coverage and Brönsted acidity through potentiometric titrations, comparing and contrasting Degussa P-25 and Q-particle TiO_2 samples in electrolyte suspensions. The seventh chapter presents the results from NMR experiments as well as a theoretical investigation, which corroborate the results in the previous chapters. Chapter eight summarizes the results of this research in the context of published literature data, and concludes with some suggestions for future research.

References

---

[1] Braun J.H. *J. Coating. Technol.*, **1997**, *69*, 59-72.

[2] Hoffmann M.R; Martin S.T.; Choi W.; Bahnemann D.W. *Chem. Rev.*, **1995**, *95*, 69-96.

[3] Pankove J.I. *Optical Processes in Semiconductors*; Dover: New York, 1975.

[4] Grela, M.A.; Colussi, A.J. *J. Phys. Chem. B.*, **1996**, *101*, 16940.

[5] Choi W., *Ph.D. Thesis*, California Institute of Technology, 1996.

[6] Zhuang, J.; Rusu, C. N.; Yates, J. T., *Phys. Chem. B,* **1999**, *103*, 6957.

Chapter 2

Infrared Spectra of Photoinduced Species on Hydroxylated Titania Surfaces

[The text of this chapter appeared in Szczepankiewicz, S.H.; Colussi, A. J.; Hoffmann M.R. *J. Phys. Chem. B*, **2000**, *104*, 9842.]

Abstract

We detect transient and persistent diffuse reflectance infrared signals from surface intermediates generated by bandgap irradiation of polycrystalline, hydroxylated TiO_2 under controlled atmospheres. Irradiation *in vacuo* or in the presence of CD_3OD(ads) leads to a new absorbance at 3716 cm^{-1}, the decline of a 3647 cm^{-1} band, and a reflectivity loss. Overall reflectivity, which gauges mobile charge, partially recovers in the dark after a few minutes, but fully upon exposure to O_2. The 3716 cm^{-1} feature persists for days in vacuum or dry O_2, but is bleached by the action of $(O_2 + H_2O + h\nu)$. It is assigned to a Ti(III)O-H^- vibration resulting from electron trapping at acidic Ti(IV)OH centers. Irradiation under O_2 yields a new band at 3683 cm^{-1}, ascribed to surface-bound OH radicals that last indefinitely in vacuum. None of the above events occur on thermally generated $TiO_{2-\gamma}$ specimens subsequently exposed to H_2O(g). We infer that: 1) O_2 is an efficient scavenger of conduction band electrons at the gas-solid interface, 2) the competition for holes between lattice oxygen photo-desorption and OH^- oxidation depends on gas pressure and composition and, 3) trapped carrier buildup eventually results in extended surface reconstruction involving Ti-OH functionalities, giving rise to restructuring hysteresis.

Introduction

Photocatalysis of chemical reactions by semiconductors is induced by bandgap excitation, and mediated by surface species (Figure 1).[1,2] The low photon efficiency of photocatalytic oxidations proceeding at practical rates prevents the implementation of large-scale decontamination processes.[3] Inefficiency largely arises from carrier recombination at surface defects (Figure 1).[4] This paper explores the nature of trapping sites in illuminated TiO_2 surfaces under controlled atmospheres by diffuse reflectance infrared Fourier transform spectroscopy (DRIFTS).[5]

Photogenerated electrons e^- and holes h^+ diffuse to the surface of the semiconductor particles, and undergo the following reactions:

$$\mathrm{TiO_2} + h\nu \rightarrow e^- + h^+ \tag{1}$$

$$e^- + \mathrm{Ti(IV)O\text{-}H}\ (A) \rightarrow \mathrm{Ti(III)O\text{-}H^-}\ (X) \tag{2}$$

$$h^+ + \mathrm{Ti(IV)O\text{-}H} \rightarrow \mathrm{Ti(IV)O^{\bullet}\text{-}H^+}\ (Y) \tag{3}$$

$$h^+ + \tfrac{1}{2}\,\mathrm{O^{2-}_{lattice}} \leftrightarrow \tfrac{1}{4}\,\mathrm{O_2(g)} + \mathrm{Vacancy} \tag{4}$$

$$e^- + \mathrm{O_{2,s}} \rightarrow \mathrm{O_{2,s}^-} \tag{5}$$

$$\mathrm{O_{2,s}^-} + \mathrm{H^+} \leftrightarrow \mathrm{HO_{2,s}} \tag{6}$$

$$h^+ + \mathrm{Ti(III)O\text{-}H^-} \rightarrow \mathrm{Ti(IV)O\text{-}H} \tag{7}$$

$$e^- + \mathrm{Ti(IV)O^{\bullet}\text{-}H^+} \rightarrow \mathrm{Ti(IV)O\text{-}H} \tag{8}$$

$$\mathrm{O_{2,s}^-} + \mathrm{Ti(IV)O^{\bullet}\text{-}H^+} \rightarrow \mathrm{Ti(IV)O\text{-}H} + \mathrm{O_{2,s}} \tag{9}$$

Reactions (2-6) are photocatalytic redox pathways, while reactions (7-9) represent recombination channels. Reactions (3) and (4) compete for holes, leading to bound OH-radicals and O-vacancies, respectively. The reverse of reaction (4) generates O-adatom intermediates upon exposing defective surfaces to O_2(g). Different surface sites are expected to favor some reactions over others.

The specific feature underlying the catalytic properties of TiO_2 may be its ability to stabilize large stoichiometry imbalances via surface restructuring.[6] Since photocatalytic TiO_2 surfaces are extensively hydroxylated,[7] the dynamics of defect creation and healing may depend not only on bulk composition and morphology, but also on the nature and density of Ti-OH species.[8] Most of the information on TiO_2 surface photochemistry deals, however, with the properties of rutile single crystals under UHV conditions.[9-20] Defects created by oxygen desorption from crystals subjected to thermal annealing, Ar^+ bombardment, electron beam or UV-bandgap irradiation under UHV conditions were monitored by STM,[6b,9,10] XPS,[11,19,21] UPS,[11] SHG,[12,14,21] TPD,[13,18] and ELS.[13,19] These techniques reveal that the partially reduced $TiO_{2-\gamma}$ surfaces are readily healed by exposure to relatively low O_2 or H_2O[22] doses at sub-ambient temperatures. Thus, second harmonic generation signals produced upon UV irradiation of (110) rutile crystals in UHV are rapidly bleached by 100 Torr O_2 at 300 K.[12] XPS shows that photogenerated Ti(III) centers are reoxidized at high H_2O dosages (up to 10^8 Langmuir).[11] In contrast, the amphiphilic character developed by hydroxylated TiO_2 films upon irradiation lasts for hours in moist air.[8,23] This suggests that photocatalyst surfaces undergo an extensive reconstruction into interpenetrating hydrophilic and hydrophobic domains that is not easily reversed.

The above considerations, plus the fact that quantum yields found for gas-phase photocatalytic oxidations on TiO_2 ($\phi \sim 0.8$) are much higher than those for aqueous suspensions ($\phi \sim 0.05$),[1-3] led us to investigate the gas-solid interface of polycrystalline titania by DRIFTS under controlled conditions. By discriminating against the bulk, DRIFTS is particularly suited to study photodynamic effects on the surfaces of illuminated TiO_2 powders.[5] Mobile carriers are expected to modify surface reflectivity across the entire infrared region.[24] In contrast, the trapped carriers X and Y (shown below) represent defects with specific TiO-H stretching frequencies that depend on the oxidation state and coordination of the attached Ti-atoms.

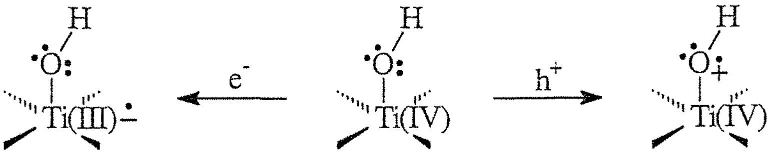

X **titanol** **Y**

The IR spectra of the hydroxylated rutile and anatase surfaces comprising actual TiO_2 photocatalysts display distinct bands in the 3300-3800 cm^{-1} region, associated with O-H stretching vibrations of TiOH, $TiOH_2$ and Ti_2OH groups.[7] Band positions, which are sensitive to both hydrogen bonding with neighboring groups and to the bonding environment of the embedded titanium atoms,[25] are expected to reflect photochemical changes. We assign the spectral features generated upon irradiation to chemically trapped photoelectrons and holes at specific surface sites, respectively, based on their redox properties. The stability of the photogenerated defects, and the conditions required for the regeneration of pristine surfaces provide useful insights into the mechanism of photocatalytic action.

Experimental

Commercial, polycrystalline TiO_2 (Degussa P-25, ~85% anatase, 15% rutile) was purified by sonication in deionized water and recovered by ultracentrifugation before being dried under vacuum. This procedure did not modify IR details, but substantially flattened the spectral baseline. Pure anatase (99.9%, Aldrich) was treated similarly. Sol-gel anatase was prepared by room temperature hydrolysis of $Ti(OCH(CH_3)_2)_4$ in the presence of HNO_3 as described in the literature.[26] The precipitate was aged at 363 K for several hours, then autoclaved at 473 K for 12 hours to digest the sol and crystallize the particulates. The powder was then subjected to the washing procedure described above. O_2 was dried through a P_2O_5 column. HCl(g) was produced by adding concentrated HCl to P_2O_5. D_2O (Alfa Aesar, 99.8% isotopic purity), CD_3OD (Cambridge Isotopes, 99.8% isotopic purity) and $Br_2(l)$ (EM Science) were used as received.

DRIFT spectra were recorded at 16 cm^{-1} resolution with a Perkin Elmer Model 1600 FTIR spectrometer equipped with a Spectra-Tech Collector diffuse reflectance accessory. TiO_2 powders were held in the sample cup of a Spectra-Tech high temperature environmental chamber (HTEC) that could be resistively heated up to 1000 K within ± 1 K. The chamber could be evacuated down to 1 μTorr. Gases were introduced through a separate inlet port. UV radiation from a 1 kW Oriel Xe lamp was focused into in the HTEC DRIFTS chamber through a KBr window. XPS was performed with an M-probe surface spectrometer (VG Instruments) pumped by a CTI Cryogenics-8 cryo pump. The crystals, mounted by pressing on double-sided tape, were irradiated with monochromatic Al Ka x-rays (1486.6 eV) that were incident at 35 from the sample surface.

Results

The DRIFT spectra of untreated TiO_2 powders display a complex, broad band spanning 2500-3900 cm^{-1} reflecting hydrogen-bonded TiO-H stretching vibrations in different atomic environments. This feature largely disappears, revealing discrete stretches within 3400-3800 cm^{-1} (Figure 2), following thermal treatment (about 12 hours at 623 K) under vacuum (~1 μTorr).[7] Exact band positions depend on TiO_2 preparation, and are affected by subsequent chemical treatment. These TiO_2 powders can be reversibly re-hydrated with water vapor.

Irradiation of dehydrated TiO_2 under vacuum reveals the fate of photogenerated electrons. The spectrum of dehydrated P-25 immediately after 30 s UV-irradiation *in vacuo* shows a raised baseline (Figure 3b), which decays with a half-life of $\tau \sim 7.50$ minutes (Figure 4) to a more persistent residual level (Figure 3d). Although the magnitude of the baseline rise increases toward the red end of the spectrum, τ is wave-number independent. The baseline rapidly relaxes to its original level by exposure to O_2 at 300 K, or by thermal treatment at 423 K. As the baseline relaxes, new discrete features, such as a prominent band at 3716 cm^{-1}, become apparent (Figure 5b). The difference spectrum (Figure 5c) reveals an additional absorbance at 3682 cm^{-1}, along with the weakening of the 3647 cm^{-1} and 3416 cm^{-1} bands. These changes persist for at least 4 days. The above phenomena are reproduced by irradiation in the presence of a hole scavenger, $CD_3OD(g)$ (Figure 6b),[27] but not under 1 atm O_2. Irradiation under 1 atm He causes the baseline shift, but no discrete bands. Pure anatase or sol-gel specimens display similar behaviors to P-25 (except for the lack of the 3416 cm^{-1} band characteristic of the rutile polymorph of TiO_2), but at much longer illumination times (30 min vs 30 s).

We assign the 3716 cm^{-1} band to a structure associated with trapped electrons (X), based on its sensitivity to redox agents. As expected, the exposure of irradiated TiO_2 powders to $H_2O(g)$ (<1 Torr) subsumes all of the above bands under the broad 2500-3900 cm^{-1} absorption described above. Upon subsequent vacuum dehydration at 300 K the 3716 cm^{-1} band reappears, revealing stability against reoxidation by water. In contrast, the partially depleted 3416 cm^{-1} peak following irradiation is fully recovered. Exposure to dry O_2 with or without further irradiation has no effect on the 3716 cm^{-1} band. The 3716 cm^{-1} band can be quenched by rehydration followed by irradiation under O_2, or by exposure to Br_2. A slight (~ 5 cm^{-1}) blue shift of some bands occasioned by increasing the pressure to 1 atm is independent of the nature of the gas, and instantly reverses upon evacuation.

The exposure of dehydrated P-25 powders to HCl(g) bleaches all bands except that at 3647 cm^{-1}, and leads to a new band at 3610 cm^{-1} (Figure 5d). This experiment, therefore, characterizes the Ti(IV)O-H group absorbing at 3647 cm^{-1} as the most acidic moiety on neutral TiO_2 surfaces.[7] Less than 1 Torr Br_2 on pristine P-25 is sufficient to yield an orange material, that is stable up to 1000 K under vacuum. The 3716 cm^{-1} band described above is readily bleached by $Br_2(g)$. Remarkably, the raised baseline following irradiation under vacuum is not completely reversed by $Br_2(g)$. Irradiation in the presence of $Br_2(ads)$ has no further effect, but irradiation under [$Br_2(ads)$ + O_2] restores the spectra of untreated surfaces. The latter samples revert in the dark within minutes to the spectra found under $Br_2(ads)$ alone.

We detect the formation of surface-bound hydroxyl radicals (Y) in TiO_2 irradiation under oxidizing conditions. Irradiation of dehydrated TiO_2 under dry O_2 (Figure 4b) yields a strong band at 3683 cm^{-1}, and a weaker one at 3726 cm^{-1} that is well resolved in the difference spectrum (Figure 7c). The 3683 cm^{-1} band persists *in vacuo*, but disappears under O_2 within a few hours at 300 K.

Deuterium labeling was used to confirm that the observed signals belong to O-H moieties (Figure 8).[7] Adsorbed CD_3OD does not exchange deuterium with the surface in the dark at room temperature, but all TiO-H bands are readily exchanged by exposure to D_2O vapor, regardless of the extent of prior dehydration. Two bands at 2927 and 2859 cm^{-1}, which do not exchange with D_2O even after extensive dehydration, correspond to hydrocarbon contaminants. An unusually large carbon peak, besides those of hydrogen, titanium and oxygen, in the XPS spectrum of P-25 confirms the presence of these hydrocarbons. Irradiation of a partially deuterated TiO_2 sample in the presence of O_2 led to the formation of a band at 2186 cm^{-1} that does not appear otherwise. This band also shows up following thermal treatment under O_2 of a sample that had been irradiated *in vacuo* several days in advance.

Discussion

The upward baseline shift following irradiation *in vacuo* is interpreted as evidence of the presence of mobile charge carriers that, by enhancing the refractive index, decrease the infrared reflectivity of TiO_2 surfaces.[24] The sensitivity of this effect to O_2 strongly suggests the mobile carriers are predominantly electrons. However, the relaxation lifetime is much longer than those associated with electron trapping in aqueous TiO_2 colloids, as measured by TRMC[28] or reflectance spectroscopy.[29] In addition, since $Br_2(g)$, a more powerful oxidant than O_2, does not fully quench the baseline shift, electron scavenging must be associated with the restoration of lattice stoichiometry, a process for which oxide ions are specific.

The band at 3716 cm^{-1} is assigned to reduced species X, resulting from the localization of conduction band electrons in a finite number of traps, because: 1) it appears by irradiation in the presence of the hole scavenger CD_3OD (Figure 6b), but not in the presence of the electron acceptor O_2 (Figure 7), and is fully bleached by Br_2, 2) its intensity reaches a saturation level, even under vacuum, that can not be enhanced by further irradiation, and 3) it is blue-shifted relative to all other TiO-H stretching vibrations. The trapped electron apparently corresponds to the species previously detected by ESR with $g_\perp = 1.957$ and $g_\parallel = 1.990$.[30] However, in contrast with the quenching behavior of the SHG[11] or ELS[12] signals in post-illuminated TiO_2 (110) crystals, the 3716 cm^{-1} band persists under 1 atm dry O_2 at 300 K, whether in the dark or under illumination. Actually, it can be bleached by illumination under O_2 *only after being partially rehydrated under H_2O vapor.* A recent *ab initio* study of oxygen-deficient rutile shows that while excess charge in the bulk remains spin-paired and localized at vacant oxygen sites, gap states in reduced surfaces are associated with spin-polarized Ti(III) $3d^1$ and Ti(II) $3d^2$ configurations.[31] In fact, electron trapping at a surface Ti(IV)OH center increases charge density on the O-atom, leading to a higher O-H vibrational frequency,[7] in accord with our assignment of the blue-shifted 3716 cm^{-1} band. The direct anticorrelation between the 3647 cm^{-1} and 3716 cm^{-1} band intensities following irradiation, plus the fact that the 3647 cm^{-1} demonstrably corresponds to the most acidic, i.e., the most electron-deficient Ti(IV)O-H group[32] (see above) are also consistent with the assignment. Saturation of the 3716 cm^{-1} peak intensity requires the presence of a finite number of such Ti(IV)O-H groups.

Remarkably, while the presence of O_2 during irradiation prevents the development of the 3716 cm^{-1} band, the addition of O_2 immediately after irradiation under vacuum enhances its intensity without shifting its position, an outcome apart from the baseline relaxation effect alluded above. Electron scavenging by O_2,[33] reaction (5), followed by protonation, reaction (6), would yield a surface hydroperoxide,[34] whose TiO_2-H stretching frequency is expected to be red-shifted relative to the literature value of the HO_2-H vibrational frequency in the gas-phase (3618 cm^{-1}), eliminating it as a candidate for the 3716 cm^{-1} band. Therefore, the 3716 cm^{-1} band magnification is probably due to O_2 dissociative chemisorption on Ti(III) clusters in defective TiO_2[35,36] (see below), followed by H-atom abstraction from weaker, neighboring TiO-H bonds. The fact that the 3716 cm^{-1} band does not appear by irradiation under 1 atm He —that, by slowing down diffusion in the gas-phase, prevents instantaneous desorption— implies that isolated oxygen vacancies in unreconstructed surfaces are rapidly and reversibly filled by O_2.

Surface-bound hydroxyl radicals (Y) vibrating at 3683 cm^{-1} (cf. with 3738 cm^{-1} in gas-phase OH radicals)[37] are also formed by irradiation (Figure 9). Y is barely formed on titania irradiated under anoxic conditions and not at all in the presence of a hole scavenger (CD_3OD). However, Y is the major species in samples illuminated under O_2. In accord with the expected reactivity of isolated hydroxyl radicals, the 3683 cm^{-1} band is indefinitely stable in vacuum, but decays within hours under O_2. By comparing the intensities of the 3716 cm^{-1} and 3683 cm^{-1} bands obtained by irradiation under vacuum and in the presence of O_2 (Figure 9), we infer the trapping of photogenerated holes under anoxic conditions yields an IR-transparent species, which we believe are the lattice O-vacancies produced in reaction (4).

Irradiation of partially deuterated TiO_2 surfaces provides additional information on these processes. The $Ti(III)O\text{-}H^-$ (3716 cm^{-1}) and $Ti(IV)OH^{+\bullet}$ (3683 cm^{-1}) band frequencies decrease by a 0.741 factor (vs. 0.707 for unbound, harmonic vibrations, or 0.728 for gas-phase, anharmonic, OH/OD radicals) to 2753 cm^{-1} for $Ti(III)O\text{-}D^-$ and 2728 cm^{-1} for $Ti(IV)OD^{+\bullet}$, respectively, and correspond, therefore, to surface-bound species.[7] The irradiation of a partially deuterated sample under O_2 yields a new band at 2186 cm^{-1} that falls in the C-D stretching region. Remarkably, the C-D band also shows up during the thermal oxidation (1 atm O_2 at 473 K) of a sample that had been irradiated under vacuum several days in advance, confirming the survival of radical centers (in the dark under O_2) that are able to initiate isotope scrambling via activated free radical processes.[38]

Considering that the 3716 cm^{-1} band does not appear on thermally generated $TiO_{2-\gamma}$ subsequently exposed to $H_2O(g)$, we infer that the photogeneration of oxygen vacancies and/or trapped electrons on hydrated, polycrystalline titania triggers a unique process. The photochemical transformations undergone by anatase surfaces under anoxic conditions require spatially uncorrelated electron trapping and oxygen desorption events. Although the desorption of a single O_2 molecule amounts to a four-hole process, the 3716 cm^{-1} band is the result of single electron trapping. Therefore, either hole accumulation is a cooperative process, i.e., the localization of the first hole seeds a specific site for subsequent trapping,[39] or oxidized species such as mobile O^- radical ions or O-atoms are able to search the surface for trapped holes prior to O_2 desorption. The participation of -OH functionalities in these phenomena is underscored by the obligatory presence of H_2O(ads) in the photochemical reoxidation of Ti(III)O-H species.[40] At variance with photochemical surface damage, thermal O_2 desorption follows the concerted four-electron transfer from 2 O^{2-} to adjacent Ti^{4+} ions. From this perspective, thermally generated defective surfaces, in contrast with irradiated samples, would contain coupled Ti(III)/O-vacancy centers. The fact that CH_3CN adsorbed on photogenerated $Ti^{16}O_{2-\gamma}$ substrates is largely converted into ^{16}O-containing species upon $^{18}O_2$ addition necessarily implies that surface reoxidation perturbs extended regions, in which the preponderant majority of ^{16}O-atoms becomes available for reaction.[41] In other words, CH_3CN photo-oxidation on defective $Ti^{16}O_{2-\gamma}$ is also incompatible with the reoxidation of independent, localized vacancies.[41]

The rather severe conditions required for healing photochemically produced surface defects in hydroxylated anatase are consistent with the existence of a sizable barrier for the deconstruction of the mesoscopic patterns underlying the amphiphilic character of irradiated titania surfaces.[8,23] Since none of these phenomena takes place on TiO_2 irradiated under 1 atm inert gas, which retards O_2 diffusion away from the surface favoring its re-absorption, surface reconstruction can be considered the outcome of a two-dimensional phase transition occurring above a critical defect concentration.

Conclusions

1. Mobile charge carriers, which are produced during bandgap irradiation of TiO_2 *in vacuo,* decrease surface reflectivity. These carriers are mobile electrons that have a lifetime of τ ~7.5 minutes toward trapping, which is very sensitive to H_2O(ads).
2. Mobile electrons are trapped into acidic Ti(IV)OH centers leading to Ti(III)O-H groups that absorb at 3716 cm^{-1}. These species are indefinitely stable, and impervious to H_2O, O_2, or UV treatment. The bleaching of these signals requires the combined action of (O_2 + H_2O + hν), consistent with defect stabilization by surface reconstruction involving OH groups.
3. The photochemical production of surface-bound hydroxyl radicals by hole oxidation of Ti(IV)OH groups is greatly increased under 1 atm O_2(g). Surface-bound OH radicals have a characteristic vibration at 3683 cm^{-1}, and decay within 5 hours under 1 atm O_2(g), but are indefinitely stable under vacuum.
4. Hole-induced, lattice-oxygen desorption competes with hydroxyl radical formation, particularly under vacuum. The resulting vacancies are segregated from the IR-active trapped electron sites.
5. Irradiation of TiO_2 surfaces under vacuum produces radical species that are stable under 1 atm O_2(g), 300 K for at least 3 days. They are able to sensitize D/H scrambling of C-H bonds in adsorbed hydrocarbons upon heating the pre-irradiated samples under O_2 at 423 K.

Acknowledgements

We thank J. A. Moss for assistance with experimental design. This work was funded by grants from the NSF and DARPA (through a cooperative program with the Northrop-Grumman Corporation).

References

---

[1] Hoffmann, M. R.; Martin, S. T.; Choi, W.; Bahnemann, D. W., *Chem. Rev.,* **1995**, *95*, 69.

[2] Linsebiger, A.; Lu, G.; Yates, J. T., *Chem. Rev.,* **1995**, *95*, 735.

[3] a) *Photocatalytic Purification and Treatment of Water and Air,* Ollis, D. F.; Al-Ekabi, H.; Eds.; Elsevier Science Publishers: Amsterdam, 1993, p.39. b) Stark, J.; Rabani, J.; *J. Phys. Chem. B,* **1999**, *103*, 8524, and references therein. c) Ibrahim, H.; de Lasa, H., Ind. Eng. Chem. Res., **1999,** 38, 3211. d) Lichtin, N. N.; Avudaithai, M., *Environ. Sci. Technol.,* **1996**, *30*, 2014.

[4] Sze, S. M., *Physics of Semiconductor Devices;* Wiley: New York, 1981; Chapter 1.

[5] Kortüm, G., *Reflectance Spectroscopy*, Springer-Verlag, New York, 1969.

[6] a) Wagner, M.; Kienzle, O; Bonnell, D. A.; Ruhle, M., *J. Vacuum Sci. Technol., A,* **1998,** *16*, 1078. b) Blanchin, M. G., *Oxides,* **1998**, *155*, 359. c) Rohrer, G. S.; Henrich, V. E.; Bonnell, D. A., *Science,* **1990,** *250,* 1239. d) Patel, R.; Guo, Q.; Cocks, I.; Williams, E. M.; Roman, E.; deSegovia, J. L., *J. Vacuum Sci. Technol., A,* **1997**, *15*, 2553.

[7] a) Contescu, C.; Popa, V. T.; Schwarz, J. A., *J. Colloid and Interface Science,* **1996**, *180*, 149. b) Hadjiivanov, K.I.; Klissurski, D.G., *Chem. Soc. Rev.,* **1996**, 25, 61.

[8] Wang, R.; Sakai, N.; Fujishima, A.; Watanabe, T.; Hashimoto, K., *J. Phys. Chem. B,* **1999**, *103*, 2188.

[9] Li, M.; Hebenstreit, W.; Gross, L.; Diebold, U.; Henderson, M. A.; Jennison, D. R.; Schultz, P. A.; Sears, M. P., *Surf. Sci.,* **1999**, *437*, 173.

[10] Dielbold, U.; Lehman, J.; Mahmoud, T.; Kuhn, M.; Leonardelli, G.; Hebenstreit, W.; Schmid, M.; Varga, P., *Surf. Sci.,* **1998**, *411*, 137.

[11] Wang, L. Q.; Ferris, K. F.; Skiba, P. X.; Shultz, A. N.; Baer, D. R.; Engerlhard, M. H., *Surf. Sci.,* **1999**, *440*, 60.

[12] Shultz, A. N.; Jang, W.; Hetherington, W. M.; Baer, D. R.; Wang, L. Q.; Engelhard, M. H., *Surf. Sci.,* **1995**, *339*, 114.

[13] Henderson, M. A.; Epling, W. S.; Perkins, C. L.; Peden, C. H. F.; Diebold, U., *Phys. Chem. B,* **1999**, *103*, 5328.

[14] Kobayashi, E.; Matsuda, K.; Mizutani, G.; Ushioda, S., *Surf. Sci.,* **1999**, *428*, 294.

[15] Epling, W. S.; Peden, C. H. F.; Henderson, M. A.; Diebold, U., *Surf. Sci.,* **1998**, *413*, 333.

[16] a) Lindan, P. J. D.; Harrison, N. M.; Gillan, M. J., *Phys. Rev. Lett.,* **1998**, *80*, 762. b) Lindan, P. J. D.; Muscat, J.; Bates, S.; Harrison, N. M.; Gillan, M., *Faraday Discuss.,* **1997**, *106*, 135.

[17] Wang, L.-Q.; Ferris, K. F.; Winokur, J. P.; Shultz, A. N.; Baer, D. R.; Engelhard, M. H., *J. Vac. Sci. Technol. A.* **1998**, *16*, 3034.

[18] a) Lu, G.; Linsebigler, A.; Yates, J. T., *J. Chem. Phys.,* **1995**, *102*, 4657. b) Lusvardi, V. S.; Barteau, M. A.; Chen, J. G.; Eng, J.; Fruhberger, B.; Teplyakov, A., *Surf. Sci.,* **1998**, *397*, 237.

[19] Göpel, W.; *Surf. Sci.* **1984,** *139*, 333.

[20] Lu, G. Q.; Linsebigler, A.; Yates, J. T., *J. Phys. Chem.,* **1994**, *98*, 11733.

[21] Shultz, A. N.; Hetherington, W. M.; Baer, D. R.; Wang, L. Q.; Engelhard, M. H.; *Surf. Sci.* **1997,** *392*, 1.

[22] Wang, L.-Q.; Baer, D. R.; Engelhard, M. H.; Shultz, A. N., *Surf. Sci.* **1995,** *344*, 237.

[23] a) Wang, R.; Hashimoto, K.; Fujishima, A.; Chikuni, M.; Kojima, E.; Kitamura, A.; Shimohigoshi, M.; Watanabe, T., *Nature,* **1997**, *388*, 431. b) Wang, R.; Hashimoto, K.; Fujishima, A.; Chikuni, M.; Kojima, E.; Kitamura, A.; Shimohigoshi, M.; Watanabe, T., *Adv. Mater.,* **1998**, *10*, 135. c) Watanabe, T.; Nakajima, A.; Wang, R.; Minabe, M.; Koizumi, S.; Fujishima, A.; Hashimoto, K., *Thin Solid Films,* **1999**, *351*, 260.

d) Fujishima, A.; Hashimoto, K.; Watanabe, T., *TiO_2 Photocatalysis, Fundamentals and Applications,* BKC, Tokyo, 1997.

[24] a) Chiaradia, P.; Del Sole, R., *Surf. Rev. Lett.,* **1999**, *6*, 517. b) Mezerreg, A.; Llinares, C.; Montaner, A., *Phys. Status Solidi B,* **1992**, *169*, 121. c) Qian, D. R., *Infrared Physics,* **1992**, *33*, 127. d) Shim, M.; Shilov, S. V.; Braiman, M. S.; Guyot-Sionnest, P.; *Phys. Chem. B,* **2000**, *104*, 1494.

[25] Hadjiivanov, K.I.; Davydov, A.A; Klissurski, D.G., *Kinetika I Kataliz.*, **1988**, 29, 161.

[26] O'Regan, B.; Gratzel, M., *Nature*, **1991**, 353, 737.

[27] a) Adsorbed CD_3OD shows well-resolved bands at 2359, 2331, 2222, 2123, 2083, and 2059 cm^{-1} (Fig. 3.a) that are not removed by evacuation or by moderate therma treatment (< 250 °C). CD_3OD is consumed during irradiation along with the formation of deuterated species, and with the enhancement of TiO-D bands. b) Chuang, C.-C.; Chen, C.-C.; Lin, J.-L., *Phys. Chem. B,* **1999**, *103*, 2439.

[28] Martin, S. T.; Hermann, H.; Choi, W.; Hoffmann, M. R., *J. Chem. Soc. Farad. Trans.,* **1994**, *21*, 3323.

[29] Furube, A.; et al., *J. Phys. Chem. B,* **1999**, *103*, 3120.

[30] Nakaoka, Y.; Nosaka, Y., *J. Photochem. Photobiol. A: Chemistry,* **1997**, *110*, 299.

[31] Mackrodt, W. C.; Simson, E.-A.; Harrison, N. M., *Surf. Sci.* **1997**, *384*, 192.

[32] Parfitt, G.D.; Ramsbothan, J.; Rochester, C.H.,*Trans. Farad. Soc.,* **1971**, *67*, 3100.

[33] Hetherington, W. M.; Koenig, E. W.; Wijekoon, W. M. K. P., *Chem. Phys. Lett.,* **1987**, *134*, 203.

[34] Ishibashi, K. I.; Fujishima, A.; Watanabe T.; Hashimoto, K., *J. Phys. Chem. B,* **2000**,*104,* 4934.

[35] Lu, G. Q.; Linsebigler, A.; Yates, J. T., *J. Phys. Chem.,* **1995**, *99*, 7626.

[36] Ishibashi, K. I.; Nosaka, Y.; Hashimoto, K.; Fujishima, A., *J. Phys. Chem. B,* **1998**, *102*, 2117.

[37] NIST Standard Reference Database Number 69 - February **2000** Release: *NIST Chemistry WebBook.*

[38] It is assumed that C-H bonds can only scramble with the surface via alkyl radicals produced by H-abstraction from OH-radicals or analogous species.

[39] Novak, D.; Garfunkel, E.; Gustafsson, T., *Phys. Rev. B,* **1994**, *15*, 5000.

[40] Obee, T.N.; Hay, S.O., *Env. Sci. Technol.,* **1997**, *31*, 2034.

[41] Zhuang, J.; Rusu, C. N.; Yates, J. T., *Phys. Chem. B,* **1999**, *103*, 6957.

[42] Shu, C.; Sukumar, N.; Ursenbach, C. P., *J. Chem. Phys.,* **1999**, *110*, 10539.

[43] Rusu, C. N.; Yates, J. T., *Langmuir,* **1997**, *13*, 4311.

[44] Serwicka, E., *Colloids and Surfaces,* **1985**, *13*, 287.

[45] Katz, G.; Kosloff, R.; Zeiri, Y., *J. Chem. Phys.,* **1999**, *111*, 7593.

[46] Wang, L. Q.; Baer, D. R.; Engelhard, M. H.; Shultz, A. N., *Surf. Sci.,* **1995**, *344*, 237.

[47] Weidmann, J.; Dittrich, T.; Konstantinova, E.; Lauermann, I.; Uhlendorf, I.; Koch, F., *Solar Energy Materials and Solar Cells,* **1999**, *56*, 153.

[48] Lee, S. K.; Robertson, P. K. J.; Mills, A.; McStay, D., *J. Photochem. Photobiol. A: Chemistry,* **1999**, *122*, 69.

[49] Lemercier, T.; Quarton, M.; Fontaine, M. F.; Hague, C. F.; Mariot, J. M., *J. Appl. Phys.,* **1994**, *76*, 3341.

[50] a) Augustynski, J., *Electrochemica Acta.,* **1993**, *38*, 43. b) Kim, W.T; Kim, C.D.; Choi, Q.W, *Phys. Rev. B*, **1984**, 30, 3625. c) Kim, W.T, *Phys. Rev. B*, **1983**, 28, 6529.

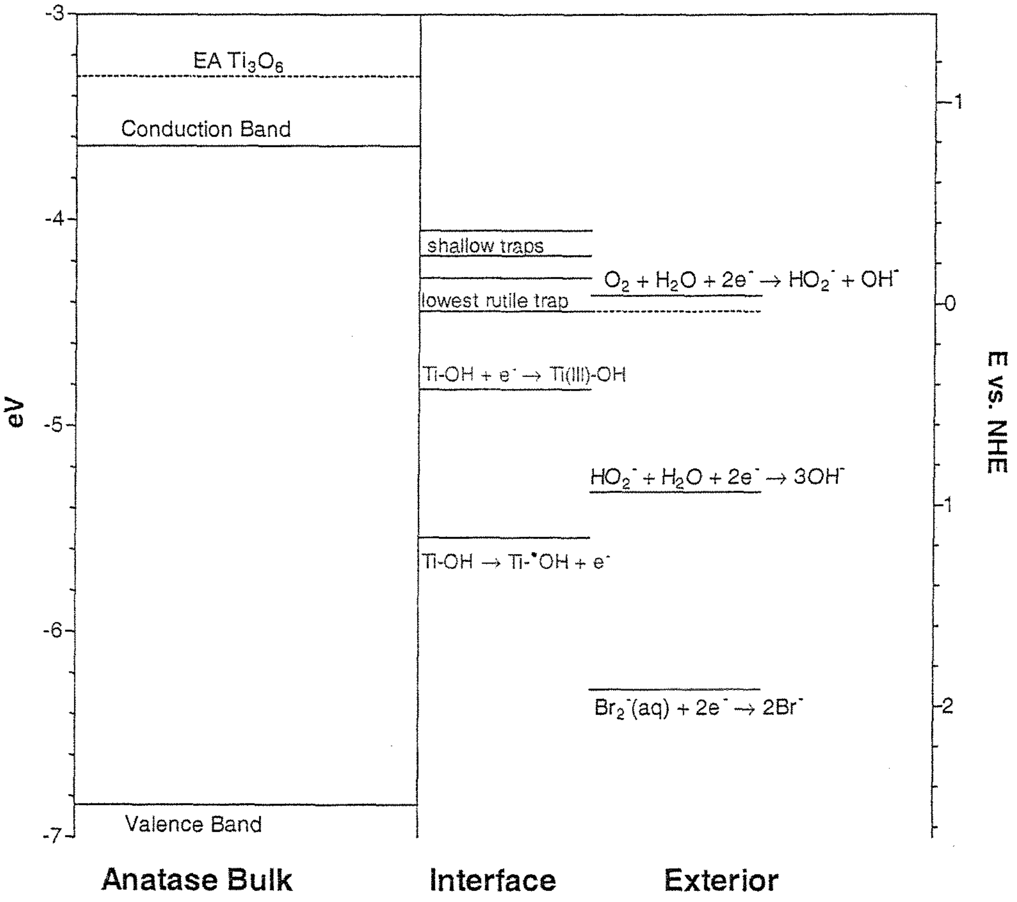

Figure 1: Quantitative diagram with literature[19,42] values of energy levels involved in TiO_2 photocatalysis.

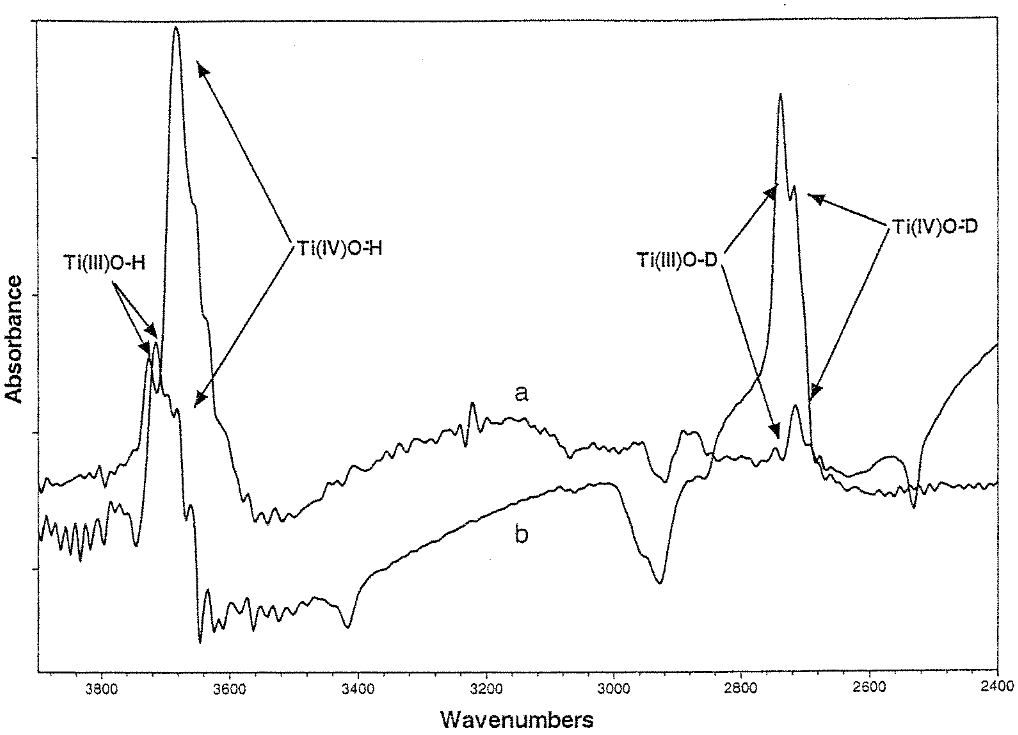

Figure 2: Sequential dehydration of P-25 TiO_2. a: at 27 °C under vacuum. b: at 27 °C under vacuum 36 hours. c: previously heated to 350 °C under vacuum, scanned at 27 °C.

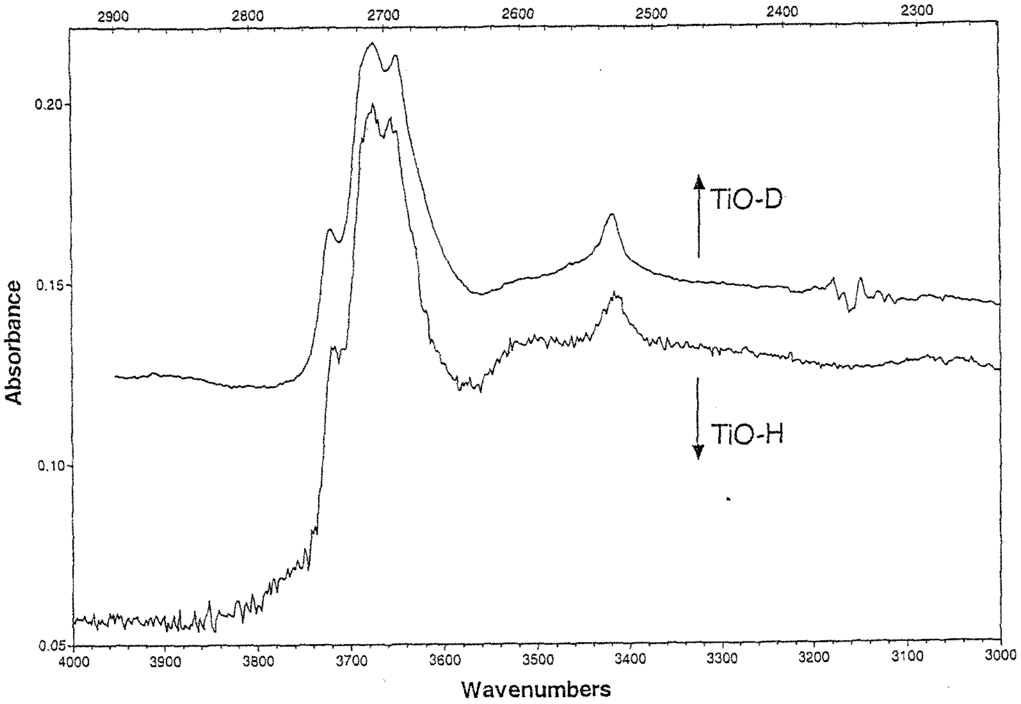

Figure 3: Baseline increase and decay. The solid black markers indicate points used for Figure 4. a: before irradiation. b: 0.5 min after irradiation termination. c: 10 min after irradiation termination. d: 20 min after irradiation termination.

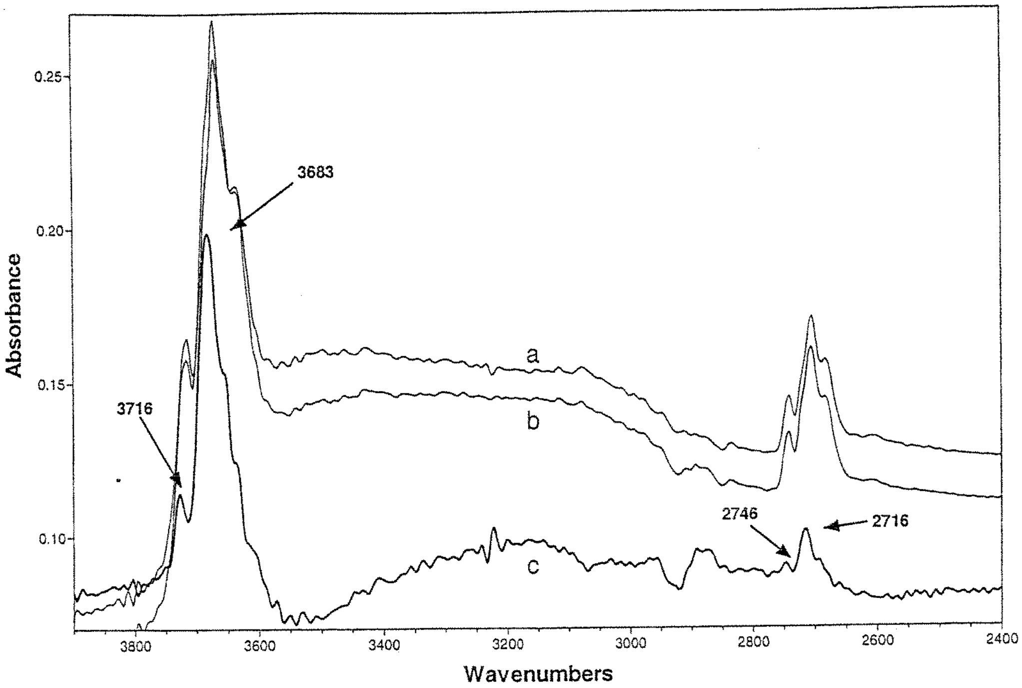

Figure 4: Kinetics of baseline relaxation. a (squares): at 2000 cm^{-1}. b (triangles): at 3000 cm^{-1}. c (dots): at 4000 cm^{-1}. Curves represent: Absorbance = A× exp(-time/τ) + B fits, to the data, consistent with a common τ = 7.5 min value.

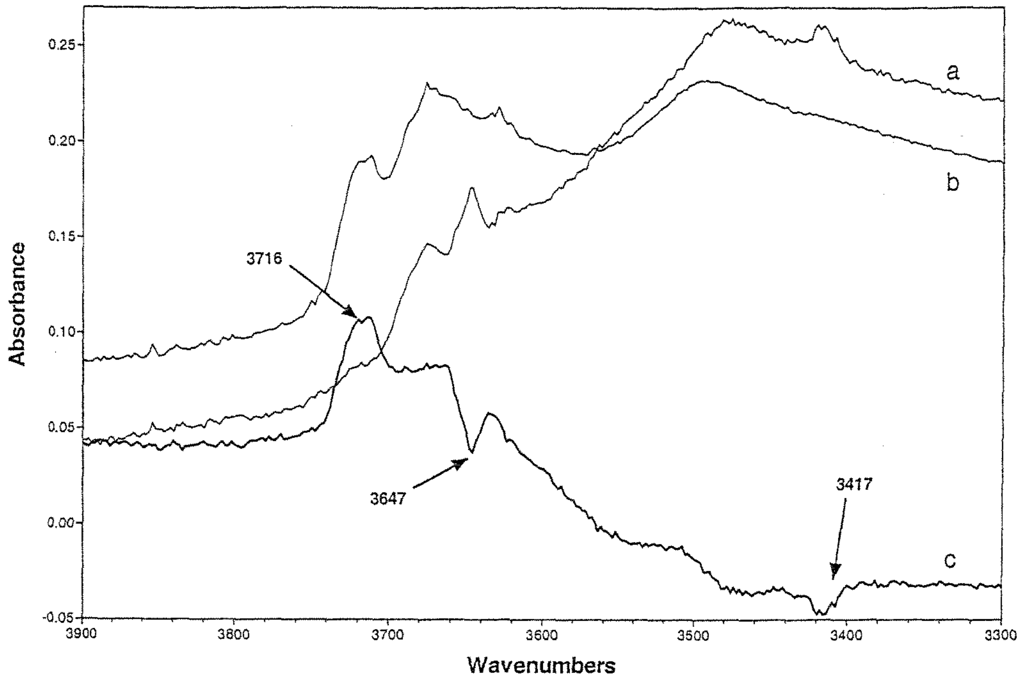

Figure 5: Effect of UV treatment on P-25 TiO_2 under vacuum. a: moderately dehydrated P-25. b: same sample following irradiation. c: difference b-a.

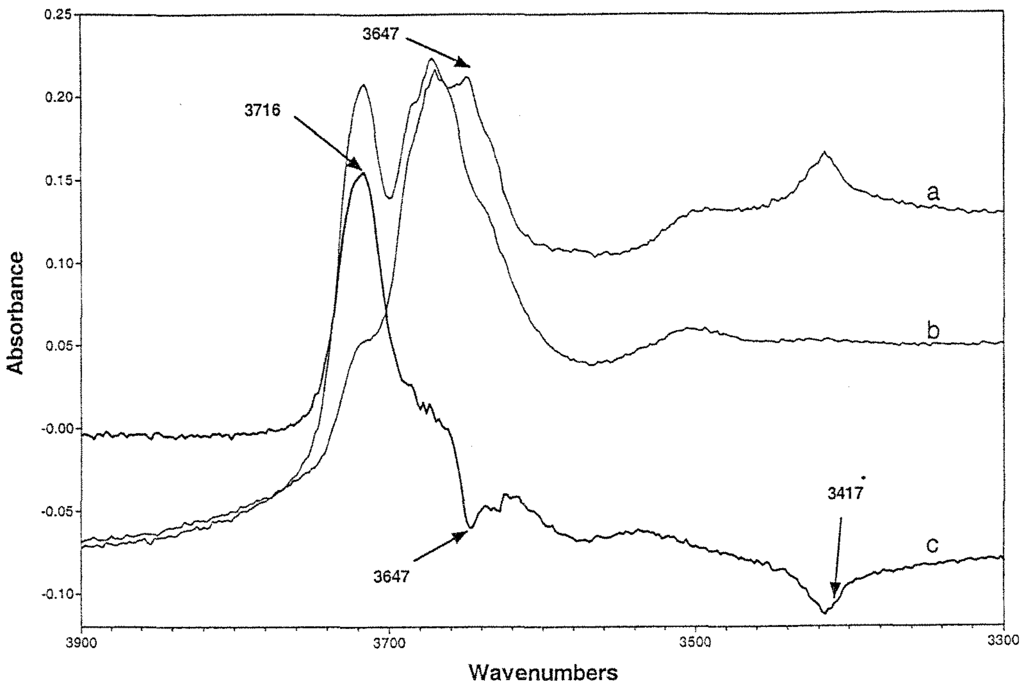

Figure 6: Irradiation of P-25 TiO_2 in the presence of CD_3OD(ads). a: dehydrated powder previously exposed to CD_3OD(g). b: same sample after irradiation. c: difference b-a.

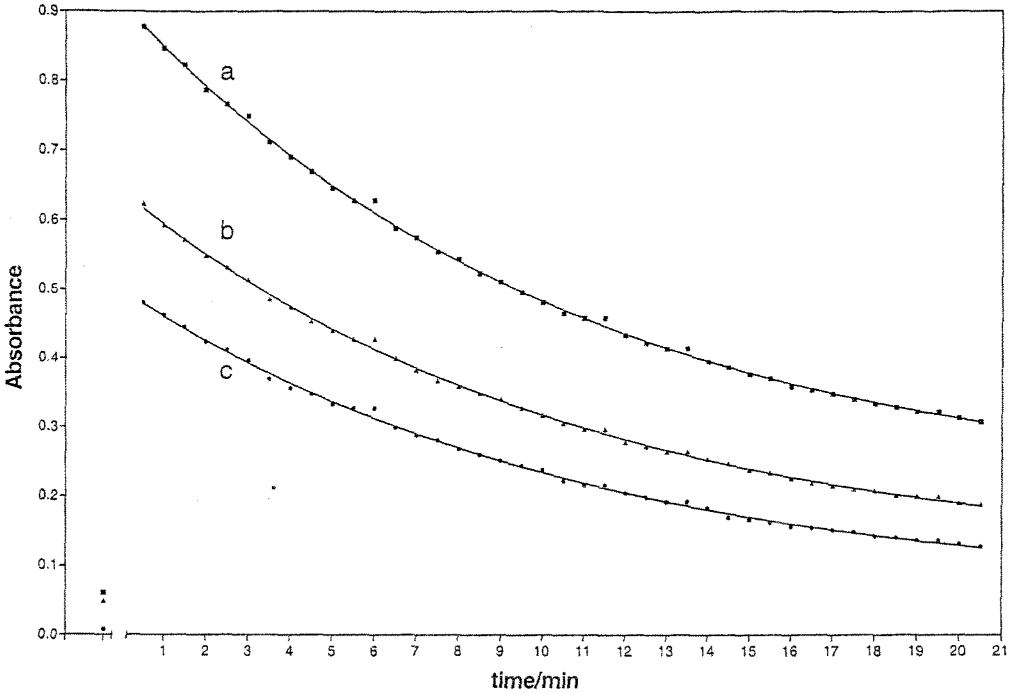

Figure 7: Partially deuterated P-25 TiO_2 irradiated under O_2. a: under O_2. b: same sample after irradiation under O_2. c: difference b-a (baseline shifted and amplified).

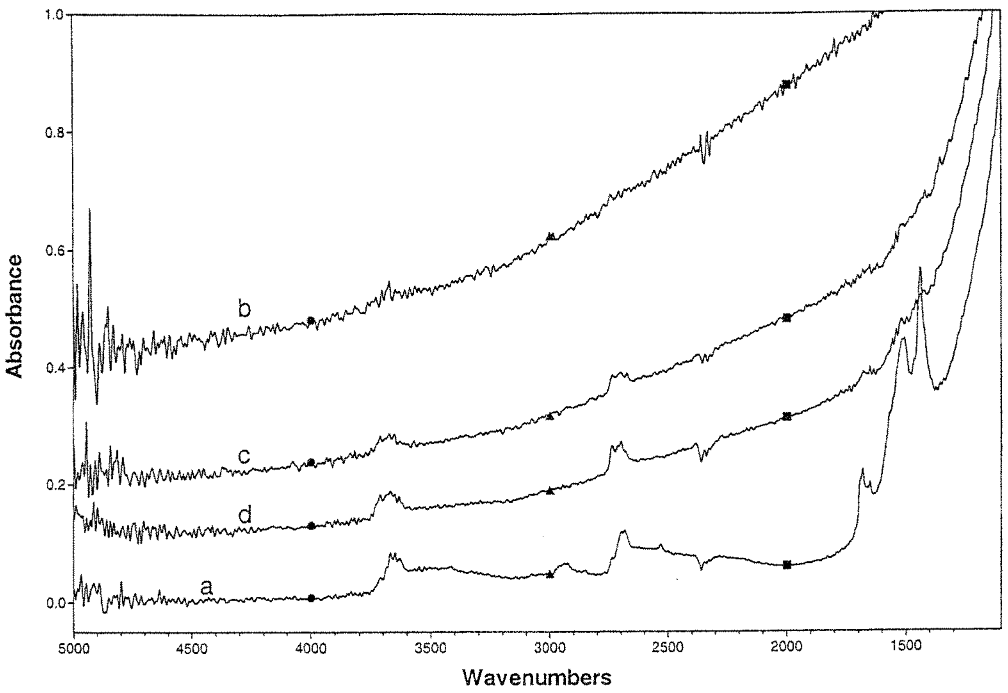

Figure 8: A typical *single spectrum* of P-25 with ~50% deuterium substitution rearranged to overlay the positions of the D bands (upper) on the H bands (lower). Note – different x scales.

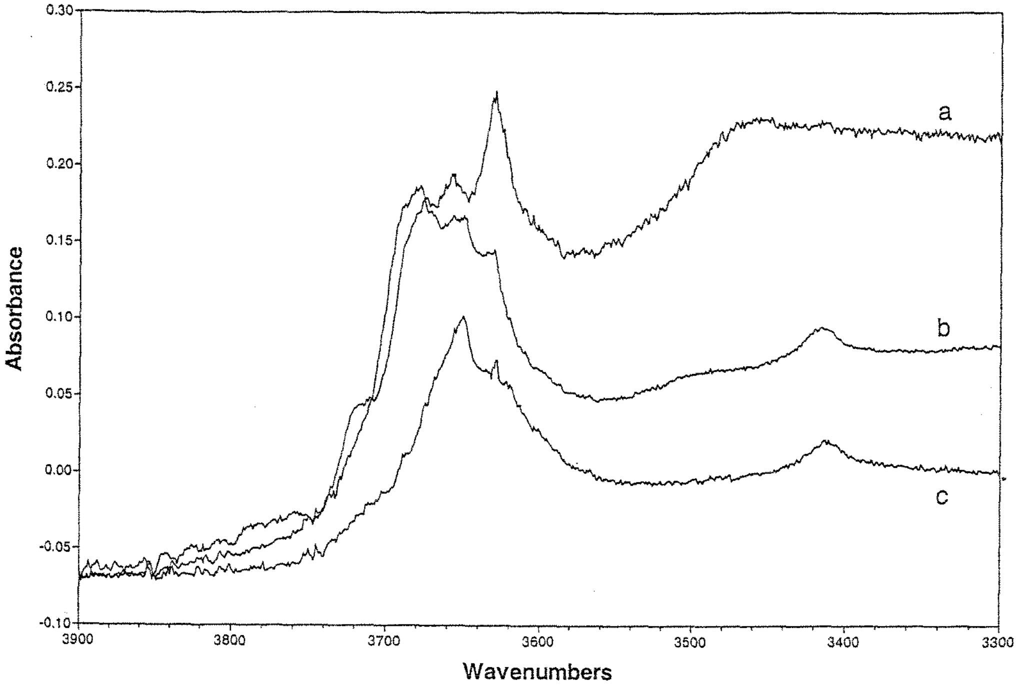

Figure 9: Overlay of partially deuterated difference spectra. a: P-25 irradiated under O_2 - P-25 under O_2. b: P-25 irradiated *in vacuo* - P-25 *in vacuo* (baseline shifted and amplified). Note that the peak positions in 'b' are blue shifted with respect to those in 'a' by the reversible effect of the O_2 atmosphere.

Chapter 3

Slow Surface Charge Trapping Kinetics on Irradiated TiO_2

[The text of this chapter is in press as Szczepankiewicz, S.H.; Moss J.A.; Hoffmann M.R. *J. Phys. Chem. B*, **2001,** *105*.]

Abstract

Free and trapped charge carriers in polycrystalline TiO_2 following bandgap irradiation are characterized by diffuse reflectance IR spectroscopy (DRIFTS). A spectrum-wide absorption signal proportional to $\lambda^{1.7}$ (λ = wavelength/μm) indicates the presence of free conduction band electrons coupled with acoustic phonons in the lattice. Free electrons appear to decay according to saturation kinetics. The fitted parameters indicate a limited number of reversible trapping states. The concentration of these states appears to be diminished by sequential UV treatments. A broad IR absorption peak centered at 3380 cm^{-1} is attributed to an electronic transition from an occupied surface electron trap 0.42 eV below the conduction band. The free carrier decay lifetime is lengthened as the samples are dehydrated. Photogenerated free electrons are comparable to conduction band electrons injected from surface-bound chromophores, and the lifetime of these electrons can be extended across several orders of magnitude.

Introduction

The nature of electron trapping on TiO_2 surfaces is of primary interest in the fields of sensitized solar energy conversion,[1] photocatalysis,[2] and pigment passivation.[3] Trapped electrons reduce adsorbed molecules at the TiO_2 surface, leading to current loss in photovoltaic cells[1] or to oxygen activation that benefits photocatalytic remediation processes,[2,4] but also causes paint to chalk.[3] In this paper, we present results from a fundamental FTIR investigation of the trapping states involved in these heterogeneous electron transfer reactions.

Whether directly injected into the TiO_2 conduction/valence band or internally photo-produced, electrons and holes migrate from the semiconductor bulk to the surface where they initiate reduction and oxidation reactions, respectively, from either a free or a trapped state.[4] Some surface traps mediate these reactions, but others lead to electron-hole recombination. Since the thermodynamic driving forces of these reactions are large, the trapping times from the free states as well as the lifetimes of the trapped states are implicated as the primary factors governing the rates of recombination.[1,2] In general, fast trapping and short residence times in the traps are believed to yield higher efficiencies for both solar energy conversion and photocatalysis, since the charges do not accumulate and recombine.

The simplified overall process of sensitized charge injection is shown in reaction (1).

$$\equiv S + h\nu \underset{r_{rec}}{\overset{r_{inj}}{\rightleftarrows}} \equiv S^{+} + e^{-}_{cb} \tag{1}$$

where $\equiv S$ is the surface-bound sensitizer, $\equiv S^+$ is the oxidized surface-bound sensitizer, e_{cb}^- is the electron in the TiO_2 conduction band, r_{inj} is the injection rate, and r_{rec} is the recombination rate.[1] Durrant and co-workers demonstrated that both the injection rate[5] and the recombination rate[6] are independent of the nature of the sensitizer used within experimental error, and the difference between the two is due to electron trapping on the TiO_2 substrate.[5] The experimental recombination kinetics are theoretically reproduced by a random-walk model demonstrating that the reaction is limited by trap-state occupation.[7] This study also shows that proximity is not the determining factor governing recombination rates, as the electron may visit the oxidized dye several times before reducing it.[7] Lian and co-workers infer that (1) injected electrons randomly populate a small region near the parent adsorbate, (2) spatial diffusion between trap states is negligible on the nanosecond time scale, and (3) injected electrons relax from shallow to deep trap states.[8] In this system, the transient injected electrons are observed by the mid-IR absorption of electrons in the semiconductor.[9] The decay of this state as measured by recombination rates, originally observed at about 100 ps,[10] is system dependent and can vary by 8 orders of magnitude depending on the trap-state population.[6,11] Although the broad, mid-IR signal is commonly used to track injected electrons sequestered in TiO_2, they could not be assigned to a free or trapped state[12] according to the spectral lineshape[13] due to the limited range of data available. In UV-Vis spectra of electrons irreversibly injected into TiO_2 from excited-state isopropanol, large stable concentrations of free conduction band electrons are observed with little evidence of trapping.[14]

Since the trapping dynamics are believed to be independent of the conduction band electron release mechanism,[5,6] the same behavior is observed following internal bandgap excitation in the absence of a sensitizer.[15] The sequence of events involving the promoted electron, that occur during bandgap irradiation, are as follows.[2]

$$TiO_2 + h\nu \rightarrow e^- + h^+ \quad (2)$$

$$e^- + O_{2,s} \rightarrow O_{2,s}^- \quad (3)$$

$$e^- + Ti(IV)O\text{-}H \rightarrow Ti(III)O\text{-}H^- \quad (4)$$

$$Ti(III)O\text{-}H^- + O_{2,s} \rightarrow Ti(IV)O\text{-}H + O_{2,s}^- \quad (5)$$

$$Ti(III)O\text{-}H^- + h^+ \rightarrow Ti(IV)O\text{-}H \quad (6)$$

$$e^- + h^+ \rightarrow \text{annihilation + heat} \quad (7)$$

This scheme shows that the electron is trapped at hydroxylated surface titania (4), in accord with our previous report.[16] Since the dynamics of the trap states are independent of surface coordination,[5,6] the same trapping reaction is expected to occur with naked surface titania. In the absence of a reducible electron acceptor, the electron remains in the particle and eventually is annihilated with an available hole,[17] which must occur with the assistance of charge trapping in an indirect semiconductor.[18] In this paper, we demonstrate that the annihilation reaction is dependent on electron trapping with the same dynamics as the recombination reaction with an adsorbed dye cation. We assign the broad, mid-IR spectral absorption to electrons in the free state based on the lineshape of the signal,[13] and by the trap-dependent saturation decay kinetics of this signal. By working with naked TiO_2 surfaces under vacuum, the electron trapping and annihilation is slowed such that the free electrons, typically monitored by ultrafast techniques,[4,19] maintain an unusually long lifetime of minutes to hours. In addition, we provide direct spectral evidence for a surface electron-trapping state on polycrystalline TiO_2.

Experimental

Commercial, polycrystalline TiO_2 (Degussa P-25, ~85% anatase, 15% rutile) was purified by sonication in deionized water and recovered by ultracentrifugation before being dried under vacuum. This procedure did not modify DRIFTS peak positions or intensities, but substantially flattened the spectral baseline. O_2 and He gases were dried by passing through P_2O_5 columns. D_2O (Alfa Aesar, 99.8% isotopic purity) was introduced as a low-pressure vapor to the sample, whose DRIFT spectrum was constantly monitored to yield a controlled H/D proportion before dehydration.

A diagram of the experimental setup is presented in Figure 1. DRIFT spectra were recorded at 8 cm^{-1} resolution with a Bio-Rad Digilab FTS-45 FTIR spectrometer equipped with an MCT detector and a Spectra-Tech Collector diffuse reflectance accessory installed in the external sampling bench. Kubelka-Munk (K-M) units were used to measure the spectral intensity. These units, which are a function of the reflected radiation (R in equation (8)), are used specifically for reflectance spectra, and are analogous to absorption units used in transmission spectroscopy.

$$K\text{–}M = \frac{(R-1)^2}{2R} \tag{8}$$

The K-M values used in the data analysis were all well below 5, which corresponds to 8% collection of reflected radiation, or an absorbance of about 1 – which is well within the linear concentration regime. TiO_2 powders were held in the sample cup of a Spectra-Tech high temperature environmental chamber (HTEC) that could be resistively heated up to 1000 ± 1 K. The chamber could be evacuated down to ~1 μTorr. Gases were introduced through a separate inlet port. UV radiation from a 1 kW Oriel Xe lamp was focused into in the HTEC DRIFTS chamber through a KBr window. A 10 cm jacketed water filter removed the IR portion of the radiation. Dynamic temperature control, maintained with a cooled air stream through the coils of the HTEC, prevented excessive heating during the UV treatment and allowed a rapid return to room temperature before analysis. A lens embedded in the compartment lid allowed for irradiation without breaking a zero-air purge. Some samples were pre-irradiated under oxygen to remove surface organic contaminants. Under typical conditions, irradiation caused the sample temperature to increase to ~130 °C under vacuum, or ~60 °C under He. Samples were heated well above these temperatures (400 °C) under 1 mTorr of O_2, then they were exposed to a vacuum condition in a final pretreatment step to eliminate the interference from strictly thermal processes.

Numerical analyses were performed with computational routines written in LabVIEW. The kinetic parameters were fit according to the saturation kinetic equation (8) in integrated, exponential form (9) by an interative solution for S_t found where $F(S_t) = 0$ for each time t.

$$\frac{dS_t}{dt} = \frac{-V_m S_t}{K + S_t} \tag{9}$$

$$F(S_t) = \frac{S_t}{S_0} - 1 + e^{\frac{S_t - V_m \cdot t}{K}} \tag{10}$$

The parameters S_0 (signal response at t = 0), K (combined kinetic constant), and V_m (maximum reaction velocity) were adjusted to globally fit the data.[20]

Results

The results of four sequential excitation/decay sequences under vacuum using a single sample are presented in detail with figures. The transient IR spectral response of TiO_2 to UV irradiation under vacuum is shown in Figure 2. The effects on the discrete TiO-H stretches in the IR spectra following UV treatment are discussed in a previous paper.[16] Since the spectral baseline increases with temperature, all spectra were recorded at 27 °C. Figure 2a shows the spectrum acquired after 2 minutes of UV treatment, and after cooling to 27 °C (~1 min lag time). Figure 2b-d show spectra acquired during the free-electron signal's decay, and Figure 2e shows the spectrum following complete relaxation of the UV-induced signal, scanned 24 hours after excitation. The signal appearance and decay were reproducible during successive photolysis/decay cycles, whether under vacuum or 1 atm He. Samples that were more extensively dehydrated qualitatively showed longer decay lifetimes. These data are not shown due to the lack of quantitative control over surface hydration.

The shape of the signal was determined by subtracting the final, relaxed state spectrum from the excited-state spectrum. Examination of these spectra in the 1427-3028 cm^{-1} region, which is free of specific IR absorption bands, reveals that the signal is wavelength dependent according to the formula

$$S(\lambda) = A\lambda^{p} \tag{11}$$

where $S(\lambda)$ is the amplitude at wavelength λ, p is a constant, and A is a proportionality factor. The inset of Figure 2 shows the data replotted on a log-log scale to demonstrate two important points. First, the logarithmic dependence is clearly shown. Rewriting equation (11) in log form gives equation (12).

$$\log\left(S\left(\lambda\right)\right)=\log\left(\mathrm{A}\right)+\mathrm{p}\cdot\log\left(10^{5}\right)\text{-}\mathrm{p}\cdot\log\left(\frac{\mathrm{E}}{\mathrm{cm}^{-1}}\right) \tag{12}$$

The linear relationship from this equation is clearly seen in the log-log plot with a linear regression, where the slope log(E) vs. log(S) is –p. The second point is that the amplitude of the signal (i.e., the magnitude of A in equation (11)), which is a function of decay time, did not affect its wavelength dependence. The best-fit p of 1.73 was independent of A (in Kubelka-Munk units), due to the constant spectral shape, independent of signal intensity, for all four subtracted spectra from Figure 2, normalized such that the signal at 2500 cm^{-1} = 1 on a log scale (offset vertically by 0.1). Even though it appears within the O-H stretching region, the characteristic peak at 3380 cm^{-1} in all spectra from Figure 2 has no deuterated counterparts (Figure 3). The 3380 cm^{-1} peak remains after the full decay of the free-electron signal, but decays completely upon standing after several hours.

Since the spectral shape does not change as the signal decays, an arbitrary point at 2500 cm^{-1} was selected to track the decay as a function of time. Figure 4 shows the time progression data for four sequential excitation/decay experiments along with fitted curves. A linear fit of the first 100 minutes of the decay curves from Figure 7 are used to approximate the initial rates. The fitted slopes and intercepts are shown in Table 1 in parentheses. The y-intercepts, which approximate the signals from free carriers at time 0, are qualitatively proportional to the UV intensity, which varied due to fogging on the lamp IR filter that partially blocked the UV beam in some of the experiments. Irradiation with an unimpeded path resulted in the greatest signal at time 0.

The complete progression curves for the signal relaxation at 2500 cm^{-1} were fitted according to saturation kinetics with the parameters shown in Table 1. A global fit of K across all four progression curves resulted in a <30% increase in the standard deviation with respect to an unrestricted fitting, and yielded parameters that are more closely comparable to the linear estimations, shown in parentheses. The values of V_m decrease with the experiment number for the four sequential irradiation/decay sequences on a single sample (Figure 5).

Discussion

The broad, featureless IR signal is assigned to free conduction band electrons according to the spectral lineshape. According to semiconductor theory, free conduction band electrons are tightly coupled with lattice phonons to conserve momentum during intraband transitions. This results in an increasing absorption of radiation with increasing wavelength, according to equation (11). The exponent has the theoretical value of $p = 1.5$ for electron momentum conservation with acoustic phonons in an indirect semiconductor. Higher values of the exponent are due to coupling with optical phonons ($p = 2.5$) and/or ionized impurities ($p = 3\text{-}3.5$).[13] The spectrum-wide signals shown in Figure 2 show such wavelength dependence, each with an exponent of $p = 1.73$. Since the fitted value of p is independent of A (which decreases with time), the nature of the signal does not change as the decay progresses. A single state is responsible for this signal, since combinations of states would change relative proportions depending on total state populations. This state is characterized as free conduction band electrons coupled with primarily acoustic phonons in the TiO_2 lattice, based on the fitted p value. A similar signal in the visible spectrum has previously been assigned to free electrons, but the limited wavelength range prevented fitting the exponential relationship.[12]

The amplitude of the signal at 2500 cm^{-1} is proportional to the free electron concentration such that $S = \alpha[e^-_{cb}]$, where α is a proportionality constant. The non-exponential decay of these free electrons over a timescale of hours is well approximated by a saturation kinetic model (Figure 4). This implies the two-step mechanism of reactions (13) and (14).

$$e_{cb}^- + T^0 \underset{k_{-1}}{\overset{k_1}{\rightleftharpoons}} T_{e^-}^{full} \tag{13}$$

$$T_{e^-}^{full} + h_{vb}^+ \underset{k_{-2}}{\overset{k_2}{\rightleftharpoons}} T^0 \tag{14}$$

Here e_{cb}^- is the conduction band electron, T^0 is an available trap site, T^{full} is an occupied trap site, and h_{vb}^+ is the valence band hole. The mechanism requires that an electron must be trapped in order for recombination to occur, in accord with our introduction reaction scheme. The rate expression for this mechanism, assuming annihilation to be irreversible, is given by equation (15)

$$\frac{dS_t}{dt} = \frac{-V_m S_t}{K + S_t} \tag{15}$$

where

$$K = \frac{(k_{-1} + k_2)}{k_1} \quad and \quad V_m = k_2 [T_{total}] \tag{16}$$

and S_t is the signal at time t. The fits of the spectral data by the saturation kinetic model are shown in Figure 4.

The data presented here show that the annihilation rate is dependent on free carrier concentration only at low concentrations. This is in contrast to the general concept that photogenerated electrons and holes behave as independent entities, which freely migrate about the TiO_2 bulk until they are irreversibly trapped at the surface (equations (2-7)).[21] Any independently trapped carrier should immediately be subject to annihilation by an opposing free carrier through coulombic attraction. Synergistically, coulombic repulsion would force nearly all traps to rapidly fill in the presence of high concentrations of free carriers, so the subsequent annihilation rate would be strongly dependent on the concentration of free carriers. To illustrate this point, consider that when half of the electron traps are filled, $[T]_{filled} = [T]_{total}/2$, equation (12) gives equation (17) and (18).

$$-\frac{dS}{dt} = rate = \frac{V_m}{2} = \frac{V_m \cdot S_{rate=50\%max}}{K + S_{rate=50\%max}} \tag{17}$$

$$K = S_{rate=50\%max} \tag{18}$$

Thus, the surface traps are only 50% filled when the free electron signal at 2500 cm^{-1} is 0.958 K-M units (the value of K/min^{-1}). This value indicates a moderately high concentration of free electrons, which is lower than the initial mobile electron concentration. However, these mobile electrons still appear to take hours to decay in the presence of available annihilation centers and valence band holes. According to the equation (16), a high value of K is possible when $k_{-1} + k_2$ is large, which could be the result of either a large k_{-1} or k_2. A large k_2 would result in a fast rate during the zero-order decay (rate = Vm = $k_2[T_{total}]$) unless $[T_{total}]$ was correspondingly small. Although $[T_{total}]$ could change as a function of dehydration as Ti-OH sites are converted to naked Ti sites, the TiO-H stretches in our spectra qualitatively indicate a high degree of H-bonding between neighboring groups, which suggests that the surface is still mostly hydroxylated.[22] Since the effect of dehydration under these conditions is observed to remove less than half of the surface hydroxylation, the concentration of surface TiOH trap sites should be relatively unaffected. Therefore, k_2 could not be large enough to cause the traps to be only ½ full at such a high free electron concentration. This implicates a relatively large k_{-1} contributing to the numerator in the K definition. That is, the de-trapping rate must be comparable to the trapping rate when $K = S_{rate=50\%\ max}$. This is only possible if (1) free carriers are relatively stable in the semiconductor bulk, (2) surface charge trapping is a reversible process, and (3) annihilation is not inevitable following charge trapping, even in the presence of an opposing charge acceptor. These are the same conclusions that describe the ultrafast electron recombination behavior in dye sensitizer studies.[7]

The lifetimes for the free electrons, known to vary in the range of picoseconds to microseconds,[11] are observed from seconds to hours in this paper, qualitatively depending on surface hydration. In our previous report,[16] we presented data for slightly more highly hydrated samples showing the baseline collapse with $t_{1/2}$=7.50 min, which is considerably shorter than the decay presented here on more extensively dehydrated samples (~100 min). Since intensity anomalies in our spectral data preclude an accurate determination of surface hydration,[23] a systematic dosing approach with controlled levels of hydration would be necessary to quantify this relationship. Although it is possible that the natures of the trap states are changing with dehydration, no structural rearrangement is believed to occur upon rehydration.[16] This suggests that the physical nature of the trap states remains invariant with respect to surface hydration. While maintaining the same forward reaction, the longer free-electron lifetimes on the extensively dehydrated samples may be attributed to the increased reversibility of the electron trapping reactions. The HO-H stretching vibration, which has an energy close to known electron trapping depths, may effectively dissipate the trapping energy loss to stabilize the trapped state, resulting in less reversible trapping by reducing k_{-1b} with respect to k_{-1a}. This suggests that the trapped electron initially occupies an excited state within the trap, which would allow reversible de-trapping.

The total concentration of annihilation centers is diminished by UV treatment under vacuum followed by relaxation. Figure 5 shows the best-fit V_m for the progression curves, along with a fitted exponential decay. Since V_m is proportional to the total trapping capacity (equation 16), T_{total} decreases exponentially with each UV treatment/decay sequence on a single TiO_2 sample. We have previously shown that a high concentration of trapped charges promotes a surface reconstruction following irradiation under vacuum.[16] Oxygen vacancy reconstruction patterns have been observed on the anatase (101) and (001) single crystal surfaces.[24] The data presented here suggests that the resulting reconstruction lowers the total charge trapping capacity of the surface. This is possible if the electron trapping/annihilation reaction consumes a portion of the electron traps. That is, for some portion of the occupied sites such that $T^0_a \neq T^0_b$ in reactions (19) and (20), which in effect diminishes T_{total}.

$$e^-_{cb} + T^0_a \underset{k_{-1}}{\overset{k_1}{\rightleftharpoons}} T^{full}_{e^-} \tag{19}$$

$$T^{full}_{e^-} + h^+_{vb} \underset{k_{-2}}{\overset{k_2}{\rightleftharpoons}} T^0_b \tag{20}$$

It is interesting to note that this effect is independent of variations in S_0 (i.e., UV flux), and only occurs following the complete relaxation from exposure to UV irradiation, suggesting that a dark process is capable of removing trapping sites.

The broad peak at 3380 cm^{-1} in the observed spectra indicates an electronic transition from an occupied electron trap with a peak value 0.42 eV below the conduction band. A similar electronic transition from a trapped state to the conduction band is observed for trapped electrons in n-type GaP.[25] We believe that this is the first direct observation of an electronic transition from a surface trap for polycrystalline TiO_2. Such transitions are well characterized from the polarized spectra of rutile single crystals.[26] The clearly defined peak shape is not consistent with the notion of a diminishing continuum of trap states below the conduction band.[7] Although the band persists well beyond the complete decay of the free electrons, it is unclear whether this trap state is serving as an annihilation mediator. In fact, the deviation of the spectral baseline fit

(Figure 3) at high energy may indicate the presence of deeper-lying traps, which could also be responsible for the observed kinetic behavior.

Conclusions

The majority of electrons in bandgap-excited TiO_2 exist in a free state, giving rise to a broad, featureless absorption with intensity proportional to $(\lambda/\mu m)^{1.73}$. These electrons decay according to a saturation kinetic mechanism that is limited by the density of trapped states. The kinetic observations suggest that (1) free charge carriers are relatively stable in the bulk phase, (2) that surface charge trapping is a reversible process, and (3) that annihilation is not inevitable following charge trapping, even in the presence of an opposing charge acceptor. The charge trapping capacity of the surface appears to be diminished following the complete annihilation of a large number of free carriers. The charge carrier annihilation rate increases with increasing surface hydration, indicating that surface hydroxylation assists annihilation reactions by allowing irreversible electron trapping. A surface electron trap state observed at 0.42 eV may be responsible for mediating the annihilation mechanism.

Acknowledgements

This work was funded by NSF and by DARPA through the Northrup-Grumman Corp.

References

---

[1] Kalayanasundaram K.; Gratzel M. *Coord. Chem. Rev.*, **1998**, *77*, 347-414.

[2] Hoffmann M.R; Martin S.T.; Choi W.; Bahnemann D.W. *Chem. Rev.*, **1995**, *95*, 69-96.

[3] Braun J.H.; *J. Coating. Technol.*, **1997**, *69*, 59-72.

[4] Tryk, D.A.; Fujishima A.; Honda K. *Electrochimica Acta*, **2000**, 2363-2376.

[5] Tachibana Y.; Haque S.A; Mercer I.P.; Durrant J.R.; Klug D.R. *J. Phys. Chem. B*, **2000**, *104*, 1198-1205.

[6] Haque S.A; Tachibana Y.; Willis R.L.; Moser J.E.; Gratzel M.; Klug D.R.; Durrant J.R. *J. Phys. Chem. B*, **2000**, *104*, 538-547.

[7] Nelson J. *Phys. Rev. B*, **1999**, *59*, 374-380.

[8] Weng Y.X.; Wang Y.Q.; Asbury J.B.; Ghosh H.N.; Lian T. *J. Phys. Chem. B*, **2000**, *104*, 93-104.

[9] Ghosh H.N.; Asbury J.B.; Lian T. *J. Phys. Chem. B*, **1998**, *102*, 6482-6486.

[10] Ghosh H.N.; Asbury J.B.; Weng Y.X.; Lian T. *J. Phys. Chem. B*, **1998**, *102*, 10208-10215.

[11] Furube A.; Asahi T.; Masahura H.; Yamashita H.; Anpo M. *J. Phys. Chem. B*, **1999**, *103*, 3120-3127.

[12] Heimer T.A.; Heilweil E.J. *J. Phys. Chem. B*, **1997**, *101*, 10990-10993.

[13] Pankove J.I. *Optical Processes in Semiconductors*; Dover: New York, 1975.

[14] Safrany A.; Gao R.; Rabani J *J. Phys. Chem. A*, **2000**, *104*, 5848-5853.

[15] Wang Y.Q.; Asbury J.B.; Lian T. *J. Phys. Chem. B*, **2000**, *104*, 4291-4299.

[16] Szczepankiewicz S.H.; Colussi A.J.; Hoffmann M.R. *J. Phys. Chem. B*, **2000**, *104*, 9842-9850.

[17] We refer to this as "annihilation" to differentiate from "recombination" of an electron with an adsorbed dye cation.

[18] Serpone N.; Lawless D.; Khairutdinov R. *J. Phys. Chem.*, **1995**, *99*, 16646-16654.

[19] Zhang J.Z. *J. Phys. Chem. B*, **2000**, *104*, 7239-7253.

[20] Duggleby R.G. Enzyme Kinetics and Mechanism Part D: Analysis of Enzyme Progression Curves by Nonlinear Regression; Abelson, J.N; Simon, M.I.; Purich D.L., Eds., Academic Press: San Diego, 1995; p 61-71.

[21] van der Zanden B.; Goosens A. *J. Phys. Chem. B*, **2000**, *104*, 7171-7178.

---

[22] Yates D.J.C. *J. Phys. Chem.*, **1960**, *65*, 746.

[23] Szczepankiewicz S.H.; Moss J.A.; Hoffmann M.R. "Electron Traps and The Stark Effect on Hydroxylated Titania Photocatalysts." Submitted for publication in *J. Phys. Chem. B.*

[24] Hengerer R.; Bolliger B.; Erbudak M.; Gratzel M. *Surface Science*, **2000**, *460*, 162-169.

[25] Spitzer W.G.; Gershenzon M.; Frosch C.J.; Gibbs D.F. *J. Phys Chem. Solids*, **1959**, *11*, 339.

[26] Khomenko V.M.; Langer K.; Rager H.; Fett A. *Phys. Chem. Minerals.*, **1998**, *25*, 338-346.

Table Caption

Regression parameters for four sequential UV treatment / decay sequences for a single TiO_2 sample. The numbers in parentheses are obtained from linear fits to the initial decay curves. K was treated as a global variable for all four curves. σ is the standard deviation from the fitted curve.

Table 1

UV treatment #	$S_{t=0}$ (int)	K (global)	V_m	$V_{t=0}$ (-slope)	$S_{t=\infty}$	$\sigma * 10^3$
1	4.26 (4.31)	0.958	0.0395	0.0333 (0.0287)	0.137	1.242
2	2.38 (2.51)	0.958	0.0195	0.0139 (0.0135)	0.0991	0.785
3	4.06 (4.07)	0.958	0.0158	0.0128 (0.0137)	-0.0283	5.112
4	1.12 (1.17)	0.958	0.0124	0.00690 (0.00487)	0.0470	0.480

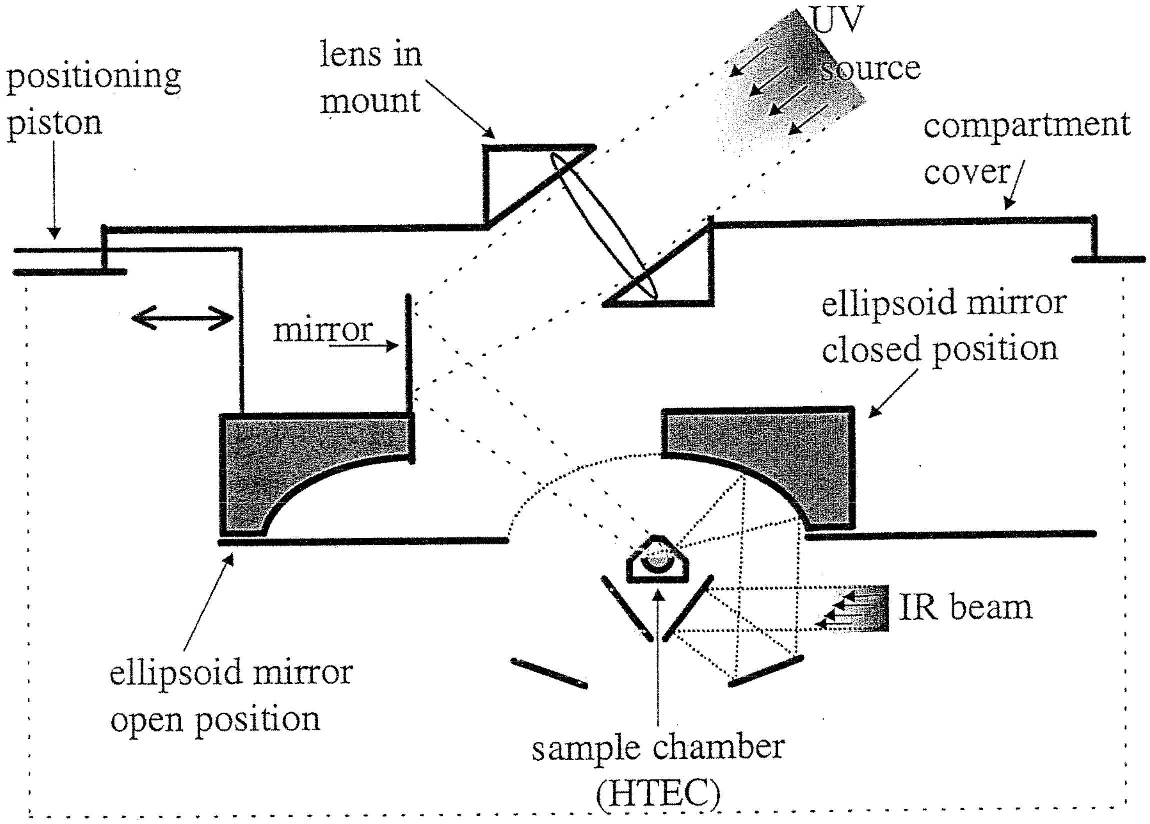

Figure 1: The experimental setup. The entire DRIFTS apparatus is enclosed in the FTIR chamber to maintain a zero-air purge and allow for rapid analysis following UV treatment. Note that the IR path is interrupted during UV treatment.

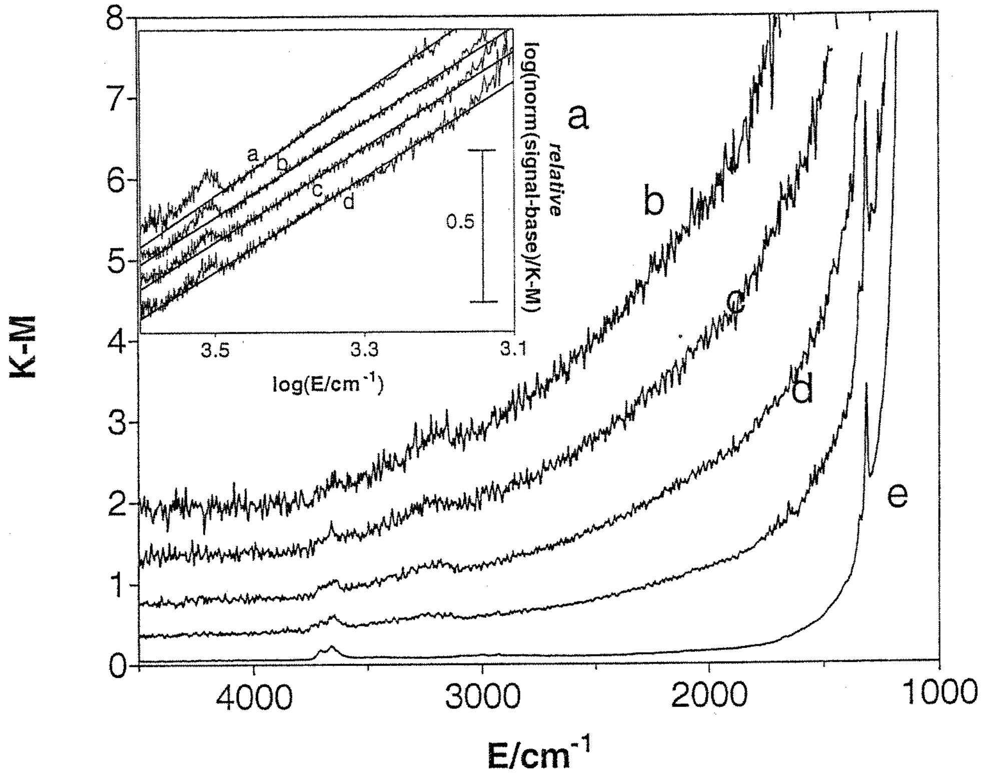

Figure 2: DRIFT spectra of TiO_2 (a) 13 minutes after UV treatment, (b) 52 minutes after, (c) 94 minutes after, (d) 135 minutes after, and (e) following full relaxation of the excited state signal. Inset: Same spectra plotted as $\log(S_{norm})$ vs. $\log(\bar{\nu}\ (cm^{-1}))$ where S_{norm} is the background subtracted signal normalized to S=1 at 2500 cm^{-1}, along with linear regression lines. For clarity, the spectra are offset by 0.1 on the y-axis. Note the electronic band centered at 3380 cm^{-1}.

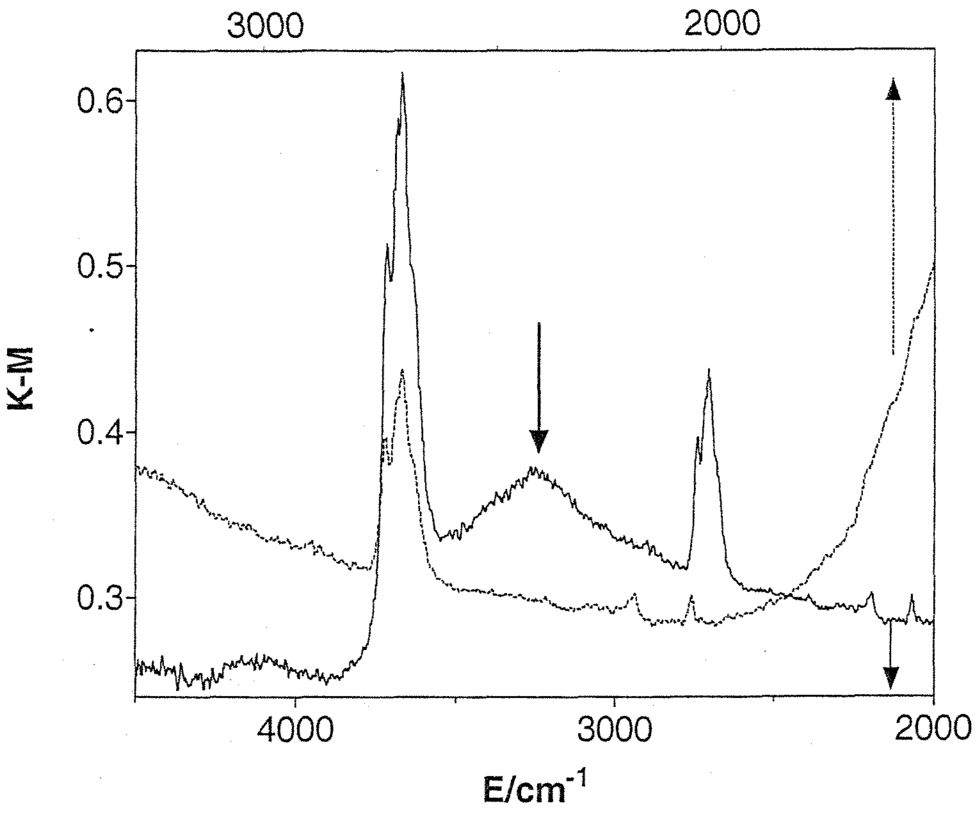

Figure 3: Spectrum of a partially deuterated sample following complete baseline relaxation under vacuum, plotted twice against different x-axes. The O-D stretches (upper x-axis) are artificially superimposed on the O-H stretches (lower x-axis) to highlight the band at 3380 cm^{-1} without a deuterated counterpart.

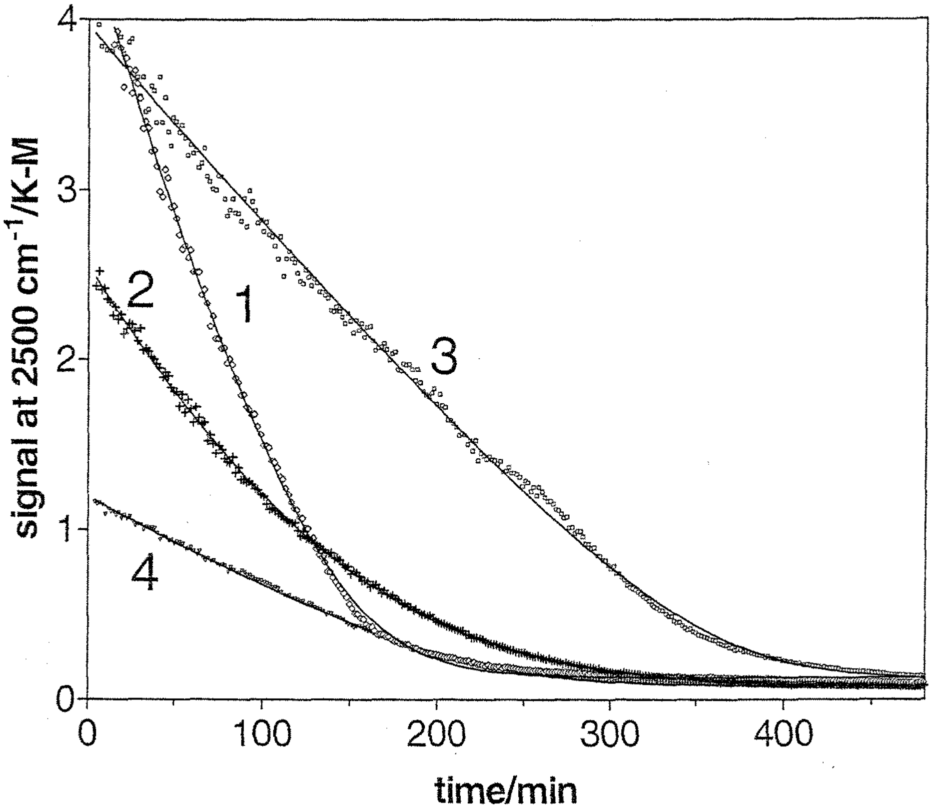

Figure 4: DRIFTS signal (at 2500 cm^{-1}) vs. time (data points) for four sequential UV treatment/relaxation sequences, along with fits according to the integrated saturation kinetic model (solid lines). The fitting parameters are given in Table 1.

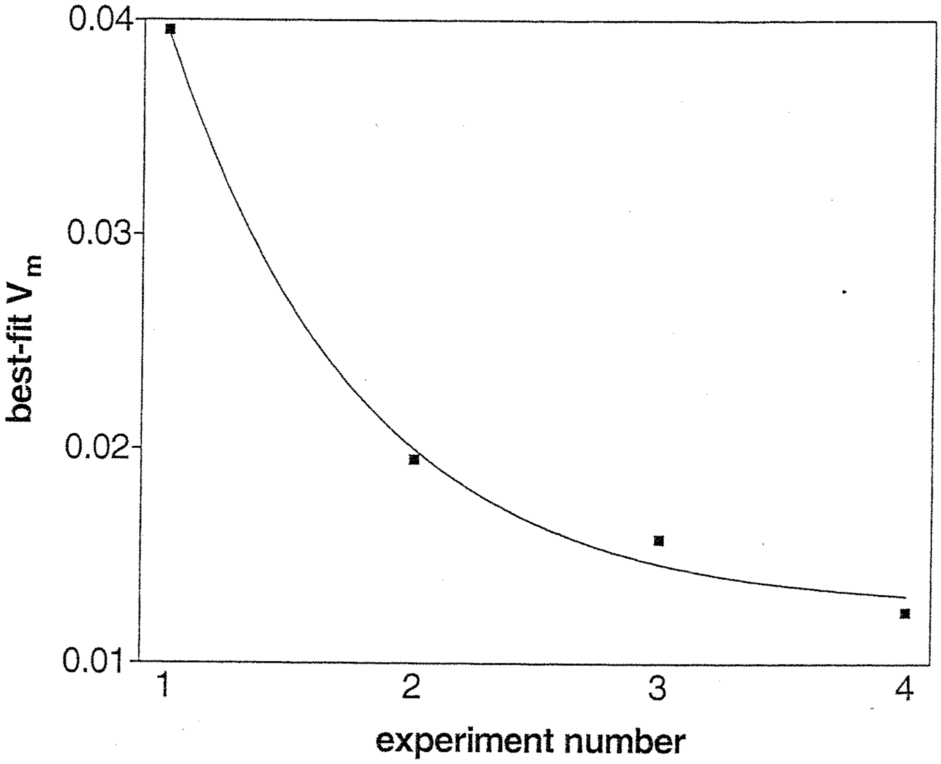

Figure 5: The fitted V_m parameters plotted vs. experiment number along with the fitted exponential decay, V_m = A*exp(-k*expt#) + P, where A = 0.0979, k = 1.29, and P = 0.0126.

Chapter 4

Electron Traps and The Stark Effect on Hydroxylated Titania Photocatalysts

[The text of this chapter is submitted for publication as Szczepankiewicz, S.H.; Moss J.A.; Hoffmann M.R. *J..Phys. Chem. B*, **2001**, *105*.]

Abstract

Electric fields generated by to photoexcited charge carriers in TiO_2 (anatase) produce Stark effect intensity and wavelength shifts for surface TiO-H stretching vibrations. Deep electron-trapping states affect a single type of TiO-H stretch (Ti(IV)O-H at 3647 cm^{-1} $\Rightarrow$ Ti(III)O-H at 3716 cm^{-1}). Shallow electron-trapping states, observed as broad absorption bands above 3000 cm^{-1}, produce an apparently homogeneous electric field. Intensity changes and corresponding wavelength shifts for ν(TiO-H) are proportional to the magnitude and polarity of the electric field. O_2 is shown to reversibly abstract electrons from shallow trapping states. These results suggest that shallow electron traps are not associated with localized structures, but rather are delocalized across the TiO_2 surface. This behavior may also explain the photon-dependent wettability of TiO_2 surfaces.

Introduction

Photoactivated TiO_2 is commonly used to assist the total oxidation of aqueous and vapor-phase organic pollutants.[1] Low conversion efficiency prevents the industrial-scale implementation of photocatalytic decontamination processes. Charge carrier recombination, which limits efficiency, is minimized when the charges are spatially separated. Bandgap irradiation of TiO_2 promotes electrons from the valence band to the conduction band, forming an electron-hole pair. Charge separation of the exciton pair is achieved by immobilizing one or both charges in mid band-gap traps.[2] The holes, which have a relatively small effective mass and high oxidizing potential (+3.0 V vs. NHE), are readily trapped at the semiconductor surface by oxidizing surface-bound hydroxyl groups to hydroxyl radicals, or by oxidizing lattice oxygen from the –2 to 0 valence state. Electrons, on the other hand, have a higher effective mass and moderate reduction potential (-0.2 V vs NHE), that allows them to remain in either the free state or to be trapped at the surface. Surface electron traps, which lower the potential of the CB electron, are defined as shallow if they lie above the reduction potential of O_2. Within seconds after irradiation, in the absence of external electron donors or acceptors, illuminated TiO_2 contains holes trapped as hydroxyl radicals and oxygen vacancies, along with electrons that are deeply trapped, shallowly trapped, and freely mobile.

Charge separation due to trapping in TiO_2 produces an electric field that can be observed as a bulk effect[3] and by its molecular influence.[4] Electric fields affect semiconductor photodynamics when the splitting of one exciton pair causes a Stark effect on the absorption of a second pair.[2,5] The Stark effect characterizes the influence of an electric field on spectroscopic transitions, which are commonly manifested as intensity and wavelength shifts. For electronic transitions, the Stark wavelength dependence (Stark tuning rate) is manifested by changing the relative potentials of the initial and/or final states, while the intensity shifts are apparent through changes in transition oscillator strength. For vibrational spectroscopy, these changes are manifested as structural modifications as the oscillating dipole responds to the electric field, changing bond lengths and orbital overlap. When the vibrational Stark effect is well-described for a system, either the dipole moment of the vibrating molecule can be determined from the influence of an external electric field, or vice versa for similar systems. Therefore, when compared with existing data, the magnitude of the Stark effect intensity and wavelength change observed for surface TiO-H vibrations on hydroxylated TiO_2 provides information about the electric field causing the changes, and hence acts as a probe for the trapping states involved in creating the electric field.

In our continuing research on TiO_2 photodynamics, we have characterized photogenerated electrons in deeply trapped states as surface Ti(III)OH moities with a characteristic stretching frequency, ν(TiO-H), at 3716 cm^{-1}.[6] We have also shown that electrons are able to exist for long times in the free state producing a broad IR absorption proportional to $\lambda^{1.7}$ where λ is the wavelength in microns.[7] We now focus our attention on the shallow electron traps. Occupied shallow electron trapping states are considered necessary for the reduction of oxygen at the TiO_2 surface, but they also facilitate the recombination of charge carriers as shown below.[1]

$$TiO_2 + h\nu \rightarrow e^-_{CB} + h^+_{VB} \tag{1}$$

$$e^-_{CB} \rightarrow e^-_{shallow\ trap} \tag{2}$$

$$e^-_{CB} \rightarrow e^-_{deep\ trap} \tag{3}$$

$$e^-_{shallow\ trap} + O_{2,s} \rightarrow O_{2,s}^- \tag{4}$$

$$e^-_{trap} + h^+ \rightarrow \text{annihilation} + \text{heat} \tag{5}$$

Despite the fundamental importance of these shallow electron-trapping states, little is known about their physical nature other than the energetic trapping depth and chemical reactivity. In this manuscript, we characterize electrons in shallow traps according to the delocalized electric field they create, which induces a Stark effect on the surface TiO-H vibrations.

Experimental

Commercial, polycrystalline TiO_2 (Degussa P-25, ~85% anatase, 15% rutile) was purified by sonication in deionized water and recovered by ultracentrifugation before being dried under vacuum. This procedure did not modify DRIFT spectrum peak positions or intensities, but substantially flattened the spectral baseline. O_2 and He gases were dried by passing through P_2O_5 columns.

DRIFT spectra were recorded at 8 cm^{-1} resolution with a Bio-Rad Digilab FTS-45 FTIR spectrometer equipped with an MCT detector and a Spectra-Tech Collector diffuse reflectance accessory installed in the external sampling bench. TiO_2 powders were held in the sample cup of a Spectra-Tech high temperature environmental chamber (HTEC) that could be resistively heated to 1000 ± 1 K. The chamber could be evacuated to ~1 μTorr. Gases were introduced through a separate inlet port. UV radiation from a 1 kW Oriel Xe lamp was focused into in the HTEC DRIFT spectra chamber through a KBr window. A 10 cm jacketed water filter removed the IR portion of the radiation. Dynamic temperature control, maintained with a cooled air stream through the coils of the HTEC, prevented excessive heating during the UV treatment and allowed a rapid return to room temperature before analysis. A lens embedded in the compartment lid allowed for irradiation without breaking a zero-air purge. Under typical conditions, irradiation caused the sample temperature to increase to ~160 °C under vacuum.

Results

Within the timescales of our experiments, irradiation of TiO_2 under vacuum produces trapped holes, and free and trapped electrons. O_2 reacts in the dark with the free and shallow-trapped electrons, leaving only deep-trapped electrons and adsorbed superoxide radicals. A typical DRIFT spectrum of dehydrated TiO_2 before UV treatment is shown in Figure 1. Following irradiation under vacuum, the broad signal from free carriers dominates the spectrum as reported previously.[7] A large band at 3716 cm^{-1}, assigned to ν[Ti(III)O-H] (deep trap),[6] is resolved when the free carriers are removed. This band appears in greatest proportion when the free carriers are quenched in the dark with O_2 rather than by self-annihilation. The spectrum following irradiation under vacuum followed by immediate exposure to O_2 is also shown in Figure 1.

Decreasing and eventually removing oxygen causes the adsorbed superoxide to desorb as O_2 following injection of an electron into TiO_2. As the electrons are injected, the total area under all of the ν(TiO-H) bands increases when the headspace O_2 is evacuated as shown in Figure 2. The intensity increase stands out in Figure 3, which shows the total peak area as a function of time, with a clear break upon evacuation. The gradual decrease in peak area after the initial rise is most likely a physical pressure effect, and can be reproduced using He instead of O_2. The initial rise is specific to an O_2-quenched system and will be discussed in the next section. Re-introduction of O_2 during this rise halts the area increase, which resumes upon re-evacuation. This sensitivity to O_2 indicates that photogenerated electrons are involved, and that those electrons are populating a shallow trap state in the TiO_2.

Electron trapping in shallow states produces an electric field, which is homogeneous as indicated by the fact that all Ti(IV)O-H stretches are affected equally. Deep traps also produce an electric field, but these fields are localized at the Ti(III)O-H centers. They appear to diminish the field effect of the shallow traps on the 3716 cm^{-1} band relative to the other TiO-H stretches. The spectrum obtained by taking the difference between the most and least intense spectra from Figure 2 does not have the same characteristic shape as the parent spectra (Figure 4). When the spectra are scaled vertically to overlay before subtraction, it is clear that the increase is not a simple spectral amplification. The proportional intensity of the 3716 cm^{-1} (deep-trap) band increases less than the other bands.

In order to investigate differences in the influence of the electric field on Ti(III)O-H and Ti(IV)O-H bands, the spectra were deconvoluted by fitting to four gaussian curves, using the appearance of distinct peaks among the TiO-H stretching bands as a basis for spectral peak fitting (Figure 5). The energy of the peak maximum for each Gaussian curve is plotted versus time in Figure 6 to highlight their sensitivity toward the elimination of O_2. A plot of peak area for each fit Gaussian curve versus time is shown in Figure 7. It is clear from Figures 5 and 7 that the spectra are dominated by contributions from peaks A and C, which constitute an average of 82% of the total peak area. While A is relatively well isolated and can be fit with minimal error, peaks B-D are overlapping. As a consequence, the largest area contributor, C, will be assumed to represent the bands in this region of the spectrum. The fraction of the total area for bands A-C is shown in Figure 8. It is clear that the area of peak A responds differently from peak C upon evacuation. In a similar fashion, the full-widths at half-maximum (FWHM) for these Gaussian curves are plotted versus time in Figure 9, showing a strong dependence for band A, but no clear change for band C.

Discussion

The Stark effect, which is observed upon removing oxygen, is manifested as a band energy and intensity change for ν(TiO-H). It is caused by an electric field due to occupied shallow electron traps. After initial irradiation *in vacuo*, introduction of O_2 in the absence of UV causes the signal from the free electrons to disappear, most likely due to the formation of O_2^-(ads).[8] A band for $\nu(O_2\text{-H})$ is not observed in the IR because O_2^- (aqueous $pK_a = 4.8$)[9] is not extensively protonated. The single-step reverse reaction causes the surfacial O_2^- to lose an electron back to TiO_2 and escape as O_2(g). This reaction does not inject electrons directly to the CB, but rather to lower-lying trap states.[10] The charge injection alters the electric field, leading to the ν(TiO-H) intensity increases observed when the O_2-quenched system is evacuated. In a previous paper, we showed that Ti(III)OH formed upon reduction of acidic Ti(IV)OH sites, resulting in a shift of ν(TiO-H) from 3647 cm^{-1} to 3716 cm^{-1} and an increase in intensity (Figure 1).[6] Using *ab initio* data presented by Hermansson for the influence of an electric field on the DO-H vibration,[11] this shift corresponds to an electric field strength change from +0.044 a.u. to 0.033 a.u. This shift directly supports the assignment of these bands to a single titanol structure type with titanium in either the +4 or +3 form (i.e., Ti(III/IV)O-H).

The observation of Stark effects for both Ti(III) and Ti(IV) centers indicates that the electric field arises from a diffuse state. When the electric field is directed along the bond axis, the wavelength and intensity shifts are approximately proportional, and exhibit a maximum whose position is sensitive to the bond polarity. However, when the bond angles change, as in the present case, the two effects clearly do not remain linear. Considering first the individual responses, the magnitude of the Stark shift of the vibrational state energy is the same for Ti(III) and Ti(IV) centers, but with a different shift in intensity as well as FWHM. When considered from a structural point of view, a static negative field is expected to contract the equilibrium bond lengths and bond angles of surface TiO-H groups as shown in Figure 10 for neutral hydroxylated TiO_2. As the bond lengths and angles contract, the energies and intensities of the vibrational frequencies change, as shown in Figure 6. Under some conditions, this can affect the very nature of the transitions involved in these vibrations (Figures 3 and 7).

The similar wavelength change observed for Ti(III)O-H and Ti(IV)O-H stretches indicates a similar potential energy change for both surface moieties. The energy of the bond length compression is nearly equivalent, but the magnitude of the change is different for Ti(III)O-H and Ti(IV)O-H. Since the Ti(III)O-H bond is already compressed with respect to the Ti(IV) bond, an equivalent potential change is manifested in a smaller displacement.

The same argument can be used to explain the difference in band intensity response to the electric field. The Ti(IV)O-H bond is slightly lengthened from its optimal orientation by the steric influence of the surface. Bond compression improves the orbital overlap, and the intensity of the vibration increases. However, the Ti(III)O-H bond is already shortened, so further compression is not as beneficial for its orbital overlap. The nature of the Ti(III)O-H vibrational transition changes slightly as a consequence of this high level of distortion, leading to band broadening. This suggests that the bond angle change for Ti(IV)O-H produces less change in the nature of the transition than for Ti(III)O-H, as indicated by the change in the FWHM.

Since the Stark effect from shallow electron trapping is observed for both Ti(III)O-H and Ti(IV)O-H vibrations, the electric field due to electrons in shallow traps is apparently homogeneous (Figure 2). In contrast, deep electron trapping appears to affect only one titanol stretching band. Since all TiO-H stretches are equally affected (Figure 4), this suggests that the shallow traps are either localized at every titanol, or that they are delocalized and affect all the titanol functionalities equally. A delocalized trap structure is supported by the influence on the band known to arise from Ti(III)O-H stretches. The shallow state must be displaced from the titania centers in order to influence both Ti(IV)O-H and Ti(III)O-H type stretches, since the latter is unlikely to accept additional charge. The observations presented above are explained by an equivalent field strength acting on both the Ti(III)O-H and Ti(IV)O-H vibrations, resulting in similar wavelength changes.

In light of these observations, we propose that the physical natures of the shallow electron traps correspond to delocalized electrons coupled with two-dimensional lattice phonons. This is similar to the two-dimensional charge traps proposed for CdSe.[12] Conduction band electrons are coupled with the bulk lattice phonons in order to conserve momentum in TiO_2.[13] This coupling is not possible as the electrons approach the surface where the phonons are not clearly defined by the lattice. It is likely that the electrons switch to coupling with two-dimensional surface phonons, which have been observed on anatase surfaces.[14] This coupling forces the electrons to occupy a two-dimensional state delocalized across the surface.

The identification of the shallow electron trapping state as a two-dimensional delocalized surface state is in agreement with much of the published data regarding TiO_2 properties and photoreactivity. The lack of a previous structural assignment to the shallow electron traps may be due to their delocalized nature. In addition, the super-wettability of the TiO_2 surface, obtained by irradiation, occurs through the formation of a checkerboard of hydrophilic and hydrophobic domains on the surface on the scale of ~50 nanometers.[15] This requires the influence of trapped charges to be transmitted across dimensions about two orders of magnitude larger than the unit cells, far beyond molecular-scale interactions, but in accord with two-dimensional polaron states.[16] The energetic depths of the shallow electron traps, which have been assigned in a range around 0.5 eV below the CB edge,[17] would be sensitive to the nature of the two-dimensional coupling. Since different crystal surfaces have different surface phonon modes,[14] they should be expected to support distinct electron trapping depths. This may account for the anisotropy in reduction rates observed on different cleavage surfaces for photoactivated rutile TiO_2.[18] Competing reduction reactions with specific surface-dependent rates could help explain the wide range of limiting efficiencies observed for different types of TiO_2 photocatalysts.[19]

Conclusions

We have shown that the intensities of surface hydroxyl stretching bands are sensitive to electric fields caused by trapped charge carriers. Using these intensity changes as a reference, we observe reversible electron abstraction from TiO_2 by O_2. We also show that the reverse reaction injects electrons to shallow trapping states, which appear to be delocalized across the surface. The assignment of this shallow electron-trapping structure corresponds well with available literature data.

Acknowledgements

This work was funded by NSF (grant # BES-9619885) and by DARPA through the Northrop-Grumman Corp.

References

---

[1] Martin S.T.; Chio W.; Hoffmann M.R. *Chem. Rev.* **1995**, *95*, 69-96.

[2] Norris D.J.; Sacra A.; Murray C.B.; Bawendi M.G. *Phys Rev. Lett.* **1994**, *72*, 2612.

[3] Komoda Y.; Rao T.N.; Fujishima A. *Langmuir* **1997**, *13*, 1371.

[4] Zaban A.; Meier A.; Gregg B.A. *J. Phys. Chem. B* **1997**, *101*, 7985.

[5] Ai X.C.; Jin R.; Ge C.B.; Wang J.J.; Zou Y.H.; Zhou X.W.; Xiao X.R. *J. Chem. Phys.* **1997**, *106*, 3387.

[6] Szczepankiewicz S.H.; Colussi A.J.; Hoffmann M.R. *J. Phys. Chem. B* **2000**, *104*, 9842.

[7] Szczepankiewicz S.H.; Moss J.A.; Hoffmann M.R. Slow Surface Charge Trapping Kinetics on Irradiated TiO_2. *J. Phys. Chem. B* submitted for publication, **2000**.

[8] Ishibashi K.; Fujishima A.; Watanabe T.; Hashimoto K. *J. Phys. Chem. B* **2000**, *104*, 4934.

[9] Buxton G.; Greenstock C.; Helman W.; Ross A. *J. Phys. Chem. Ref. Data* **1988**, *17*, 513.

[10] Ishibashi K.; Nosaka Y.; Hashimoto K.; Fujishima A. *J. Phys. Chem. B* **1998**, *102*, 2117.

[11] Hermansson K; *J. Chem. Phys.* **1993**, *99*, 861.

[12] Bawendi M.G.; Carroll P.J.; Wilson W.L.; Brus L.E. *J. Chem. Phys.* **1992**, *96*, 946.

[13] Pankove J.I. *Optical Processes in Semiconductors*; Dover: New York, 1975.

[14] Durinck G., et al. *Sol. State Commun.* **1991**, *80*, 579.

[15] Wang R., et al. *Adv. Mater.* **1998** *10*, 135.

[16] Sumi H.; Sumi A. *Sol. St. Comm.* **1991**, *78*, 883.

---

[17] For example: 1) Weng Y.X.; Wang Y.Q.; Asbury J.B.; Ghosh H.N.; Lian T. *J. Phys. Chem. B* **2000**, *104*, 93-104. 2) Boschloo G.; Fitzmaurice D. *J. Phys. Chem. B* **1999**, *103*, 2228. 3) Boschloo G.; Goosens A. *J. Phys. Chem. B* **1996**, *100*, 19489.

[18] Lowekamp J.B.; Rohrer G.S.; Hotsenpiller P.A.M.; Bolt J.D.; Farneth W.E. *J. Phys. Chem. B* **1998**, *102*, 7323.

[19] For example: Herrmann J.M.; Tahiri H.; Guillard C.; Pichat P. *Catalysis Today* **1999**, *54*, 131.

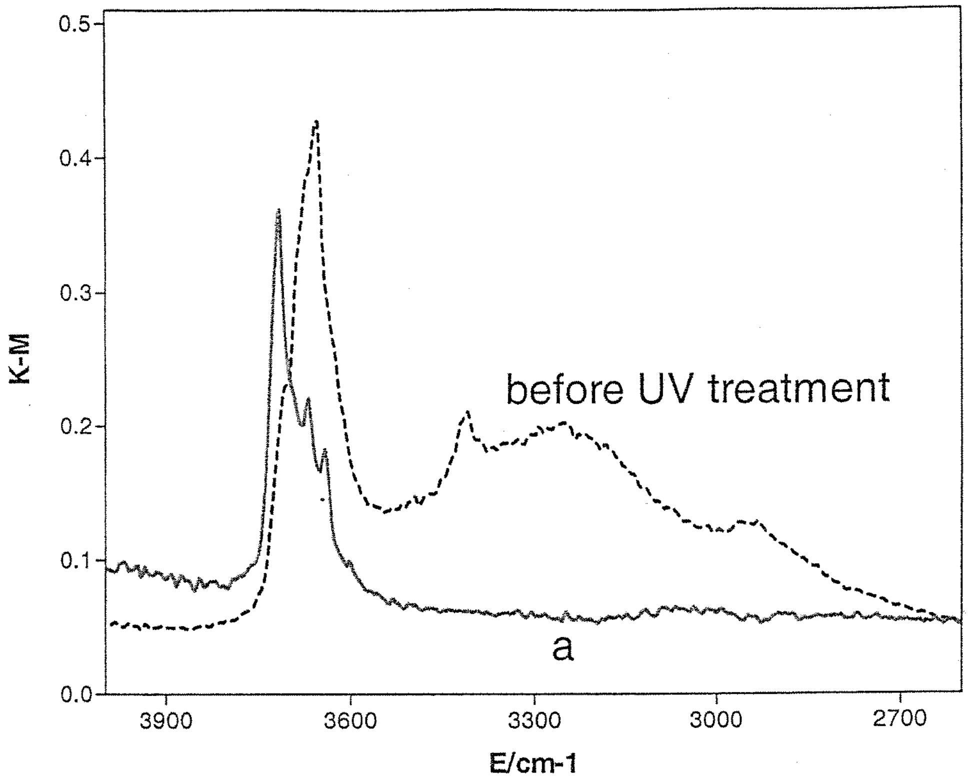

Figure 1: DRIFT spectra of dry TiO_2 that highlight the effects of charge trapping on the stretching vibrations of surface TiO-H bands. Spectrum (a) was acquired following immediate exposure of UV irradiated TiO_2 to O_2 in the dark at 298 K.

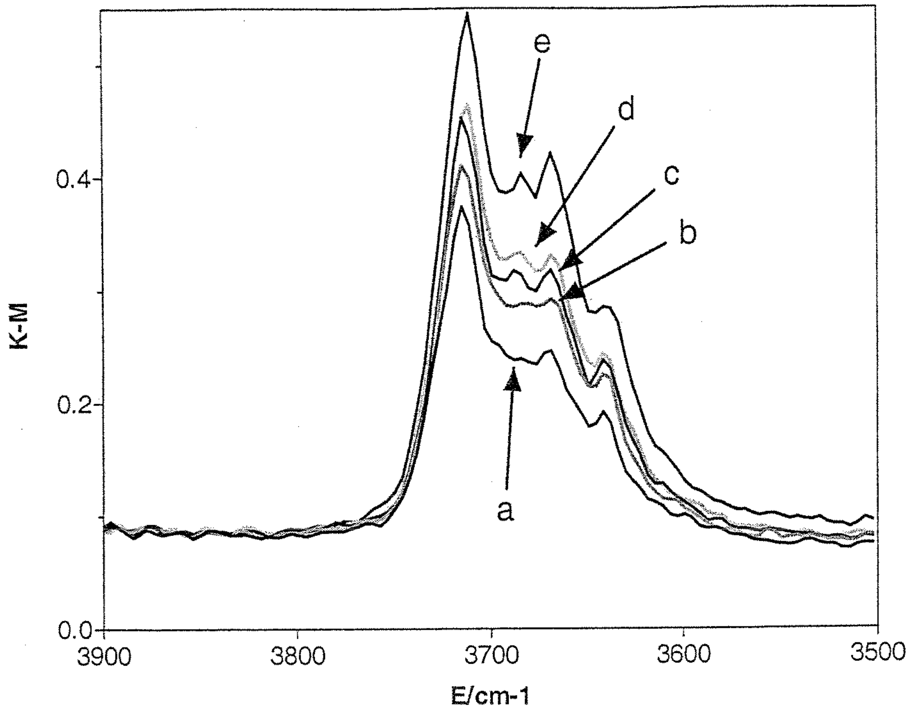

Figure 2: Selected spectra from series acquired during evacuation of HTEC chamber in the dark after irradiation under vacuum followed by addition of O_2. The changes are due to decrease in O_2 pressure from approximately 760 to 10^{-6} Torr. (a) O_2 at ~ 760 Torr (Figure 1a). (b-d) spectra changing upon removal of O_2. (e) O_2 at ~10^{-6} Torr.

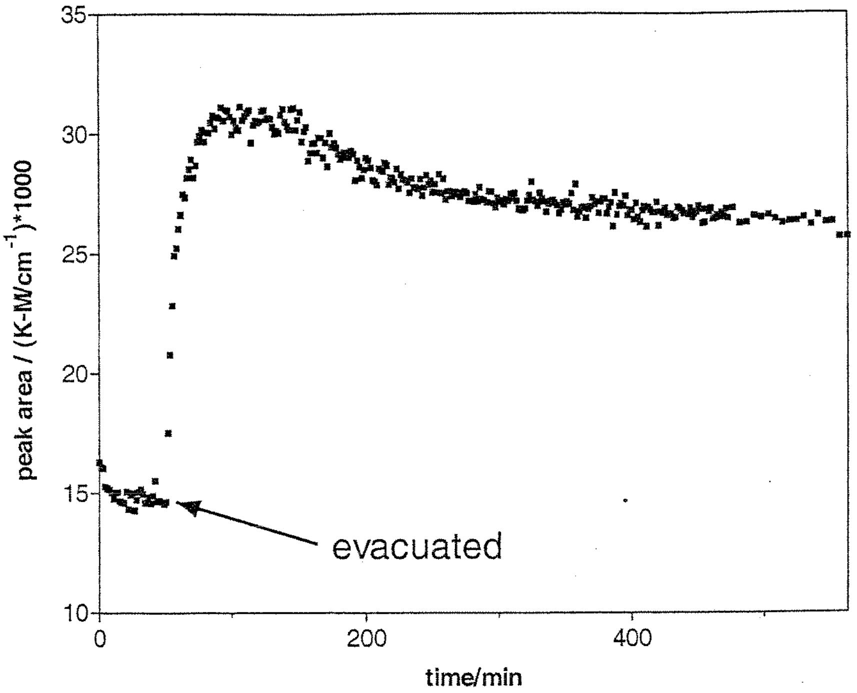

Figure 3: The sum of ν(TiO-H) peak area for all bands as a function of time. Time 0 corresponds to spectrum (a) from Figure 2. The maximum area following O_2 evacuation corresponds to spectrum (e) from Figure 2.

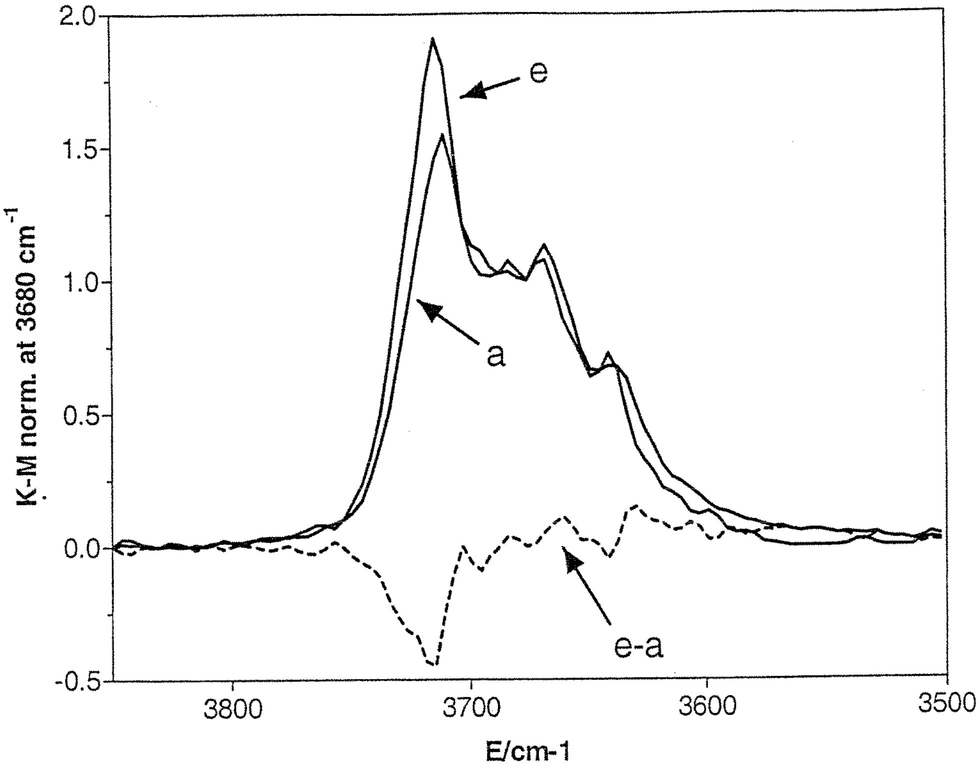

Figure 4: Spectra (a) and (e) from Figure 2 normalized to Y=1 at 3680 cm^{-1} and difference spectrum (e-a). Note that the peak at 3716 cm^{-1} is prominent when all others are subtracted out.

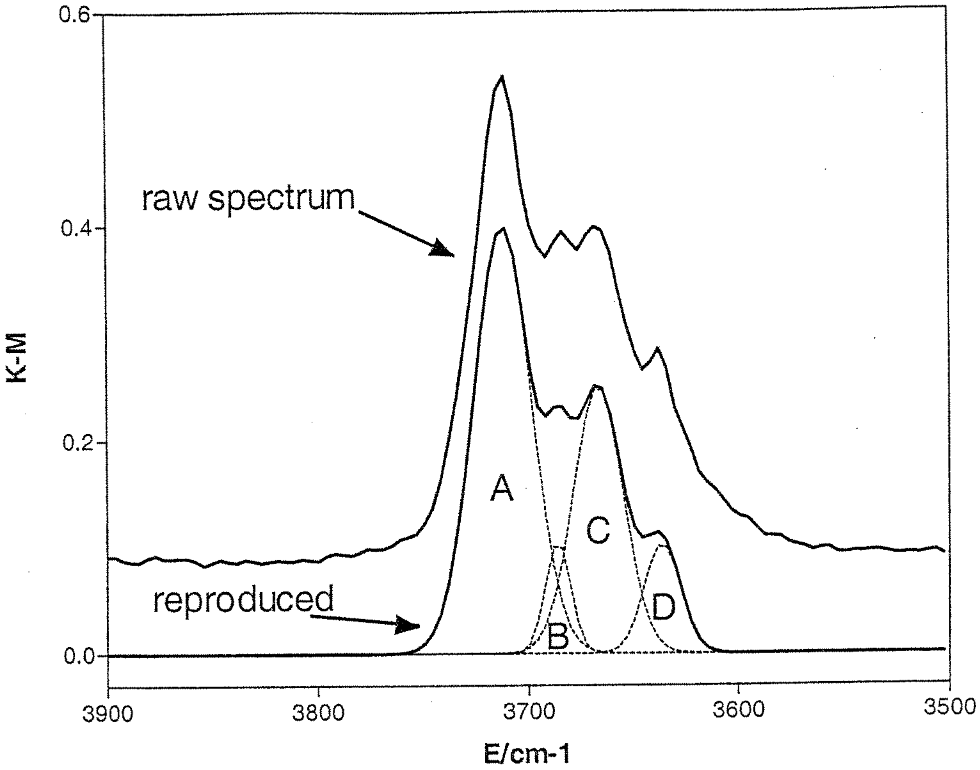

Figure 5: A typical spectrum of TiO-H stretching bands along with Gaussian fits for bands A-D and the resulting spectrum (sum of Gaussian fits) without baseline correction.

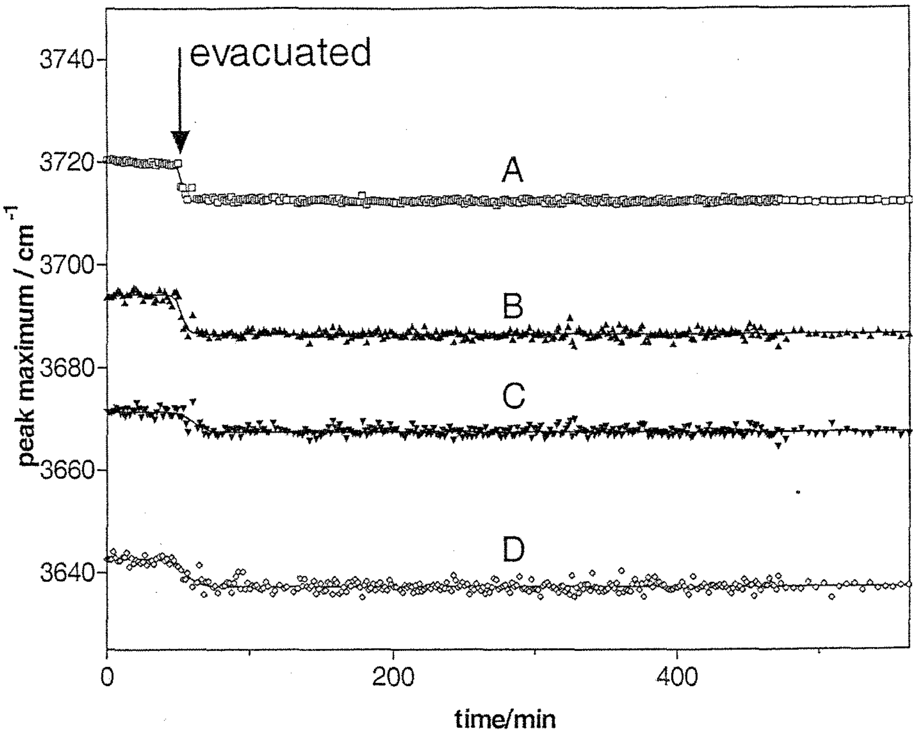

Figure 6: Plot of peak maximum (cm^{-1}) versus time for the Gaussian fits to the spectral series in Figure 2. The sigmoidal fits are included to illustrate the wavelength shift of each fitted band upon the evacuation of O_2.

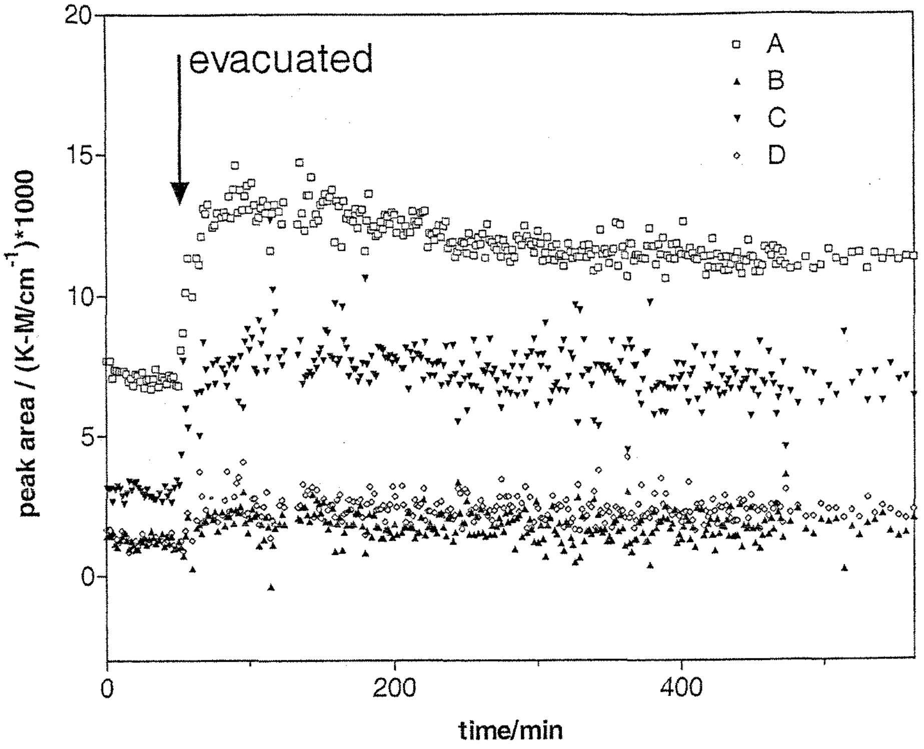

Figure 7: Plot of peak area versus time for the fitted spectra in the series from Figure 2. Note that the areas of peaks B and D are small compared to the scatter in the data.

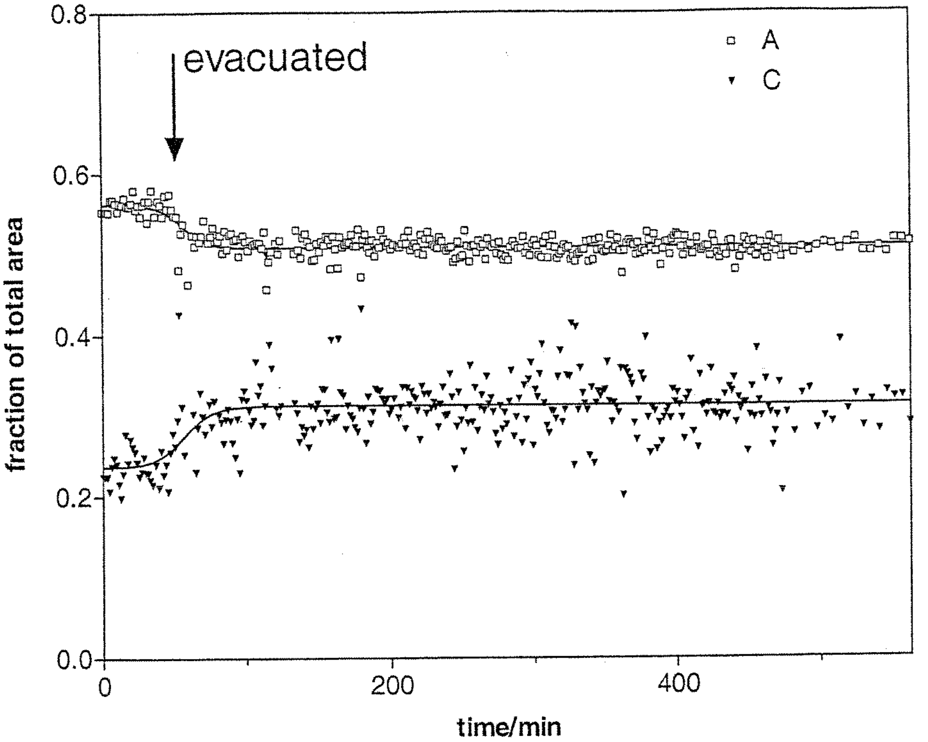

Figure 8: Plot of fraction of the total ν(TiO-H) peak area versus time for peaks A and C from the fit spectra in the series from Figure 2. The small contributions from peaks B and D are not shown. The sigmoidal fits are included to illustrate the relative influence of each fitted band on the total area upon the evacuation of O_2.

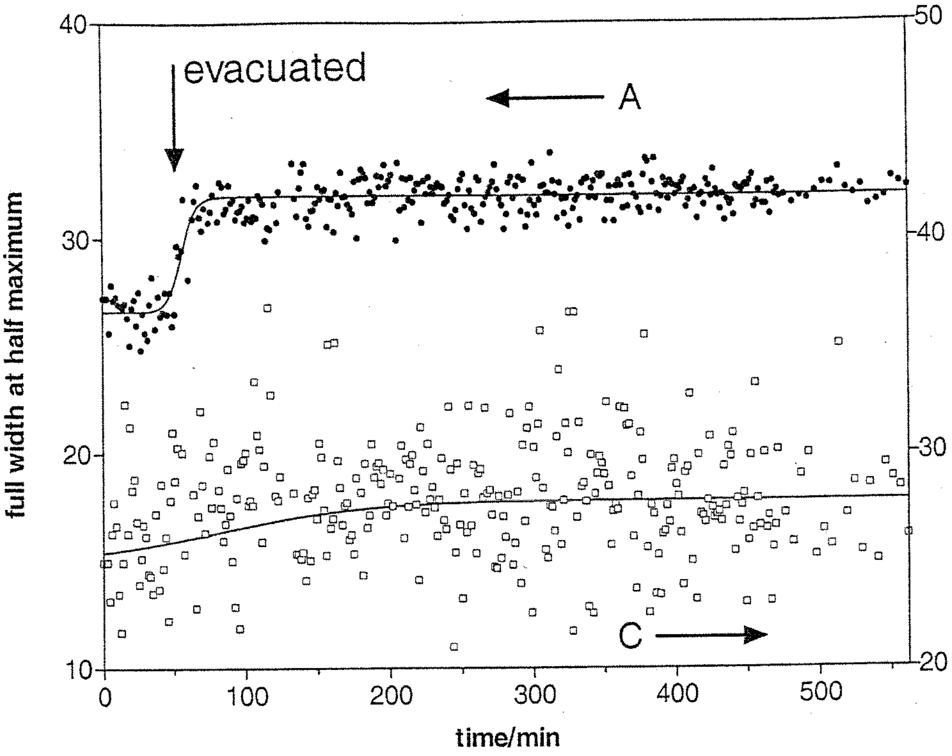

Figure 9: Plot of FWHM versus time for the fit spectra in the series from Figure 2 along with the sigmoidal fits. Note that peak A shows a clear dependence on the evacuation event, but peak C does not.

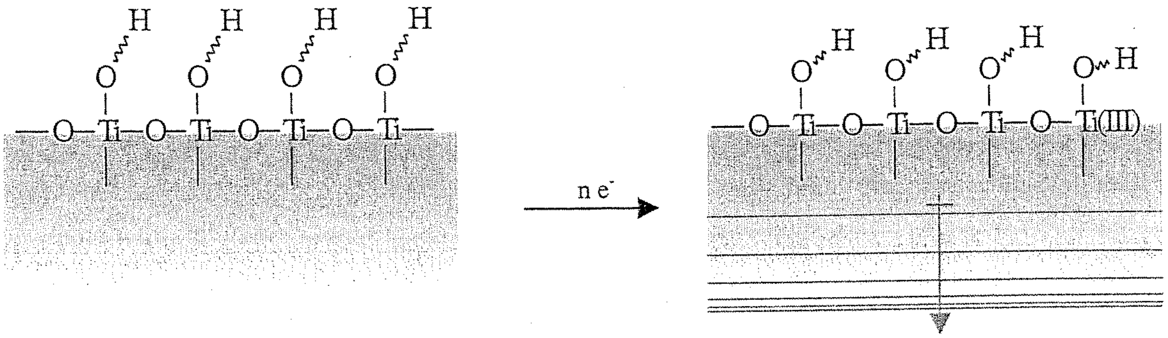

Figure 10: Diagram illustrating the relative influence of localized and diffuse electric fields on the bond lengths and angles of surface TiO-H bonds.

Chapter 5

Adsorption and Photodegradation of DMMP Vapor at TiO_2 Surfaces

Abstract

The adsorption and degradation of the nerve agent simulants dimethylmethylphosphonate (DMMP) and diethylmethylphosphonate (DEMP) vapor over UV-irradiated TiO_2 powders and thin films is investigated in the vapor phase. The adsorption of these compounds on TiO_2 powder is characterized and quantified by diffuse reflectance infrared Fourier transform spectroscopy (DRIFTS). Photochemically assisted oxidation of adsorbed DMMP is carried out *in situ* by irradiation of samples in the DRIFTS accessory, giving kinetic data and information on specific site binding of DMMP and catalyst poisoning. Gas phase intermediates from a static vapor phase reaction are identified by GC-MS analysis, and surface-bound intermediates and products are analyzed by HPLC-MS and ion-chromatography of both aqueous and organic extractions from the TiO_2. A proposed mechanism suggests rapid degradation of DMMP, but with extensive poisoning of the catalyst by surface-bound phosphonate products.

Introduction

As a class of compounds used in such diverse applications as pesticides, chemical warfare agents, plasticizers, lubricants, and flame-retardants, organophosphorous compounds pose a significant environmental threat.[1] Heterogeneous reactions, catalytic and stoichiometric, have been investigated as a means of removing these pollutants from aqueous and atmospheric environments, as well as for the destruction organophosphorous waste, especially stockpiled chemical warfare agents. Of particular importance is the removal of these contaminants from breathing air on a range of scales from personal protection (gas-masks) to large indoor air purification systems for storage areas.

Current technology for capture and destruction of chemical nerve agent vapors involves trapping the contaminant in a carbon bed followed by a separate chemical decontamination step involving hydrolysis or chemical oxidation. Heterogeneous strategies employ reactive surfaces, such as metal oxides, to capture and degrade the contaminants to benign gas-phase and surface-bound products. The applicability of this method is largely determined by the surface chemistry of the organophosphorous compound and the properties of the reactive surface.

Of particular interest has been the adsorption and decomposition of organophosphonate compounds on metal or metal oxide surfaces. The specific adsorption of dimethylmethylphosphonate (DMMP), a simulant for nerve agents such as Sarin or VX has been investigated on supported metal catalysts (Pt/Al_2O_3),[2-4] single crystal metals (Rh(100),[5] Ni(111),[6] Pd(111),[6] and Mo(110)[1,7]), and oxides[8] (Al_2O_3,[9,10] SiO_2,[11] a-Fe_2O_3,[11,12] MgO,[13,16] AMO,[17] and others). These surfaces degrade DMMP either catalytically or stoichiometrically by dealkylation, hydrolysis, or oxidation to give desorbable small-molecule products and surface-bound phosphates. The high surface area of the oxide materials provides a large adsorption capacity, allowing subsequent thermal destruction of the captured contaminants. The mode of DMMP binding to the surface and the mechanism of reaction have been investigated in these systems by FTIR, HREELS, SIMS, TPD, Auger electron spectroscopy, and other techniques.

An alternative strategy is to employ the high surface area of a metal oxide for contaminant adsorption, but with photocatalytic degradation of the substrate. Titanium dioxide has been shown to be an effective photocatalyst for the degradation of a large number of organic and inorganic compounds in both aqueous solution and the gas phase. For organophosphorous compounds, namely DMMP, a number of studies have examined aqueous phase heterogeneous photocatalytic degradation. Only a few studies have examined the reaction of gas-phase DMMP with TiO_2 or the DMMP-TiO_2 surface interaction. Obee and Satyapal investigated intrinsic rates, products, and catalyst poisioning for DMMP photodegradation in a single-pass reactor.[18] An additional report detailed the IR spectra of DMMP adsorbed on TiO_2, but found no evidence for photodegradation.[19] Recently, a mechanistic investigation of the adsorption and photo-oxidation of DMMP on titania by FTIR spectroscopy at non-standard conditions was reported.[20] Here we investigate the adsorption and photocatalytic degradation of DMMP vapor on Degussa P-25 TiO_2 powders by diffuse reflectance Fourier transform infrared spectroscopy (DRIFTS) with an aim for establishing the background surface chemistry necessary for developing photocatalytic filter devices for the removal of chemical warfare agents from breathing air.

Experimental

Materials

Polycrystalline TiO_2 (Degussa P-25) and fumed silica (SiO_2) (Aldrich, 14 nm particle size) was purified by sonication in deionized water and recovered by ultracentrifugation before being dried under vacuum. Dimethylmethylphosphonate (DMMP) and methylphosphonic acid (MPA) were obtained from Aldrich and used as received. All chemicals were reagent grade or better and used as received. O_2 was dried by passing through a P_2O_5 column. N_2 and He were purified by passing through $CaCl_2$, P_2O_5, and an Oxy-Trap column.

Instrumental Methods

Gas chromatography-mass spectrometry (GC-MS) was carried out using a HP 5890 GC with a HP 5989A mass-selective detector using either a 30 M length x 0.25 mm diameter x 0.25 um thickness HP-FFAP column (for DMMP and other organophosphonates) or a 25 M length x 0.25 mm diameter x 1 μm thickness HP-1 column (CH3OH, HCOOH, HCHO, and CO2). Liquid chromatography-mass spectrometry (LC-MS) was performed by gradient elution in methanol/water with a HP 1100 LC/MSD fitted with a normal-phase CN column. Mass spectra were acquired in both positive and negative APCI and electrospray modes. Analysis for anions by ion chromatography (IC) was performed using a Dionex Bio-LC with conductivity detection and 1 mM - 100 mM OH^- gradient elution on an AS-11 column (Dionex). Infrared spectra in CCl_4 solution were acquired using a Bio-Rad FTS-45 FTIR spectrometer in transmission mode at 4 cm^{-1} resolution with a DTGS detector using a 0.1 mm pathlength demountable liquid cell with NaCl windows.

DRIFTS

DRIFT spectra were acquired on the same FTS-45 instrument with a liquid N_2-cooled MCT detector at 8 cm^{-1} resolution using a Spectra-Tech Collector diffuse-reflectance accessory mounted in an external sample compartment which was continuously purged with dry, CO_2-free air. Solid samples were held in the diffuse reflectance accessory in the sample cup of a Spectra-Tech high temperature environmental chamber (HTEC). The sample could be resistively heated to 1000 K (± 1 K) and the chamber evacuated to 1 μTorr. Gases and vapors were introduced through a separate port via a manifold (Figure 1). N_2, O_2, and He were admitted to the manifold through separate valves after passing through a drying column as described above. DMMP and CD_3OD vapors were admitted in reproducible amounts by first closing off the evacuated manifold and opening it to a Schlenk tube of either DMMP or CD_3OD. The Schlenk was then closed, and the manifold opened to the evacuated HTEC.

Prior to adsorption and photolysis experiments, TiO_2 or SiO_2 samples were dried in the sample cup under vacuum (~1 μTorr) at 25 °C or 325 °C until the broad, overlapping hydrogen-bonded TiO-H stretching vibrations from 2500-3800 cm^{-1} were largely removed to reveal discrete stretches in the 3400-3800 cm^{-1} region.

Irradiation of samples was carried out within the HTEC chamber and without breaking the external sample compartment purge by irradiating with a 1 kW Xe lamp (Oriel) focused directly into the HTEC chamber through a quartz lens mounted in the top of the sample compartment. Following irradiation, the sample temperature was allowed to cool to 27 °C before a spectrum was acquired.

Product Analysis – Gas Phase

The identification of gas-phase products was carried out by GC-MS analysis of the headspace gases in a static batch reactor. A powder of P-25 TiO_2 or a film of P-25 on a glass microscope slide was introduced to a 50 mL volume quartz tube reactor. Nitrogen gas bubbled through DMMP at 50 °C was flowed through the reactor for 30 minutes. After stopping the N_2 flow, the TiO_2 was exposed to UV irradiation from a 450 W Oriel Xe lamp which was passed through a H_2O IR filter and a 300-400 nm bandpass filter (Oriel UG-1). Throughout the irradiation, 50 μL samples of the headspace gas were analyzed by GC-MS.

Product Analysis – Surface

Surface-bound products from the bulk photolysis and the DRIFTS experiments were removed from the TiO_2 by washing with CH_2Cl_2, then deionized H_2O. The CH_2Cl_2 fractions were analyzed by GC-MS as described above. The CH_2Cl_2 was then extracted with H_2O, and both this H_2O fraction and the H_2O wash fraction were analyzed by LC-MS and IC.

Results

DMMP on KBr and SiO₂

Infrared absorption band frequencies for DMMP in hexane and CCl_4 solution (transmission mode) and DMMP vapor adsorbed on KBr and SiO_2 powder (diffuse-reflectance mode) are presented in Table 1 along with band assignments. For adsorption on KBr, the IR spectrum closely matches that of DMMP in solution. On SiO_2, the IR spectrum of DMMP closely matches that of DMMP in solution, but the OH stretch band at 3728 cm^{-1} for SiO_2 disappears upon DMMP adsorption. The band assignments were obtained from normal mode analysis of DMMP and taken from the literature.[21,22]

DMMP on TiO₂

Prior to DMMP adsorption experiments, samples of TiO_2 were dried in the DRIFT accessory under vacuum and with heating. Heating the sample as high as 325 °C expedited the dehydration process but did not change the IR spectra of the dehydrated TiO_2 or the subsequently absorbed DMMP compared to vacuum dehydration at room temperature. IR spectra acquired during dehydration of P-25 TiO_2 under vacuum at room temperature are shown in Figure 1.

Upon addition of DMMP vapor to the sample chamber, bands corresponding to the IR absorptions of DMMP appear in DRIFT spectra of the TiO_2 (Figure 2,3). The most prominent bands are the methyl stretches which appear in the 2800-3000 cm^{-1}

region and the CH_3-P methyl deformation at 1310 cm^{-1}. The bands assigned to the symmetric and asymmetric C-H stretch for the methoxy group are each split into two bands, with one at the same energy as the solution DMMP spectrum and one at 23 cm^{-1} lower energy. The strong P=O stretch at 1250 cm^{-1} for DMMP in solution or adsorbed on KBr is shifted ~40 cm^{-1} to lower energy upon adsorption of DMMP onto TiO_2, and is distorted in the spectra by its proximity to the intense Ti-O lattice vibrations. The TiO_2 O-H stretches in the 3550-3750 cm^{-1} region disappear completely upon DMMP adsorption.

Photodegradation

Upon irradiation under an O_2 atmosphere of DMMP-loaded TiO_2 samples in the DRIFT chamber, a reduction of the IR peak intensity for the bands assigned to DMMP methyl stretches and the PC-H deformation is seen along with the concomitant appearance in the IR spectrum of a doublet for CO_2 at 2361 and 2337 cm^{-1}. Additionally, the ν(TiO-H) bands between 3600 and 3716 cm^{-1} reappear in the spectra of DMMP loaded TiO_2 following evacuation to remove the adsorbed H_2O photolysis product.

Products and Kinetics by FTIR

Plots of A_i/A_o versus irradiation time fit to a first order decay for DMMP $\nu(CH_3)$ and $\delta(PCH_3)$ are shown in Figure 6. The rate for the loss of P-bound methyl groups is smaller than the rate for the loss of methoxy groups. The signal for CO_2 in the gas-phase of the DRIFTS chamber increases with irradiation time. No evidence for other products is observed in the IR spectra of irradiated DMMP on TiO_2.

Rates of successive loading and Inhibition of DMMP degradation by PO_4^{3-} products

The capacity of the P-25 surface for DMMP adsorption decreases with sequential adsorption/degradation cycles, Figure 8, as PO_4^{3-} and phosphonate intermediates block adsorption sites. This leads to an inhibition of UV degradation by the products of previous degradation reactions, Figure 9.

Product Analysis – Gas Phase

Gas-phase product formation during photolysis of DMMP adsorbed on TiO_2 in a static reactor was followed by GC-MS analysis throughout the course of the reaction. The gas phase products were identical for reactions with excess DMMP directly applied to the TiO_2 surface and for DMMP adsorbed on TiO_2 from the vapor phase. Figure 10 is a plot of gas-phase product evolution. The major gas-phase constituents were DMMP,

CO_2, and H_2O with trace amounts of methanol and formic acid detected. No phosphorous containing products or intermediates (other than DMMP) were detected in the gas phase.

Product Analysis – Surface

The phosphorous-containing products of DMMP photodegradation remained adsorbed to the TiO_2 surface throughout the reaction. They were identified as methyl methylphosphonate (MMP), methylphosphonic acid (MPA), and phosphate by IC and LC-MS analysis of organic and aqueous extractions of the TiO_2 and comparison to authentic samples of these compounds. An additional intermediate, methylmethylphosphonic acid (MMPA), was identified by LC-MS, but was not compared to an authentic sample. Kinetic simulation (see discussion), however, supports the assignment of this intermediate. For photocatalytic DMMP degradation in the static reactor, samples of the TiO_2 were removed at selected intervals and the surface-bound products and intermediates analyzed as above. A plot of the relative distribution of products throughout the reaction is given in Figure 11.

Discussion

The DRIFTS technique is a convenient and versatile method for examining the surface chemistry of organophosphonate compounds adsorbed on TiO_2 and other metal oxide surfaces. Changes in the spectra of both the organophosphonate (adsorbent) and oxide (adsorbate) can be monitored with DRIFTS, allowing a more complete understanding of the photochemical processes involved than is provided by traditional chromatographic analysis of reaction intermediates and products, or adsorbent-sensitive techniques such as thermogravametric analysis or differential scanning calorimetry.

Adsorption and DRIFTS

As has been observed for other metal oxides, DMMP adsorbs strongly on P-25 TiO_2 from the vapor-phase. The adsorption process can be monitored by DRIFTS, examining the change in the spectra of both DMMP and the TiO_2 hydroxyl stretches. DMMP adsorbs specifically to surface hydroxyl groups on the TiO_2 surface as shown by the disappearance of the TiO-H stretch upon addition of DMMP to a clean TiO_2 surface. The adsorption of DMMP follows first-order association kinetics, where A is the DRIFTS peak area ($A \propto$ concentration), A_{max} the maximum peak area, k the first-order association rate constant, and t the time exposed to DMMP at a fixed concentration in the DRIFTS chamber. For the integrated C-H stretching peaks from 2800-3010 cm^{-1}, $k = 0.11\ min^{-1}$ and for the 1310 cm^{-1} peak, $k = 0.12\ min^{-1}$.

$$A = A_{max}(1 - e^{-kt}) \qquad (1)$$

Photodegradation

DRIFT spectra acquired during the photodegradation of DMMP adsorbed on TiO_2 show the sequential loss of methoxy groups, to form MMPA and MPA, then the loss of the P-bound methyl group to leave a surface-bound PO_4^{3-} species. The final gas-phase product CO_2 is observed in the DRIFT spectra, with no DRIFTS evidence for CH_3OH or HCOOH intermediates. The loss of DMMP was monitored by the decrease in the combined peak areas for the ν_{OC-H} asymmetric (2957 and 2929 cm^{-1}) and symmetric (2855 and 2827 cm^{-1}) stretching bands. The peak area data was normalized by dividing by the maximum peak area observed during the photodegradation experiment. The decrease in ν_{OC-H} area is exponential (Figure 6) with an observed rate constant $k_{obs} = 0.25$ min^{-1}. The peak area for the δ_{PC-H} bend at 1310 cm^{-1} is proportional to the surface concentration of DMMP, MMPA, and MPA and also decreases exponentially with $k_{obs} = 0.11$ min^{-1}. The peak-area CO_2 increases during the initial irradiation period. The IR bands for CO_2 at 2360 and 2333 cm^{-1} disappear immediately upon opening the HTEC to vacuum, indicating that the CO_2 is not adsorbed to the TiO_2 but is present in the gas-phase. No evidence of C=O containing products is observed in DRIFT spectra of the irradiated TiO_2.

Photodegradation results in the static batch reactor are in agreement with those from the DRIFTS experiments. In the batch reactor, gas phase products were monitored throughout the photolysis by removing aliquots of the headspace gas and analyzing them by GC-MS. The major gas-phase product, detected at early reaction times and increasing in concentration throughout the reaction, was CO_2. Methanol and formic acid were also detected as gas-phase intermediates. Methanol concentrations increased rapidly immediately after the start of irradiation, but the levels fell quickly and never reached more than a trace amount, even at peak concentrations. Formic acid concentrations increased more slowly, but also never reached more than a trace level. The production of toxic gas-phase products is a concern in systems for potential use in air purification. In this case, small amounts of harmful gas-phase methanol and formic acid are produced, but this is for a low surface-area test material. Provisions would be made for re-capture and continued degradation of these intermediates in a filter/photodegradation device of an actual air purification application. The low intermediate concentrations and rapid conversion of intermediates to CO_2 should allow this to be readily accomplished.

The surface-bound product distribution in the static batch reactor also parallels that of the DRIFTS experiments. An initial rapid decrease in $[DMMP]_s$ leads to an increase in intermediate $[MMPA]_s$ and $[MPA]_s$ followed by a slower increase in $[PO_4^{3-}]_s$. The formation of the complete mineralization product PO_4^{3-} is slow, and a high surface concentration of bound MMP remains even after long irradiation times. This is not a problem from a toxicological standpoint, however, as oxidation of DMMP to MMPA in the model system corresponds to the decontamination step for organophosphorous nerve agents and pesticides. For DMMP, breaking the P-O bond in this first step is thermodynamically more difficult than breaking the P-F bond of GB or GD. Further degradation of MMPA to PO_4^{3-} may occur more slowly and not impact the effectiveness of photodegradation as a viable chemical nerve agent destruction technique.

Data obtained from DRIFTS and product analysis lends valuable insight into the mechanism of DMMP photodegradation. The photochemical destruction of DMMP adsorbed on TiO_2 may be described by the mechanism shown in equations (2-6), a stepwise loss of CH_3OH from the phosphate core followed by a multi-step oxidation of CH_3OH to CO_2.

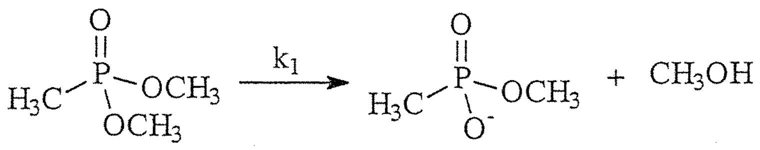

(2)

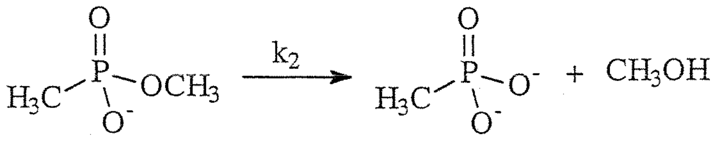

(3)

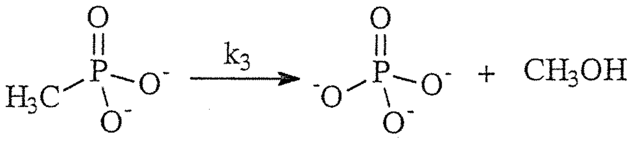

(4)

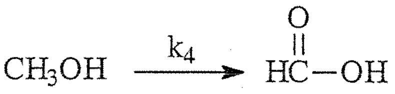

$$\mathrm{CH_3OH} \xrightarrow{k_4} \mathrm{H\overset{\overset{O}{\|}}{C}-OH}$$

(5)

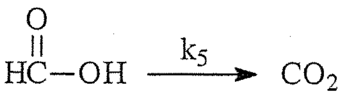

$$\mathrm{H\overset{\overset{O}{\|}}{C}-OH} \xrightarrow{k_5} \mathrm{CO_2}$$

(6)

A simulated degradation following this mechanism is shown by the solid lines in Figure 12. The data points in Figure 12 are obtained from the $\nu_{OC\text{-}H}$ (circles) and $\delta_{PC\text{-}H}$ data described above. The $\nu_{OC\text{-}H}$ and $\delta_{PC\text{-}H}$ peak areas do not correspond directly to the concentrations of single species, but rather to the sum of the contributions from each species containing that particular vibrational mode. For [DMMP] the $\nu_{OC\text{-}H}$ data was used as obtained from the DRIFT spectra. An estimate of the time-progression of [MPA] was made by subtraction of the normalized peak area for $\nu_{OC\text{-}H}$ from $\delta_{PC\text{-}H}$ (triangles). This is valid for the mechanism if $k_2<k_3$ so that MMPA will be a minor contributor to the intensity of $\delta_{PC\text{-}H}$ relative to MPA.

Similarly, reactions carried out in a static batch reactor for product analysis studies also support the mechanism shown above. Figure 13 shows the simulated normalized concentration (C/C_{max}) versus time curves for DMMP and MMPA (solid lines) plotted along with data points for these two species. The presence of MMPA was not identified conclusively as an intermediate, as no known standard was available. LC-MS analysis of CH_2Cl_2 extractions of TiO_2 from early reaction times indicated the presence of an ion of mass 109 (negative ion ES mode) or 111 (positive ion ES). Additionally, the IC peak at earliest times, indicating an ion of -1 charge, fits the simulated kinetic profile of MMPA. In the batch reactor, inhomogeneous DMMP distribution and the uncertainty of the efficiency of extraction of phosphate from TiO_2 may lead to the deviation of PO_4^{3-} formation from the mechanism above. These experiments were designed to identify possible reaction products, and the conditions were not controlled for factors affecting kinetic analysis such as light distribution and quantitative product determination. The results as obtained, however, lend support to the mechanism suggested by the DRIFT experiments and the product identity.

Inhibition by Surface-Bound Products

The inhibition of DMMP degradation by the surface-bound phosphate oxidation products was investigated by a series of DMMP loading-photodegradation experiments. The MPA and PO_4^{3-} products from previous degradation reactions decrease the DMMP adsorption capacity of the TiO_2 on subsequent DMMP additions as shown in Figure 8. This is due to the PO_4^{3-} and MPA products remaining bound to surface adsorption sites, blocking further adsorption of DMMP vapor. Additionally, the observed rate of DMMP loss decreases with subsequent degradation reactions, Figure 9. Effects due to the decreasing initial surface concentration of DMMP for subsequent photolysis experiments were removed by dividing the observed rate constant from Figure 6 by the initial surface concentration ($\nu_{OC\text{-}H}$ or $\delta_{PC\text{-}H}$ peak area). Obee and Satyapal reported a similar inhibition, and catalytic activity of the TiO_2 could be restored by washing the surface with H_2O to remove the P-containing products.[18]

Implications for Real-world Devices

The above results have important implications for the use of TiO_2 in devices for photocatalytic degradation of gas-phase pollutants. First, the photocatalytic decomposition of DMMP has been examined on both bulk Degussa P-25 TiO_2 powder and on a thin film of P-25 on glass. In both cases the gas-phase and surface-bound products are the same. This indicates that the TiO_2 surface preparation may be optimized for maximum contaminant absorption and UV distribution without affecting the product distribution. Additionally, comparison of DRIFTS results obtained on highly dehydrated TiO_2 samples with bulk static reactor data for TiO_2 exposed to air at 50% RH indicate that the hydration state of the TiO_2 is a relatively unimportant factor in determining the product distribution for DMMP photodegradation. This observation is important in two respects: 1. the mechanistic data obtained by the DRIFTS technique should be directly applicable to scaled-up reactor prototypes, and 2. characteristics of a filter feed gas such as humidity and O_2 concentration may not contribute to the effectiveness of degradation for highly adsorbed (low-volatility) compounds such as DMMP. For any gas-phase filter/reactor design, of course, these characteristics will have to be determined specifically, but the above results indicate that for DMMP and other organophosphorous vapors, vapor capture ability is the critical parameter with photomineralization of the surface-bound contaminants occurring with minimal formation of toxic gas-phase intermediates. This is in contrast to photomineralization of halogenated organic compounds such as trichloroethane where toxic gas-phase intermediates (i.e., phosgene) are often observed.

Conclusions

DRIFT spectroscopy is an ideal technique for examining the interaction of gas or vapor-phase compounds with TiO_2 for several reasons. DRIFTS is relatively simple and inexpensive compared to other surface techniques such as XPS and HREELS. Bulk materials may be examined in their native state as powders or films without special preparation such as adsorption on sample grids. Finally, DRIFTS provides functional group information (e.g., alkyl vs. alkoxy) for elucidation of mechanistic details and inhibitory effect of intermediates and products on subsequent degradations, and these details are available for both the adsorbent and adsorbate. In the study reported here, vapor-phase DMMP is adsorbed onto TiO_2 powder, and both the adsorption and subsequent photocatalytic decomposition of the adsorbed DMMP may be followed by DRIFTS. Adsorbed DMMP can be photocatalytically degraded in a stepwise fashion to give MPA, PO_4^{3-}, H_2O and CO_2 as products. This is counter to a previous report.[19] Trace amounts of CH_3OH and HCOOH are detected in the gas-phase, but a properly designed gas-phase reactor should re-capture and completely mineralize these intermediates.

Acknowledgements

Funding by DARPA and Northrop-Grumman Corp.

References

---

[1] Eckerdt, J.G.; Klabunde, K.J.; Shapley, J.R.; White, J.M.; Yates, J.T., Jr. *J. Phys. Chem. B*, **1988**, 92, 6182.

[2] Tzou, T.Z.; Weller, S.W. *Catalytic oxidation of dimethyl methylphosphonate*, 1994; Vol. 146, pp 370.

[3] Baier, R.W.; Weller, S.W. *Ind. Eng. Chem. Process. Des. Dev.*, **1967**, *6*, 380.

[4] Graven, W.M.; Weller, S.W.; Peters, D.L. *Ind. Eng. Chem. Process. Des. Dev.*, **1966**, *5*, 183.

[5] Hedge, R.I.; Greenlief, C.M.; White, J.M. *J. Phys. Chem.*, **1985**, *89*, 2886.

[6] Guo, X.; Yoshinobu, J.; Yates, J.T., Jr. *J. Phys. Chem.*, **1990**, *94*, 6839.

[7] Smentkowski, V.S.; Hagans, P.; Yates, J.T., Jr. *J. Phys. Chem.*, **1988**, *92*, 6351.

[8] Mitchell, M.B.; Sheinker, V.N.; Mintz, E.A. *J. Phys. Chem.*, **1997**, *101*, 11192.

[9] Templeton, M.K.; Weinberg, W.H. *J. Am. Chem. Soc.*, **1985**, *107*, 774.

[10] Templeton, M.K.; Weinberg, W.H. *J. Am. Chem. Soc.*, **1985**, *107*, 97.

[11] Henderson, M.A.; Jin, T.; White, J.M. *J. Phys. Chem.*, **1986**, *90*, 4607.

[12] Barja, B.C.; Tjedor- Tjedor, M.I.; Anderson, M.A. *Langmuir*, **1999**, *15*, 2316.

---

[13] Wagner, G.W.; Bartram, P.W.; Koper, O.; Klabunde, K.J. *Reactions of VX, GD, and HD with Nanosize MgO*, 1999, Vol. 103, pp 3225.

[14] Li, Y.X.; Koper, O.; Atteya, M.; Klabunde, K.J. *Adsorption and decomposition of organophosphorous compounds on nanoscale metal oxide particles. In Situ GC-MS studies of pulsed microreactions over magnesium oxide*, 1992; Vol. 4, pp 232.

[15] Li, Y.X.; Klabunde, K.J. *Nano-scale metal oxide particles as chemical reagents. Destructive adsorption of a chemical agent simulant, dimethyl methylphosphonate, on heat-treated magnesium oxide*, 1991; Vol. 7, pp 1388.

[16] Li, Y.T.; Schlup, J.R.; Klabunde, K.J. *Fourier-Transform Infrared Photoacoustic Spectroscopy Study of the Adsorption of Organophosphorous Compounds on Heat-Treated Magnesium Oxide*, 1991; Vol. 7, pp 1394.

[17] Segal, S.R.; Suib, S.L. *Chem. Mater.*, **1999**, *11*, 1687.

[18] Obee, T.N.; Satyapal, S.J. *J. Photochem. Photobiol. A: Chem.*, **1998**, *118*, 45.

[19] Aurian-Blajeni, B.; Boucher, M.M. *Langmuir*, **1989**, *5*, 170.

[20] Rusu, C.N.; Yates, J.T., Jr. *J. Phys. Chem. B*, **2000**, *104*, 12299.

[21] Moravie, R.; Froment, F.; Corset, J. *Spectrochim. Acta*, **1989**, *45A*, 1015.

[22] Van Der Veken, B.; Herman, M. *Phosphorous Sulfur*, **1981**, *10*, 357.

Table 1 - DMMP IR Bands on Background Surfaces

	IR frequency (cm^{-1})			
vibrational mode[a]	solution		surface adsorbed	
	hexane[b]	CCl_4	KBr	SiO_2
$\nu_a(CH_3P)$	2992	3006	3003	3006
$\nu_a(CH_3O)$	2957	2961	2956	2961
$\nu_s(CH_3P)$	2926	2935	2925	2935
$\nu_s(CH_3O)$	2852	2857	2855	2857
$\delta_a(CH_3O)$	1467	1462	1487	
$\delta_s(CH_3O)$	1452	1448	1457	
$\delta_a(CH_3P)$	1421	1417	1423	
$\delta_s(CH_3P)$	1314	1309	1314	
$\nu(P{=}O)$	1246	1251	1252	
$\rho(CH_3O)$	1185	1186	1186	
$\nu(CO)$	1061	1066	1061	
$\nu(CO)$	1033	1039	1040	
$\rho(CH_3P)$	914	915	917	
$\nu(PO_2)$	820	895	821	
$\nu(PO_2)$	789		794	
$\nu(PC)$	711		712	

[a] Assignments from [Van Der Veken, 1981 #3; Moravie, 1989 #2]. [b] Values from [Mitchell, 1997 #1]. ν = stretch, δ = deformation, ρ = rock, $_s$ = symmetric, $_a$ = antisymmetric.

Table 2- DMMP and MPA IR Bands on P-25

	IR frequency (cm^{-1})	
vibrational mode[a]	DMMP	MPA
$\nu_a(CH_3P)$	3002	3002
$\nu_a(CH_3O)$	2957	
	2929	
$\nu_s(CH_3P)$	2898	2899
$\nu_s(CH_3O)$	2855	
	2827	
$\delta_a(CH_3O)$	1467	
$\delta_s(CH_3O)$	1452	
$\delta_a(CH_3P)$	1421	1419
$\delta_s(CH_3P)$	1309	1312

[a] Assignments from [Van Der Veken, 1981 #3; Moravie, 1989 #2]. ν = stretch, δ = deformation, $_s$ = symmetric, $_a$ = antisymmetric.

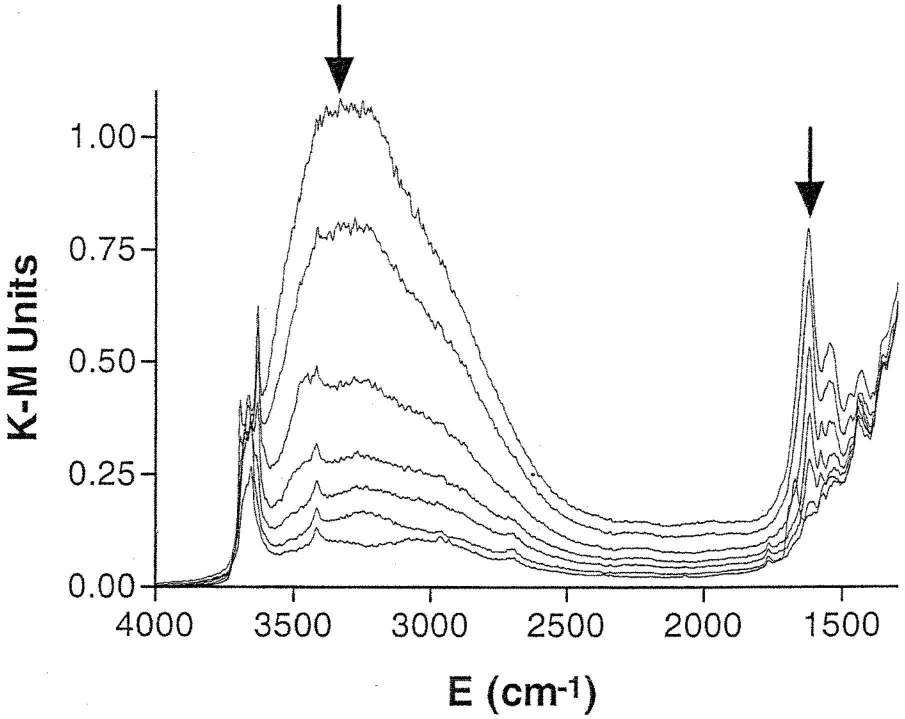

Figure 1: Vacuum dehydration of P-25 TiO_2 at RT.

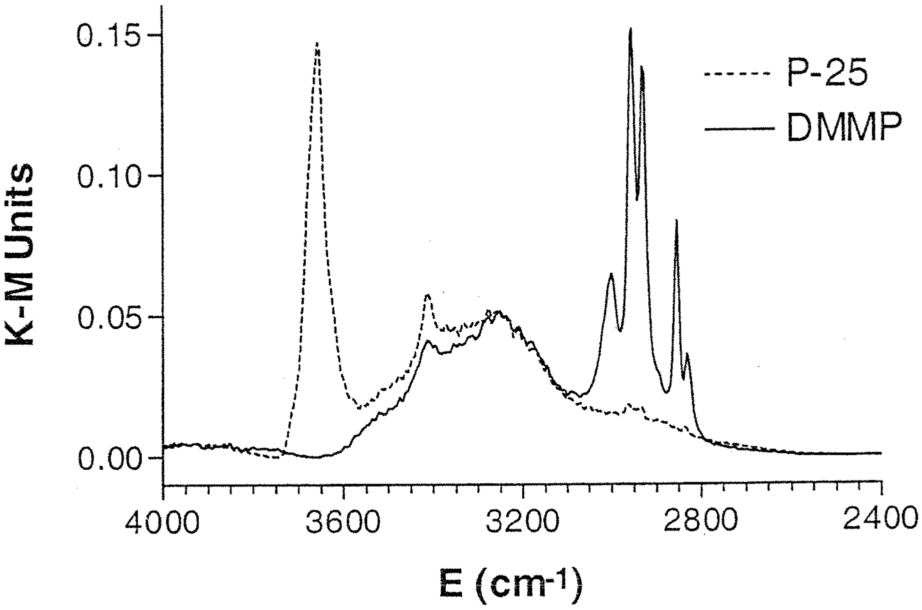

Figure 2: DMMP loading on P-25.

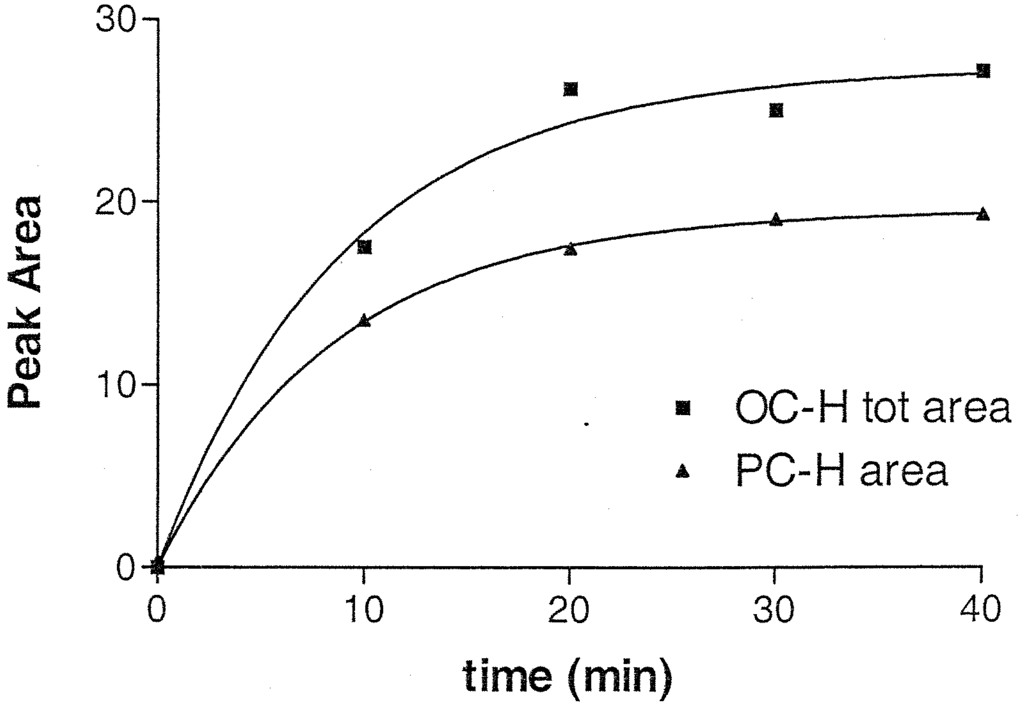

Figure 3: Loading rate of DMMP on P-25.

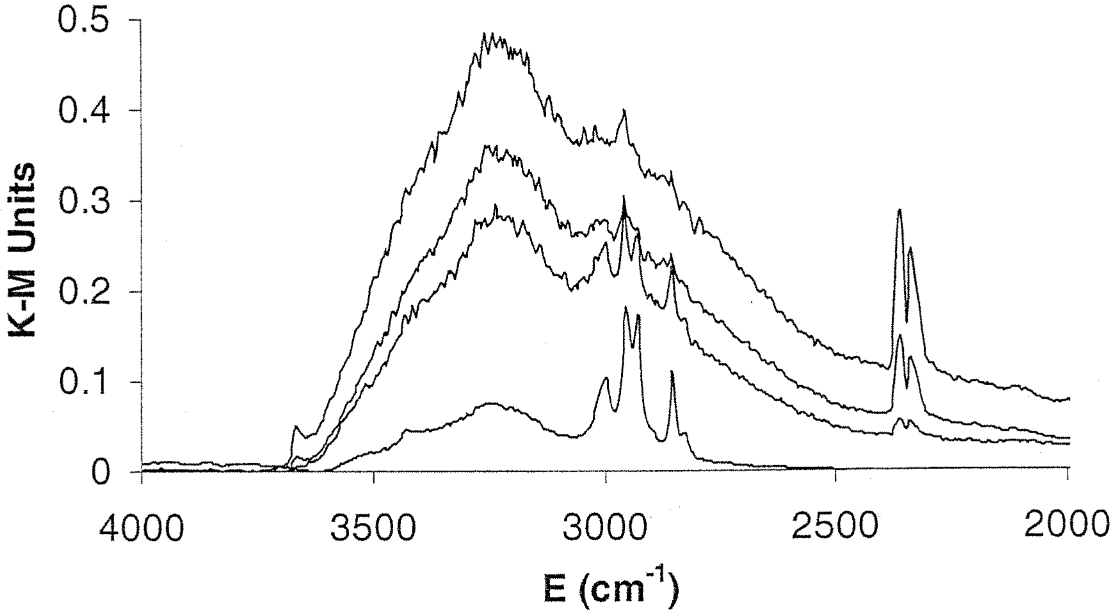

Figure 4: Photodegradation of DMMP on TiO_2 scanned under O_2.

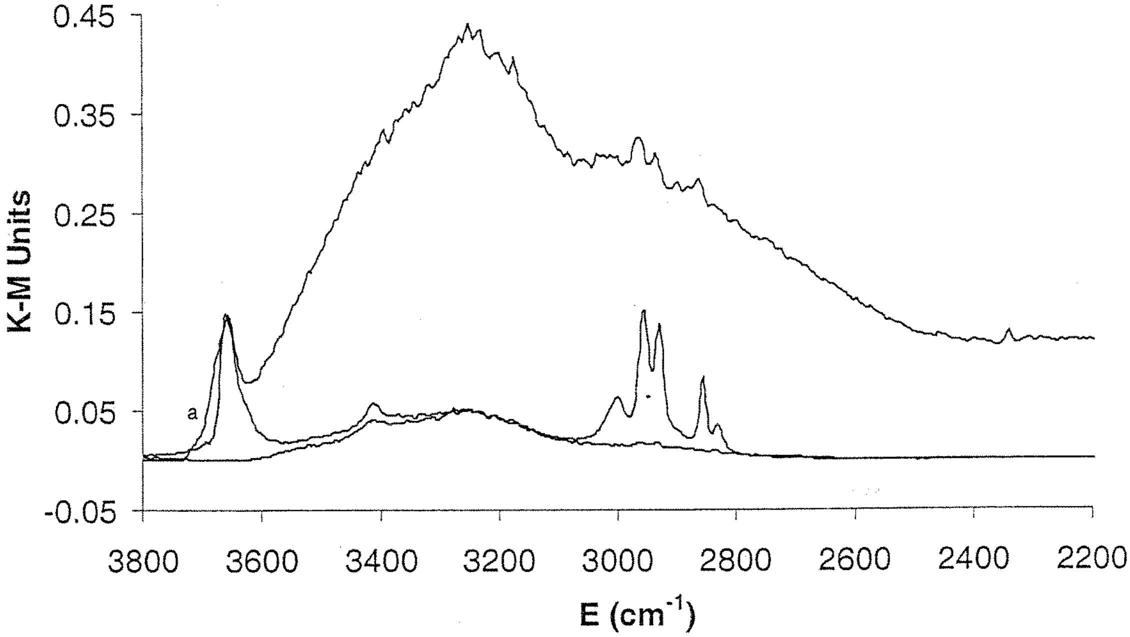

Figure 5: Photodegradation of DMMP on TiO_2 scanned under vacuum.

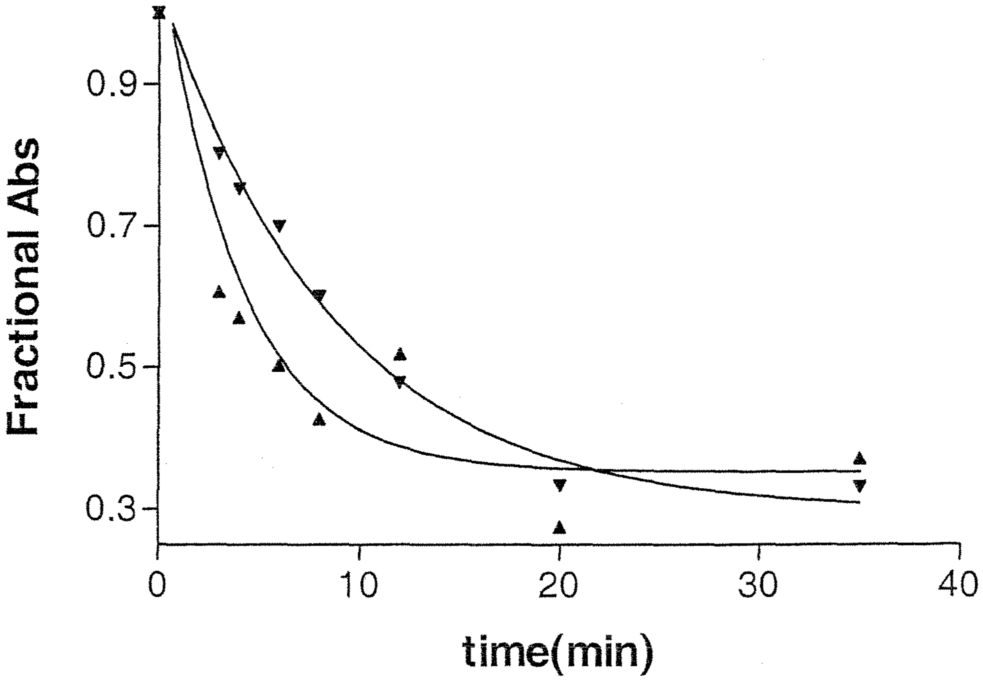

Figure 6: Plot of peak area versus time for a) nOC-H (sum of areas of doublets at 2943 and 2841 cm^{-1}) and b) dPC-H (area of 1310 cm^{-1} peak) during photodegradation shown in Figure 4.

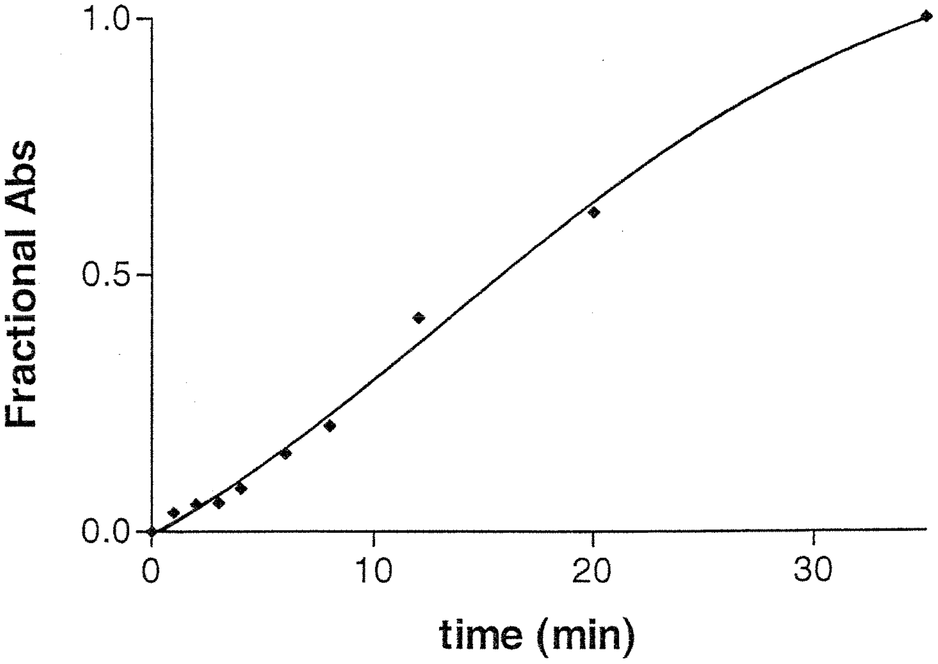

Figure 7: Plot of peak area versus time for CO_2 (doublet at 2347 cm^{-1}) during photodegradation shown in Figure 4.

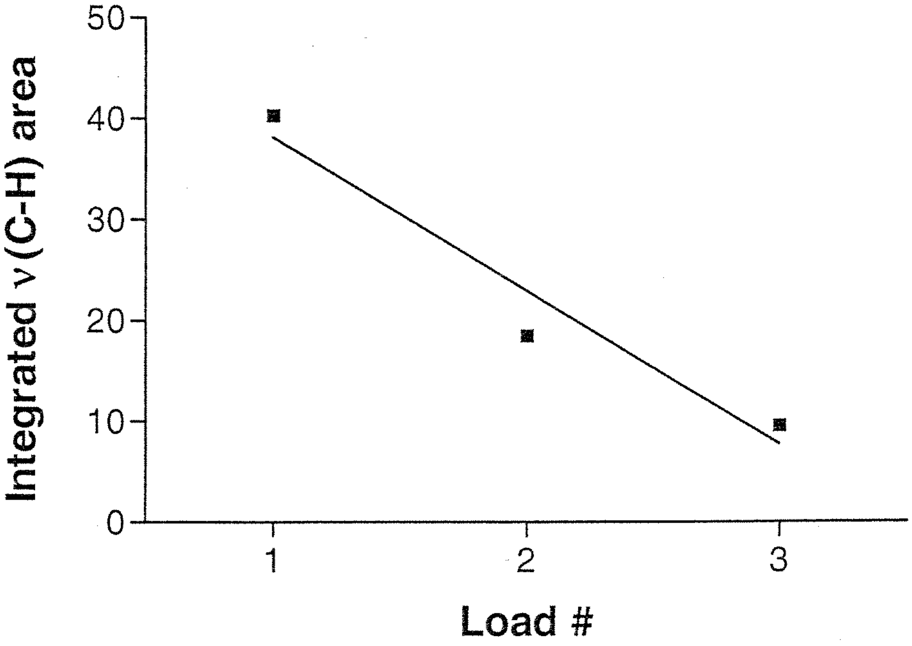

Figure 8: Plot of total integrated nC-H area versus load number for sequential DMMP loading/photodegradation cycles.

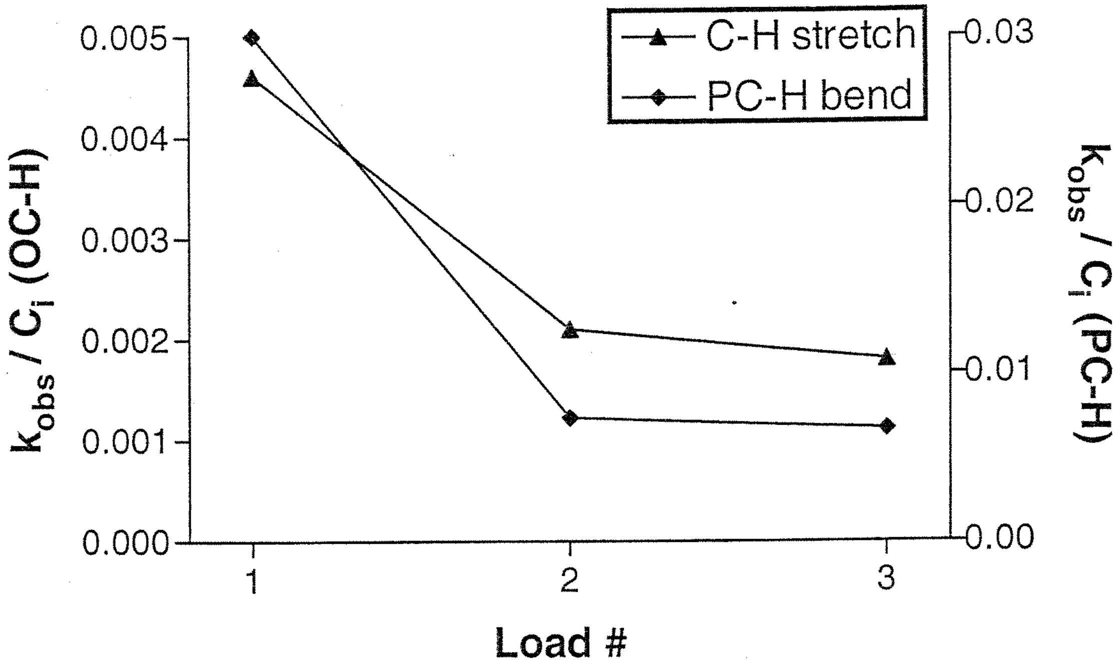

Figure 9: Plot of DMMP decomposition rate versus load number for sequential loading/degradation cycles. The decomposition rate is plotted as observed rate, k_{obs}, from Figure 4 divided by initial DMMP concentration (as integrated peak area from Figure 8).

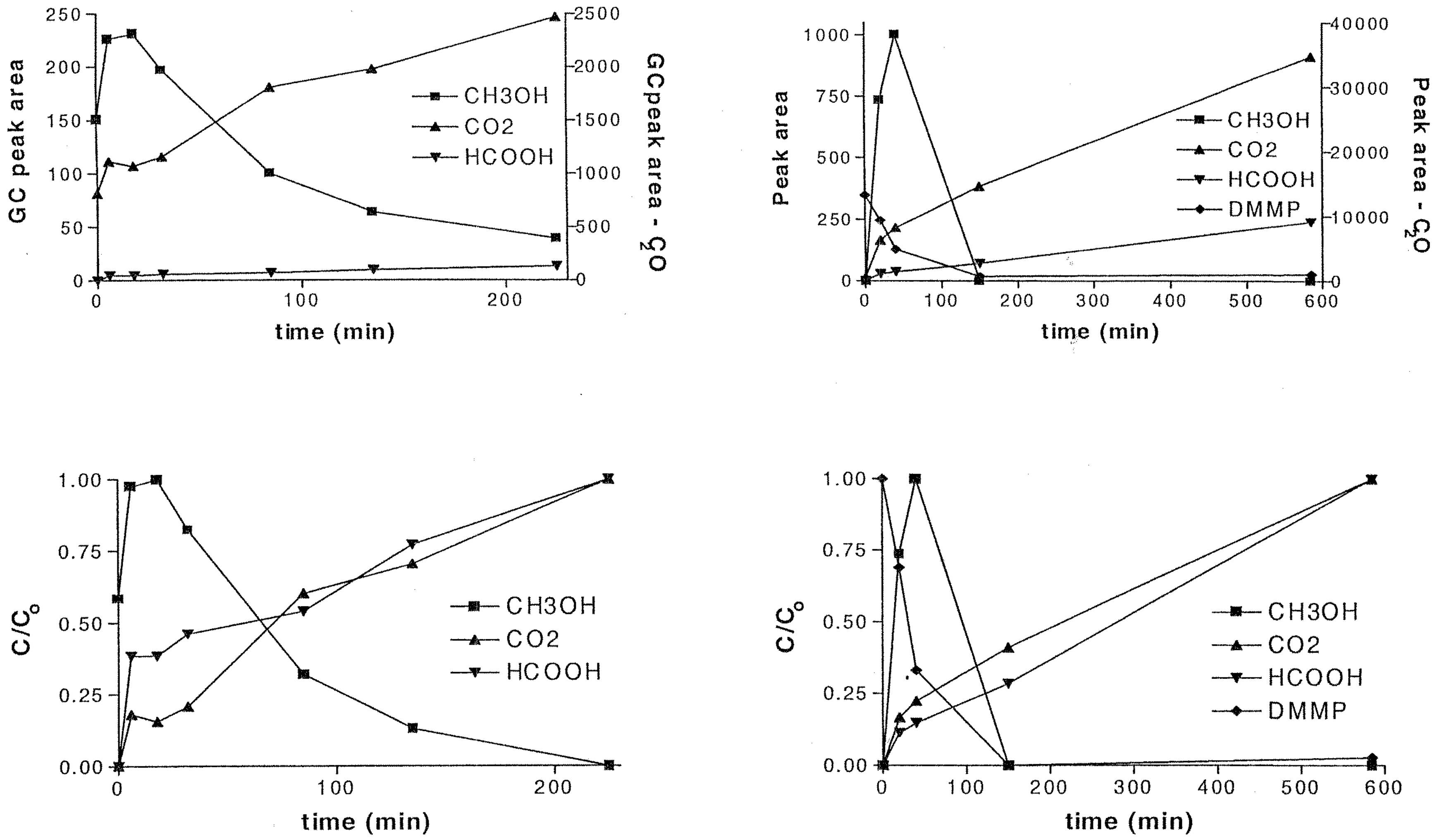

Figure 10: Concentration versus time data for gas phase products in bulk static reactor degradation experiments. a) heavily loaded (30 min exposure to DMMP aerosol from Collison nebulizer) and b) lightly loaded (30 min exposure to flowing DMMP vapor at RT).

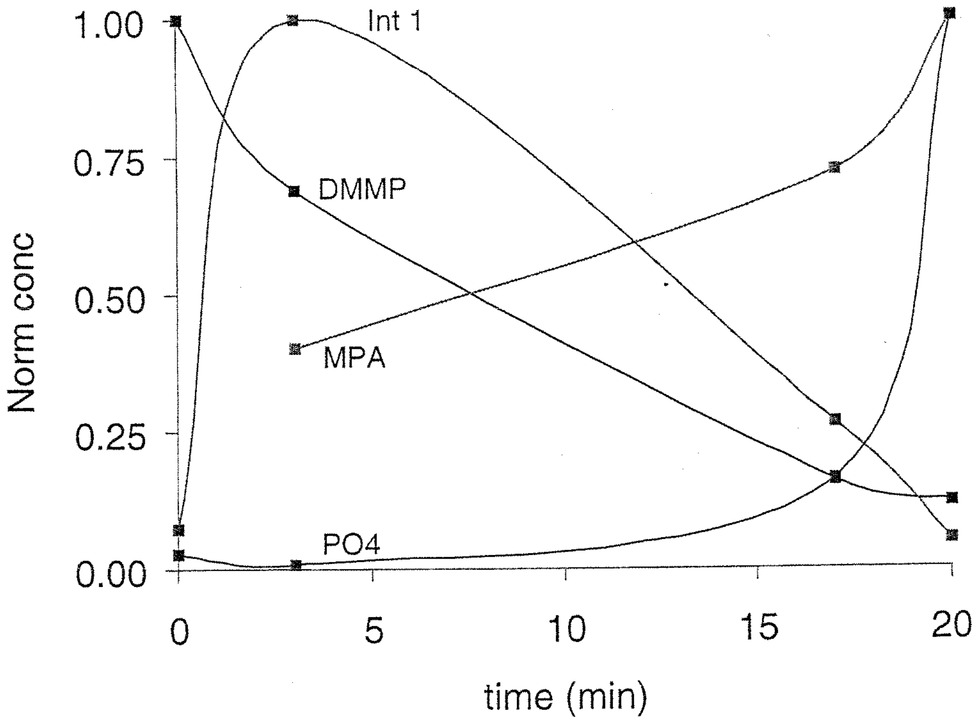

Figure 11: Surface-bound product concentration versus time plots for photodegradation reaction in static batch reactor with lightly loaded DMMP.

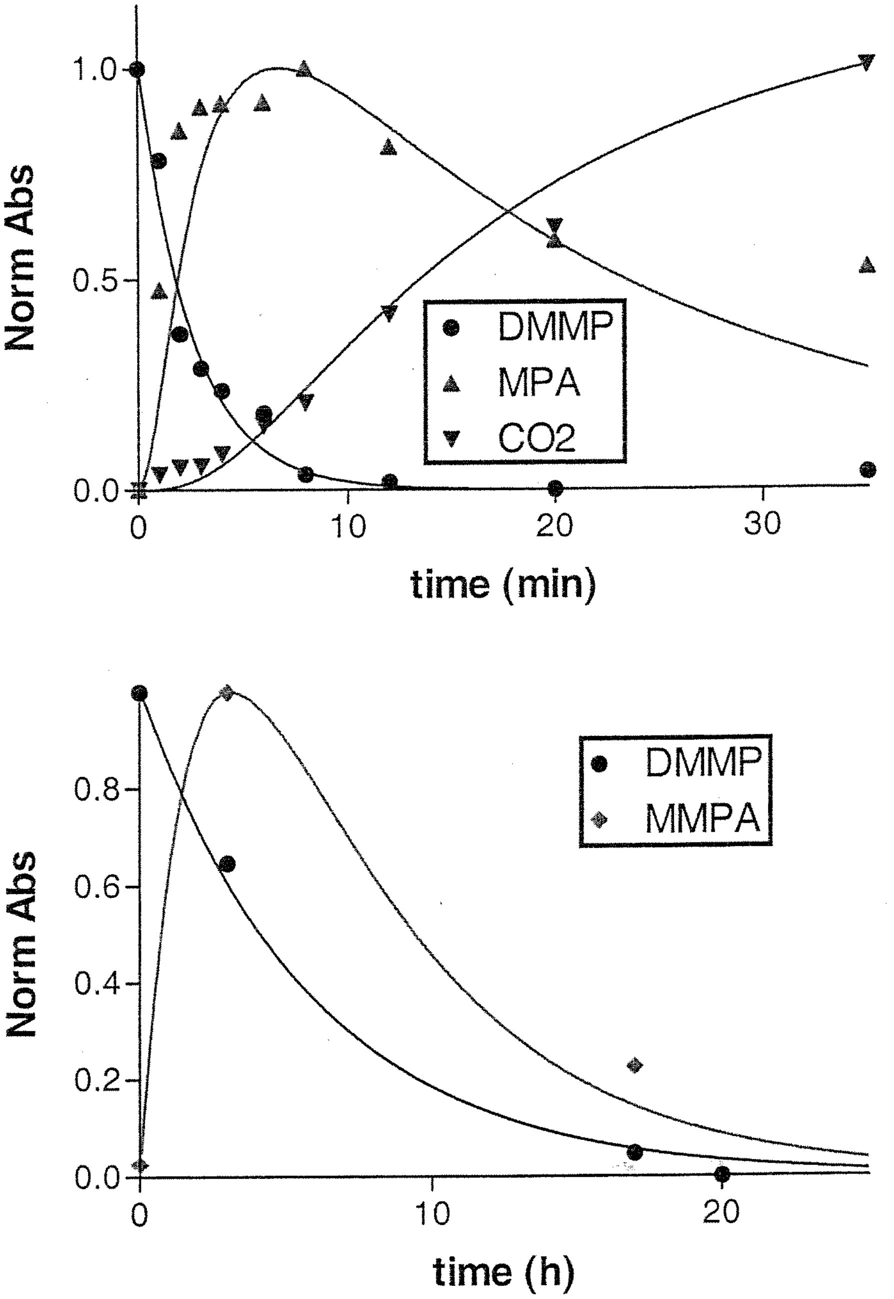

Figure 12: Simulated kinetic data for Scheme I and (a) DRIFT data for DMMP, MPA, and CO_2 and (b) static batch reactor data for DMMP and MMPA.

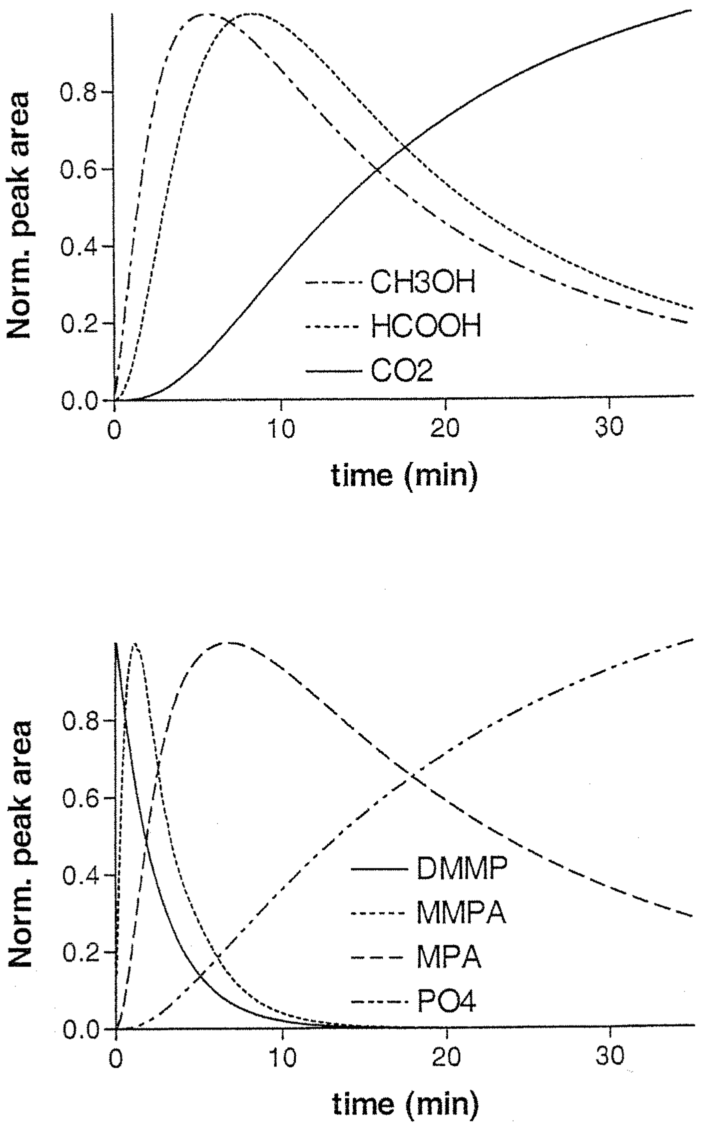

Figure 13: Plots of normalized concentration versus time for simulated kinetics according to Scheme I for (a) gas-phase products and (b) surface-bound products.

Chapter 6

Surface Acidity of TiO_2 Q Particles

Abstract

Ultrasmall TiO_2 Q particles have been synthesized. Individual anatase crystallites of approximately 2 nm in diameter are observed by TEM. An extremely high surface proton capacity is determined by potentiometric titrations. The surface functional groups appear to be much more acidic than those observed on larger TiO_2 particles. The unusual photochemical reactivity of the Q-particles is explained in terms of a hydrated gel layer on the surface.

Introduction

Anatase TiO_2 is an excellent heterogeneous photocatalyst for assisting the total oxidation of aqueous and vapor-phase organic pollutants because it is chemically and photostable, and inert in the absence of UV. When excited with UV light above the bandgap energy (3.2 eV), the photogenerated electrons initiate O_2 reduction, and the holes oxidize water to form hydroxyl radicals. Hydroxyl radicals oxidize organic pollutants by H-atom abstraction. However, the O_2 reduction process is believed to limit the overall photonic conversion efficiency.[1] Increasing the driving force of the reaction by raising the conduction band edge through size quantization can accelerate the O_2 reduction rate.

Semiconductors such as TiO_2 exhibit size quantization when the individual crystallite size approaches the same physical dimensions as the charge carriers.[2] Quantum confinement increases the potential of the charge carriers and causes the bandgap to widen as the crystallite size decreases from bulk-like dimensions. For anatase TiO_2, the threshold maximum crystallite diameter to exhibit size quantization is about 4 nanometers.[3] Particles below this critical size are called Q (quantum) particles, because of these quantum effects. TiO_2 Q particles prepared through the sol-gel method have exhibited increased photocatalytic reaction efficiencies with respect to their larger counterparts.[3] In addition to the thermodynamic advantages of Q particles, they also have a very large specific surface area for the heterogeneous reactions to occur, thereby increasing the kinetics. However, reactions using Q particles have not exceeded the efficiencies observed with other bulk-like photocatalysts.[4] While the bulk thermodynamics are increased, it is possible that the charge carriers are deactivated at the particle surfaces.

Photogenerated charges can be localized at the surface according to the following reactions:

$$TiO_2 + h\nu \rightarrow e^-_{CB} + h^+_{VB} \qquad (1)$$

$$e^-_{CB} + \equiv Ti(IV)OH \rightarrow \equiv Ti(III)OH \qquad (2)$$

$$h^+_{VB} + \equiv Ti(IV)OH \rightarrow \equiv Ti(IV)O^{\bullet}H \qquad (3)$$

The nature of the accepting ≡Ti(IV)OH group determines whether charge trapping will occur and the energetic depth of the resulting charge traps. These surface titanol groups are sensitive to the local structure of the TiO_2,[5] such as the orientation on a cleavage surface. [6] The Lewis acid/base properties of the surface moities are correlated to their Brönsted acid/base chemistry.[7] Amphiphilic surface titanol functional groups can undergo the following Brönsted acid base reactions.

$$\equiv TiOH_2^{\oplus} \xrightleftharpoons{K_{a1}} \equiv TiOH \xrightleftharpoons{K_{a2}} \equiv TiO^{\ominus} \qquad (4)$$

The K_a values are related to the electron trapping capability since more acidic structures are expected to be correspondingly more electronegative. Therefore, the Brönsted acidity of these groups, which is related to their Lewis acid/base chemistry, can be used to qualitatively determine their charge-trapping capability.

In this paper, we determine the acid/base chemistry of surface ≡TiOH groups on Degussa P-25 TiO_2 and TiO_2 Q particle surfaces. The total concentration of ≡TiOH functional groups and their microscopic pKa values are presented and compared with the photocatalytic reactivity of each type of TiO_2. The results suggest that the Q particle surface is covered with a highly protonated gel layer, which limits interfacial electron transfer reactions.

Experimental

Commercial TiO_2 was obtained from the Degussa Corp. (P-25). Anatase TiO_2 particles were prepared by the sol-gel method. 1 L Milli-Q (18 MΩ) water was acidified with HNO_3 to pH=1.5 and cooled to 1 °C in an ice bath. Controlled hydrolysis was performed by adding 5 mL of $Ti(OCH(CH_3)_2)$ dissolved in 100 mL isopropanol dropwise to the cold water with vigorous stirring, yielding a transparent solution. The TiO_2 was isolated at room temperature by rotary evaporation. The powder residue was dried under high vacuum at room temperature overnight, removing most of the water and some of the residual HNO_3 to crystallize the particulates. The highly hygroscopic Q particles were stored in a dessiccator. The Q particles produced transparent suspensions when remixed in pure water for several weeks after synthesis, but would yield cloudy mixtures after extended aging.

Titrations were performed in the presence of swamping KNO_3 electrolyte that provided a constant ionic strength not less than 10 times excess of the concentration of functional analyte. The residual HNO_3 remaining from the synthesis of the Q particles provided the initial acidification of the suspensions. P-25 suspensions were acidified with calibrated aliquots of an HNO_3 solution. The suspensions were titrated with a KOH solution of the same ionic strength, calibrated against a potassium hydrogen phthalate primary reference. The titrant was dispensed in 5 or 0.5 μL increments for a total burette volume of 10 or 1 mL, respectively, from a Radiometer ABU-80 autoburette. The pH was read by a Radiometer PHM85 pH meter with a radiometer glass pH electrode referenced against an external standard electrode. Saturated. calomel and silver/silver chloride electrodes were used as references, using the background electrolyte in the salt bridge to minimize junction potentials. A glass sleeve barrier was used on the silver/silver chloride electrode to eliminate clogging effects from the porous frit barrier of the other electrodes. The mV potential read by the pH meter was input to a desktop computer, which also controlled the autoburette using LabVIEW software. Under standard conditions, the system required stability to ±0.01 mV over 30 seconds before measuring the value and dosing more titrant. The solution was enclosed under a nitrogen atmosphere to eliminate interference from CO_2. The titrant was dispensed through a thin (0.33 mm ID) HDPE tube whose end was momentarily lowered by a solenoid piston to contact the solution after the burette dispensed the dose, eliminating both drop error and idle diffusion out of the burette tip. A typical titration took about 20 hours to complete. The conversion of mV to pH was performed during the analysis, not the acquisition, to allow for internally referenced calibration of each data set. Blank titrations of background electrolyte were performed to provide additional external referencing as well as to check the performance of the system.

Photocatalytic decoloration of dilute aqueous methyl orange solutions were performed in the presence of both P-25 and Q particle TiO_2 catalysts. UV radiation from a 1 kW Oriel Xe lamp was focused into in the vigorously stirred slurry chamber through a quartz window. A 10 cm jacketed water filter removed the IR portion of the radiation. Q particles were used as synthesized, resulting in a transparent solution with pH of about 3. P-25 suspensions were prepared and acidified to match the pH of the Q-particle suspensions. O_2 was bubbled through the solution during irradiation. Absorbance values were recorded in a flow through quartz cuvette on an HP 8452 diode array UV-Vis spectrometer.

TEM images were recorded with a Philips EM430 microscope operating at 300kV. Unwashed sol-gel samples were ground in 2-propanol with a mortar and pestle to disperse the particles. A drop of the suspension was then placed on a copper grid with a holey carbon support. The drop was allowed to settle, excess solvent wicked off, and allowed to dry before imaging.

Results

TEM images of the Q particles show non-aggregated particulates about 2 nm in diameter (Figure 1). Diffraction patterns indicate anatase and amorphous phases with no evidence of rutile. The proportion of anatase to amorphous could not be determined because of the small crystallite size. An expanded image of a single crystallite (Figure 2) shows evidence of diffraction on the lattice planes, which confirm the original size estimate.

The Q particles dried under high vacuum were extremely hygroscopic. Figure 3 shows the increasing mass of a Q particle sample exposed to air, along with a langmuir adsorption isotherm. The mass increase suggests that about 30% of the mass of Q particles in air is due to adsorbed water. The mass fraction of water is factored into the surface-charging calculations.

Before and after the slow surface titrations, the pH meter was externally calibrated to a near continuum of concentration references by titrating a pure HNO_3 solution with the KOH titrant in swamping KNO_3 electrolyte. The electrode response was then calibrated numerically to the observed titration curve (Figure 4). When mixed with pure water, the Q particles form a completely transparent suspension with a low pH due to residual HNO_3 from the Q particle synthesis. Raising the pH or ionic strength causes the suspension to turn cloudy as the particles aggregate. Increasing the dessiccation time under high vacuum reduces the amount of HNO_3, but causes the Q particles to form cloudy suspensions at all pH values. Titrations of Q particles showing the aggregating effects of varying ionic strengths are shown in Figure 5. A titration of the Q particles is compared with a titration of P-25 at 1 M ionic strength in Figure 6. P-25, which is prepared by flame-hydrolysis of $TiCl_4$, contains HCL as a synthetic by-product that accounts for less than 0.2% of its total mass. Added HNO_3 provided the initial acidification of the P-25 suspension.

The effect of UV irradiation on the proton release from Q particles was determined by measuring the pH of a suspension of as-synthesized Q particles in pure water as the UV beam was turned on and off. A rapid decrease in pH is observed when the lamp is turned on, which reverts in the dark (Figure 7). A slow decrease in pH, which is independent of irradiation, is observed in all Q particle suspensions.

Dilute solutions of methyl orange were rapidly photocatalytically decolorized using P-25 photocatalyst suspensions (~0.01 g/L). The reaction proceeded much more slowly using Q particles under otherwise identical conditions, whether or not a much higher catalyst loading was used. Since the two sets of raw decoration data did not directly compare, the data was plotted on an arbitrary time axis vs. a normalized absorbance axis, to demonstrate the relative profiles of the decoloration curves (Figure 8). The decoloration over P-25 appeared to proceed with pseudo first-order kinetics, while the decoloration over Q particles appeared to be auto-catalytic. Adding more methyl orange during the rapid (auto-catalyzed) phase resulted in continued rapid decoloration. Addition of more methyl orange after complete decoloration resulted in the appearance of a new lag period before the autocatalytic phase. The partially decolorized solution, separated from the Q-particles by aggregation and centrifugation, acted to eliminate the lag period from a fresh mixture of Q-particles and methyl orange. These experiments indicated that a reaction intermediate in the solution was inducing the autocatalytic behavior.

Discussion

The surface chemistry of metal oxides, including titration behavior, is a well-studied field.[8] Microscopically, the individual titanol functionalities act as solution species with distinct pKa's. The effect of being embedded in the surface allows these functional groups to interact with each other according to their charge. In general, this causes coulombic repulsion as the surface develops a charge, which makes the approach of like-charged species in solution less favorable. The net effect is to distort the pKa values away from the neutral condition with increasing surface charge. This effect necessitates the use of a more involved analysis than is used for solution phase titrations. Since the early experimental characterization of the acid-base behavior of anatase surfaces,[9] theoretical models have been developed that describe the chemistry on a molecular level,[10,11] which can be used for pH-dependent adsorption behavior in general.[12] Because of the wealth of knowledge already present on this subject, our purpose is not to describe the system in detail, but rather to understand the underlying differences between highly efficient TiO_2 photocatalysts and other types of TiO_2.

The preferred method for analyzing surface titration data is to express the data in terms of surface charge as a function of pH.[*] At acidic pH, the surface charge is determined by the discrepancy between the H^+ added to the suspension, and the amount observed in solution, and similarly for OH^- at basic pH. The concentrations of H^+ and OH^- are determined from the pH, which is calibrated to a concentration scale instead of the more common activity scale. The equation to determine the surface charge is then

---

[*] The pH must be measured as a function of H^+ concentration rather than the more common activity scale. This is achieved by maintaining a constant ionic strength.

$$q_m = \left[\left(10^{-pH_{blank}} - 10^{-pH_{measured}}\right) - \left(10^{-pOH_{blank}} - 10^{-pOH_{measured}}\right)\right]\frac{V}{m} \qquad (5)$$

where q_m is the mole equivalent of adsorbed proton charge per gram of solid, V is the total volume of suspension, and m is the mass of solid. The blank is the predicted pH or pOH in the absence of the adsorbing species, determined by the amount of acid or base added.

This analysis works well with P-25 because the powder forms nearly neutral suspensions out of the bottle. Analysis of the P-25 titration curves (Figure 9) gives a point of zero (proton) charge (PZC) at pH = 5.45. This is slightly lower that the value measured for pure anatase (6.39),[9] and close to the value for pure rutile (5.8).[11] Since P-25 is a mixture of the two phases, an intermediate value is expected. The low value is most likely an artifact of the resiual HCl from the synthesis. The pKa values, from the 2-pKa model, provided by the titration curves are 3.34 and 7.68.

The situation is more complex for the analysis of the Q particle titration curves (Figure 10). The as-synthesized Q particles have a large quantity of acid inherent in the samples. Proper analysis of the surface chemistry requires an initially acid-free sample, but removing the acid from Q particles inherently changes their physical properties by aggregation, and may change their chemical properties as well since they cannot be de-aggregated. Since the acid region is the primary focus for this paper, the particles were titrated without removing the acid synthetic by-product. The quantity of "acid added" used in the analysis was then determined by assuming the same PZC observed for pure anatase and back-calculating from that point in the titration curve. Although this analysis precludes the assignment of titration features near the PZC, the highly acidic region provides qualitative information.

A common prominent feature observed in the pKa vs. surface charge plots is the relatively flat data in the highly acidic region (Figure 10). The deviation from this flat region corresponds to the onset of aggregation. Because the flat regions have small slopes, their extrapolation to zero charge is rather insensitive to slight changes in the assumed PZC. It is clear that the flat region is most prominent in the titrations performed at low ionic strength. The diminished prominence in the higher ionic strength titrations is due to the aggregating effect of the electrolyte to "salt out" the particles at progressively lower pH values. In fact, the 1 M ionic strength titration, which exhibited agreggation at all pH values, shows only a slight tailing in the acid region that indicates the transition from a flat region. The lack of a common intersection of the extrapolated linear portions is most likely due to a combination of non-equilibrium measurements as well as the error in estimating the PZC.

There are three main conclusions that can be drawn from these titrations. First, if we assume that the linear portion is the "true" data to be extrapolated for the lower pK_a value, then the lower pKa extrapolated for Q particles (2-3.5) is much more acidic than for bulk anatase (4.98).[9] Second, the low pK_a vs. charge slope for Q particles relative to P-25 indicates that the protonation events are more molecular-like protonations rather than double layer charging effects. Third, the data corresponding to very high charge layers suggests that Q particles can accommodate ~8 sites/nm^2. This is about twice as large as the cleaved surfaces can allow, which indicates this presence of a hydrated gel layer that is permeable to H^+.[13] Each conclusion has implications for the reactivity of TiO_2 Q particles.

The presence of highly acidic sites on Q particles indicates a great capacity for deep electron trapping. In a previous paper, we demonstrated that deep electron trapping occurs only at the most acidic, i.e., the most electronegative TiOH moieties.[7] A lower pK_a value suggests that the sites are even more electronegative on Q particles, as well as being in great abundance. Since deep electron trapping inevitably leads to charge recombination, a high coverage of these traps is expected to lower the photocatalytic efficiency, as observed.

The presence of highly acidic sites is likely due to the synthesis of the particles at a very low pH. As the sol-gel collapses to form crystals under these conditions, all but the most acidic sites become protonated, restricting their incorporation into the final surface structure by charge repulsion. Also, the small particle size may contribute to lowering the pK_a as the curvature of the particles allows coulombic repulsion to affect more sites than those immediately proximate as on a flat surface. This effect would be expected to shift the low pK_a lower, and the high pK_a higher, much like the effect of spatial proximity of functional groups on diprotic molecules. The presence of a gradual pK_a slope vs. pH indicates molecular-like buffering behavior. The negative slope observed for the 0.01 M ionic strength titration is discussed later.

The high site capacity calculated for the surface indicates that protons penetrate the surface gel layer. This gel layer, which most likely has a photo-inactive amorphous form, is expected to be a detriment toward photocatalysis. However, the presence of this layer may help explain the behavior of TiO_2 sol-gel electrodes to accommodate local charging effects. As a potential is applied to the electrodes, the local surface charges are offset by the intercalation of electrolyte.[14] Therefore, the nature and concentration of the electrolyte is very important,[15] as well as the capacity of the surface to accommodate the electrolyte's influence.[16] The presence of this gel layer allows the surface to accommodate a higher asdorbate charge, which in turn can offset a high internal charge. This has implications for applications such as solar cell electrodes, where local field effects from injected electrons can limit the overall efficiency.

The negative slope in the pKa vs. surface charge plot for the 0.01 M ionic strength titration indicates the excessive release of protons during the titration. This may indicate the irreversible collapse of the protonated porous gel layer. This would cause more protons to be released than those neutralized by the hydroxide ions that are added in, within the time allowed between measurements. The net effect then is to lower the pH as base is added during the initial part of the titration. The proposed mechanism of proton release is shown below.

(6)

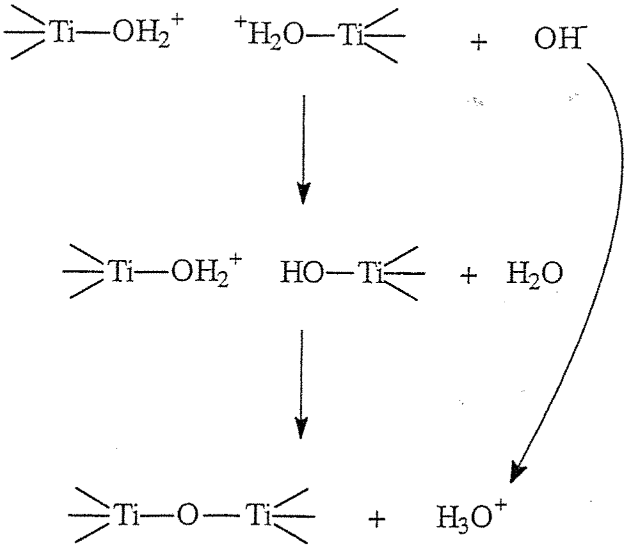

A similar proton release effect occurs in response to UV illumination (Figure 7). As photogenerated charge carriers are localized at the surface, the electron environment at the surface is apparently altered enough to affect the acidity of the surface groups. A proposed mechanism for the photoactivated proton release is shown below.

(7)

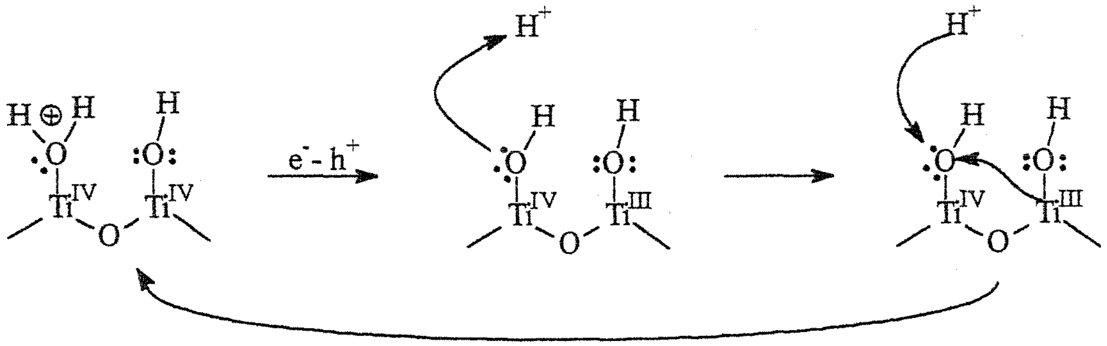

A consequence of this hydrated gel layer on the surface of TiO_2 Q particles is that the surface photodynamics during photocatalytic reactions are altered with respect to other photocatalysts. A clear example of differing surface reactions is seen in the photocatalytic decoloration of methyl orange solutions with either Q particle or P-25 photocatalysts. P-25 rapidly decolorizes the solution with pseudo first-order kinetics. However, the reaction over Q particles clearly has a sigmoidal shape. The initial lag period shows that some of the reaction intermediates act as co-catalysts with the Q particles, enhancing the overall reaction, and causing an auto-acceleration. It is likely that these intermediates intercalate into the gel layer where they can serve as a mediator for electron transfer in what would otherwise be an insulating layer.

Conclusions

As-synthesized anatase TiO_2 Q particles are covered with a hydrated gel layer. This layer is permeable to H^+ ions, giving the particles an extremely large acid capacity. It is likely that this layer acts as an insulator against the heterogeneous electron transfer required for photocatalytic reactions. The auto-acceleration of the photocatalytic decoloration of methyl orange over Q-particles is due to a co-catalytic intermediate, which is able to penetrate this gel layer.

References

---

[1] Martin S.T.; Choi W.; Hoffmann M.R. *Chem. Rev.*, **1995**, *95*, 69-96.

[2] Brus L.E. *J. Chem. Phys.*, **1984**, *80*, 4403.

[3] Hoffman A.J. *Ph.D. Thesis*, California Institute of Technology, 1993.

[4] Choi W. *Ph.D. Thesis*, California Institute of Technology, 1996.

[5] Paxton A.T.; Thien-Nga L. *Phys Rev. B*, **1997**, *57*, 1579.

[6] Chung Y.W.; Lo W.J.; Somorjai G.A. *Surface Science*, **1977**, *64*, 588.

[7] Szczepankiewicz S.H.; Colussi A.J.; Hoffmann M.R. *J. Phys. Chem. B* **2000**, *104*, 9842.

[8] Morgan J.J. and Stumm W. Aquatic Chemistry. In *Environmental Science and Technology*. 1996. John Wiley & Sons, New York. pp. 516-599.

[9] Schindler P.W.; Gamsjager H. *Kolloid-Z. u. Z. Polymere*, **1972**, *250*, 759.

[10] Hiemstra T.; Van Riemsdijk W.H.; Bolt G.H. *J. Coll. Int. Sci.*, **1989**, *133*, 91.

[11] Hiemstra T.; De Wit J.C.M.; Bolt G.H. *J. Coll. Int. Sci.*, **1989**, *133*, 105.

[12] Ludwig C.; Schindler P.W. *J. Coll. Int. Sci.*, **1995**, *169*, 284.

---

[13] Busch K.W.; Busch M.A.; Gopalakrishnan S.; Chibowski *E. Coll. Polym. Sci.*, **1995**, *273*, 1186.

[14] Boschloo G.; Fitzmaurice D. *J. Phys. Chem. B*, **1999**, *103*, 7860.

[15] Ravichandran C.; Noel M.; Anantharaman P.N. *J. App. Electrochem.*, **1996**, *26*, 195.

[16] Lyon L.A.; Hupp J.T. *J. Phys. Chem. B*, **1999**, *103*, 4623.

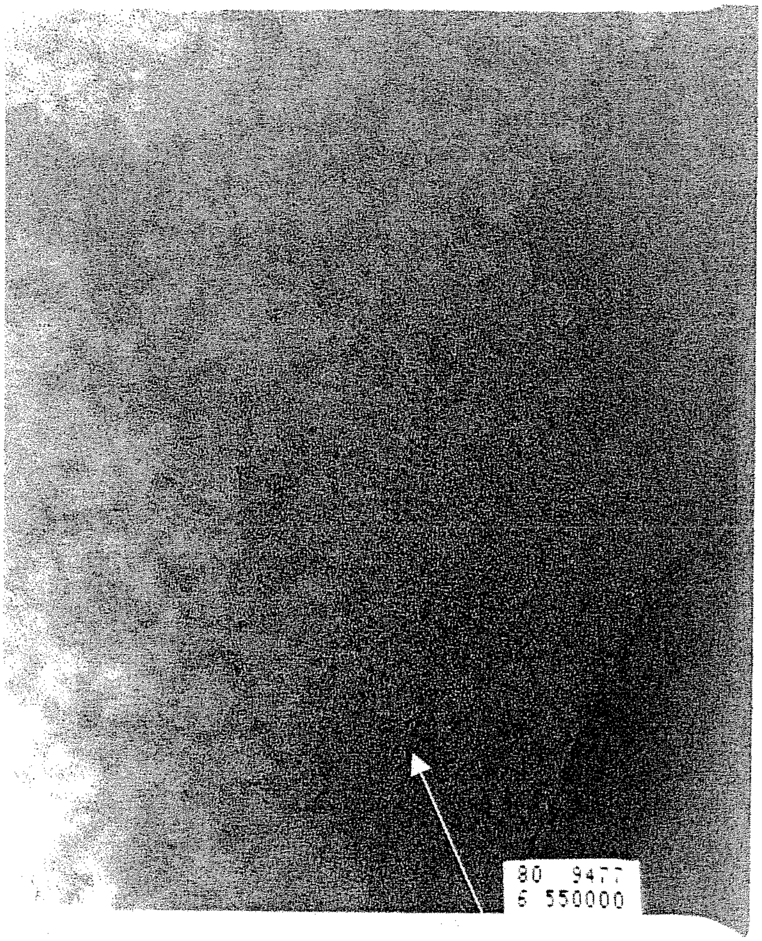

Figure 1: TEM image of Q particles showing individual crystallites about 2 nm in diameter. The arrow indicates the particle shown in Figure 2.

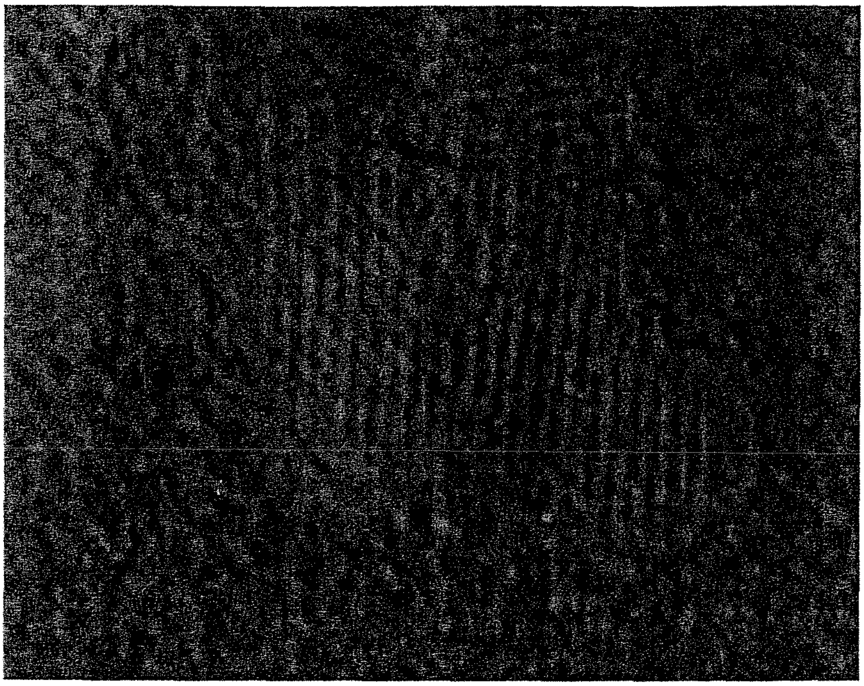

Figure 2: TEM image of a single Q particle showing lattice diffraction planes.

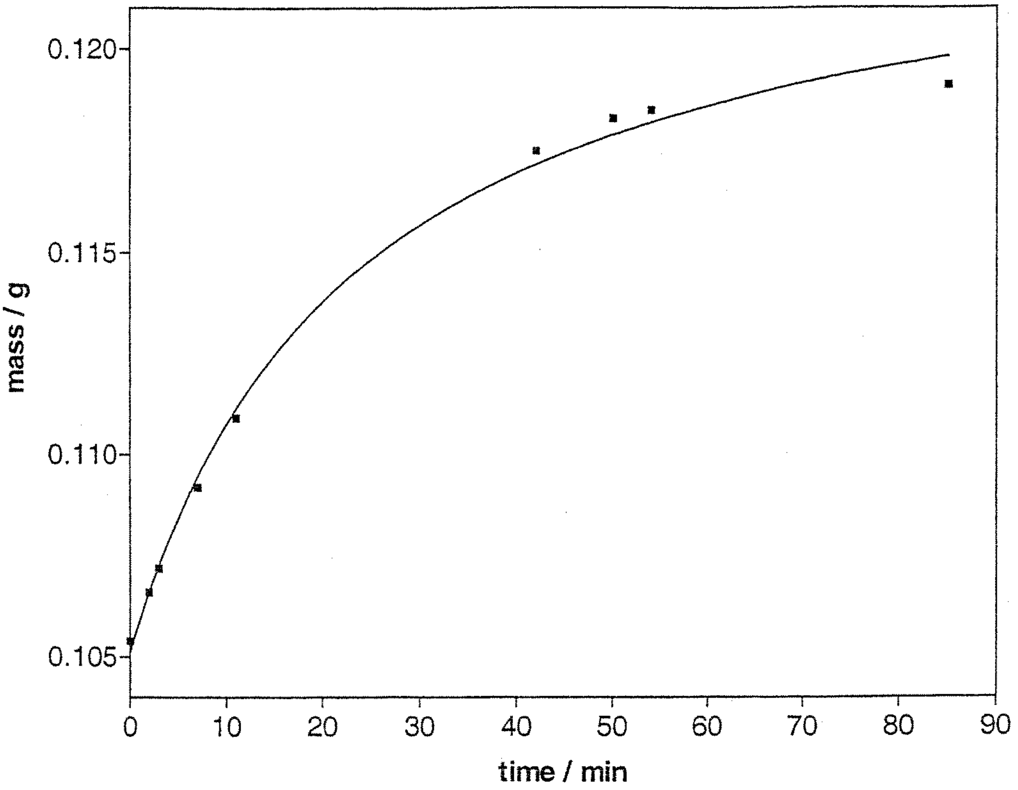

Figure 3: Mass increase due to water adsorption on Q-particles in air.

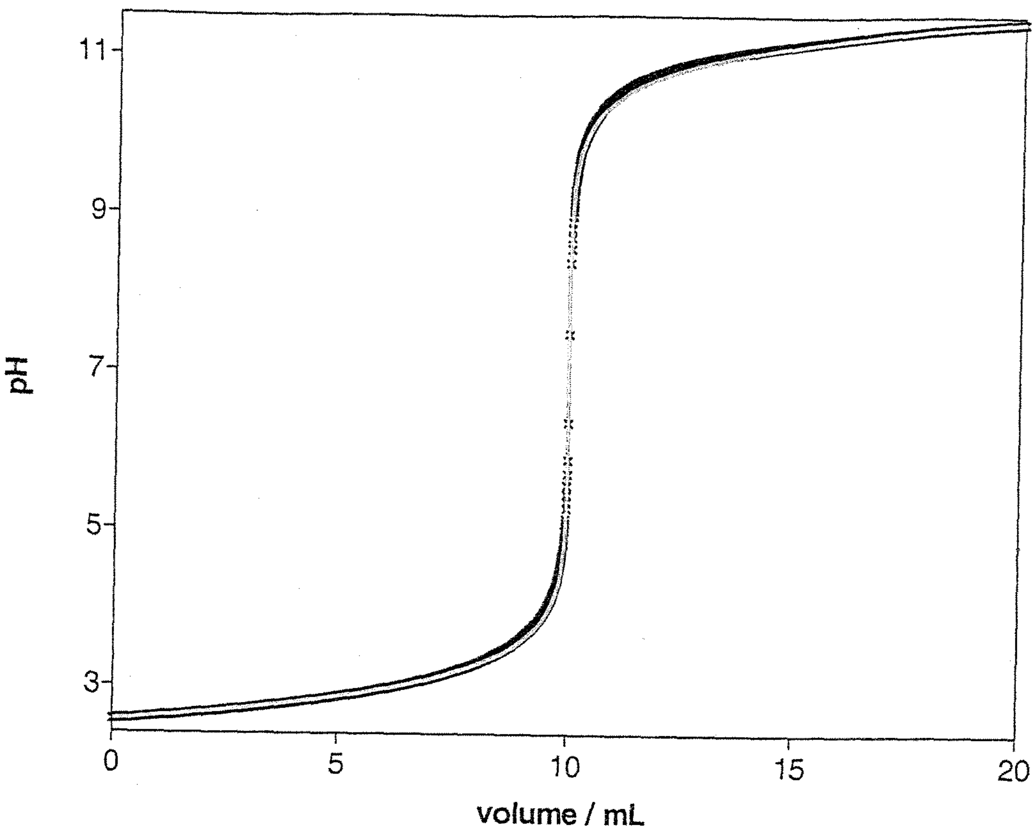

Figure 4: 2.033 mmol HNO_3 in 750 mL of KNO_3 electrolyte at1 M ionic strength titrated with 0.2040 M KOH for external calibration reference vs. a saturated calomel electrode. The calibration parameters are m = 0.9408 and b = 0.4356 where

$$pH=-\frac{m}{59.1}mV+\left(\frac{333}{59.1}+b\right)$$

Note the agreement between the system performance (data points), and the predicted response (solid line).

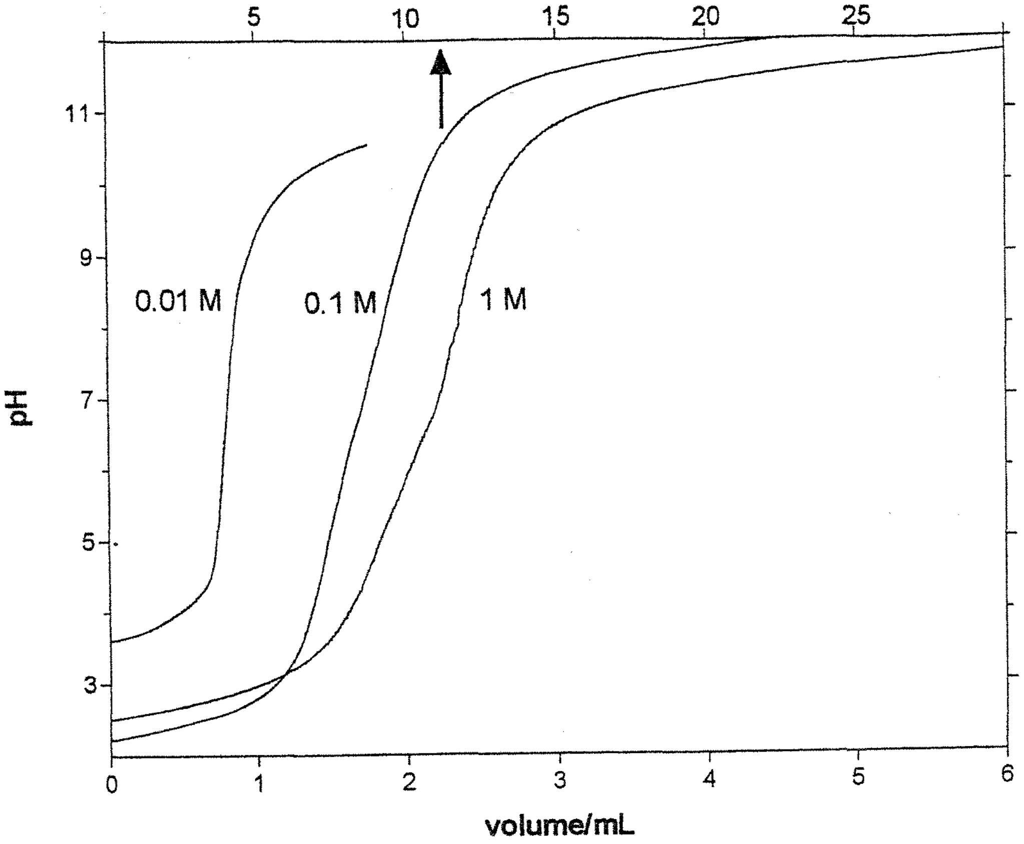

Figure 5: Typical Q particle titration curves at varying ionic strength. 1 M - 0.0858 g in 100 mL suspension titrated with 0.2040 M KOH. 0.1 M - 0.1110 g in 50 mL suspension titrated with 0.05626 M KOH (upper X axis). 0.01 M - 0.0108 g in 100 mL suspension titrated with 0.05626 M KOH.

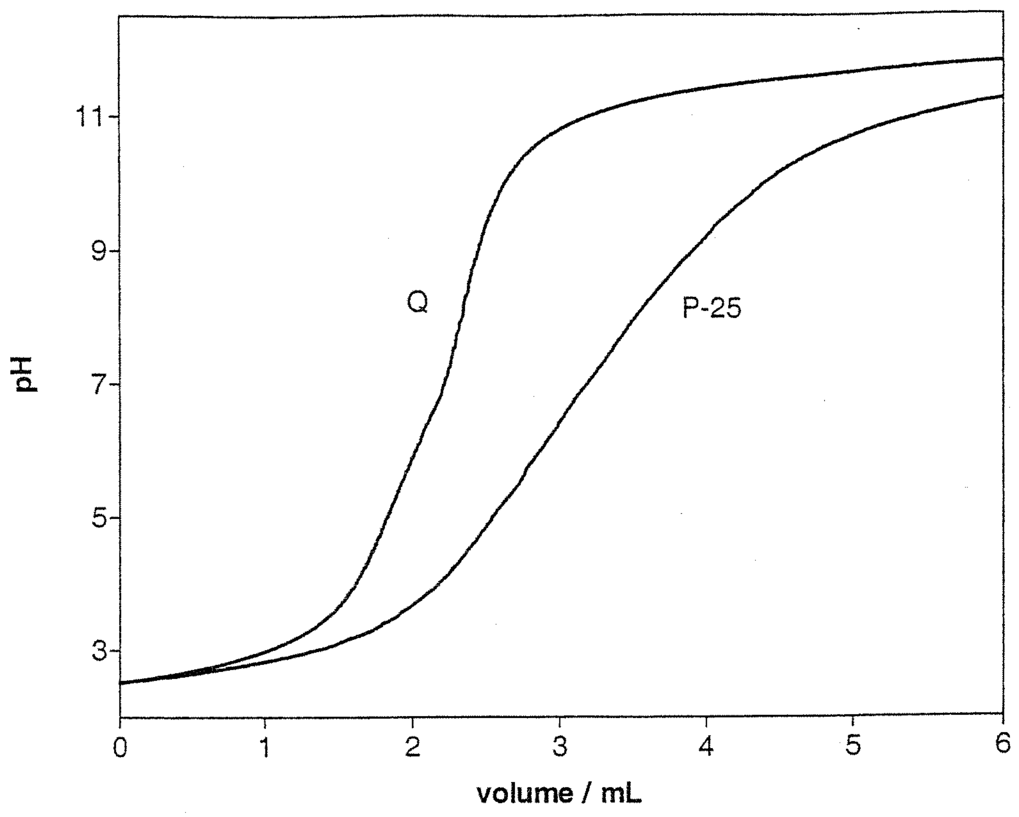

Figure 6: Titrations of Q particles and P-25 at 1 M ionic strength. Q - 0.0858 g in 100 mL suspension titrated with 0.2040 M KOH. P-25 - 5.6380 g in 750 mL suspension titrated with 0.7465 M KOH.

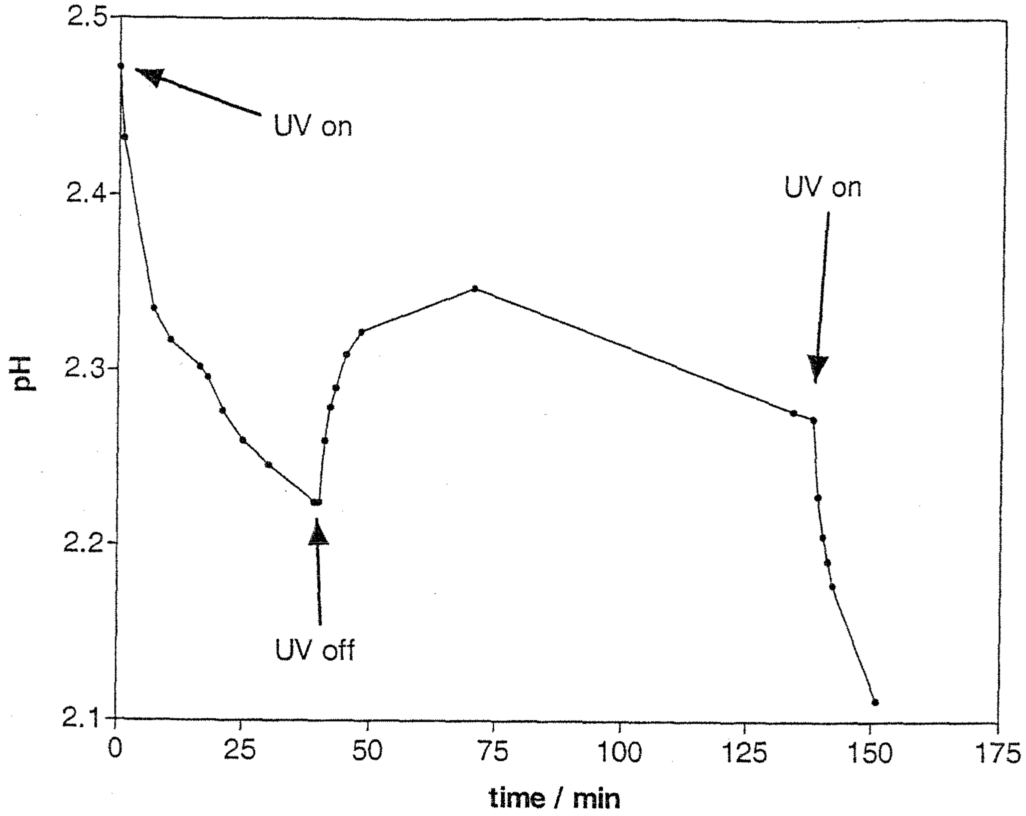

Figure 7: UV induced H^+ release from Q-particles in aqueous suspension.

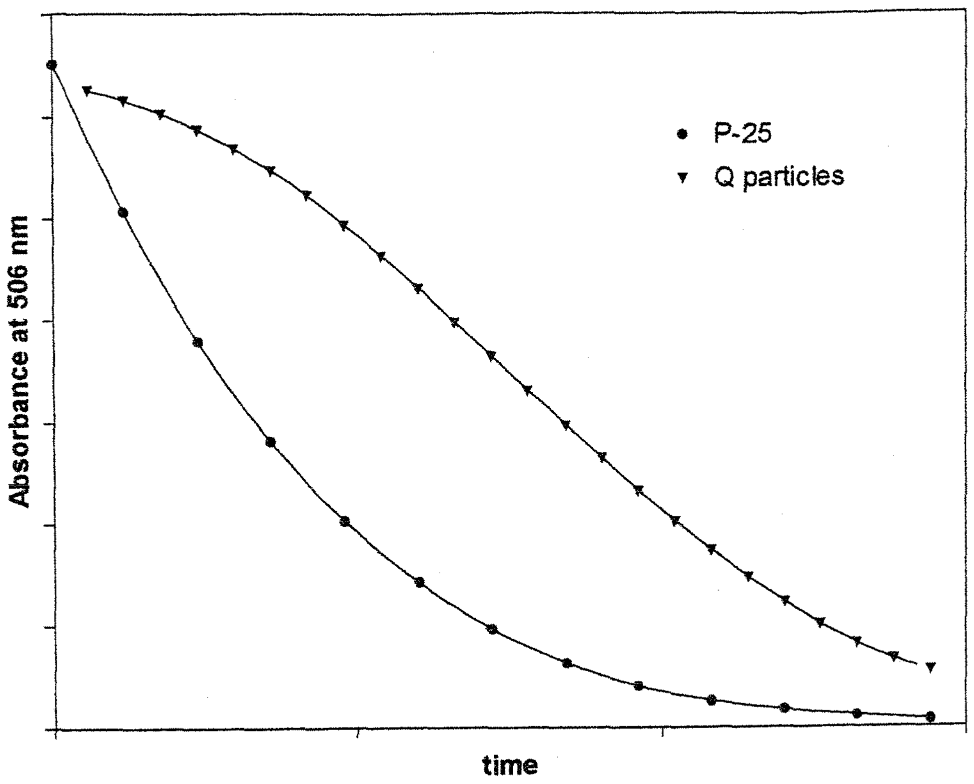

Figure 8: Photocatalytic decoloration of methyl orange over P-25 and Q particles. The data sets are arbitrarily superimposed on the x axis, and normalized on the y axis to contrast the curve profiles.

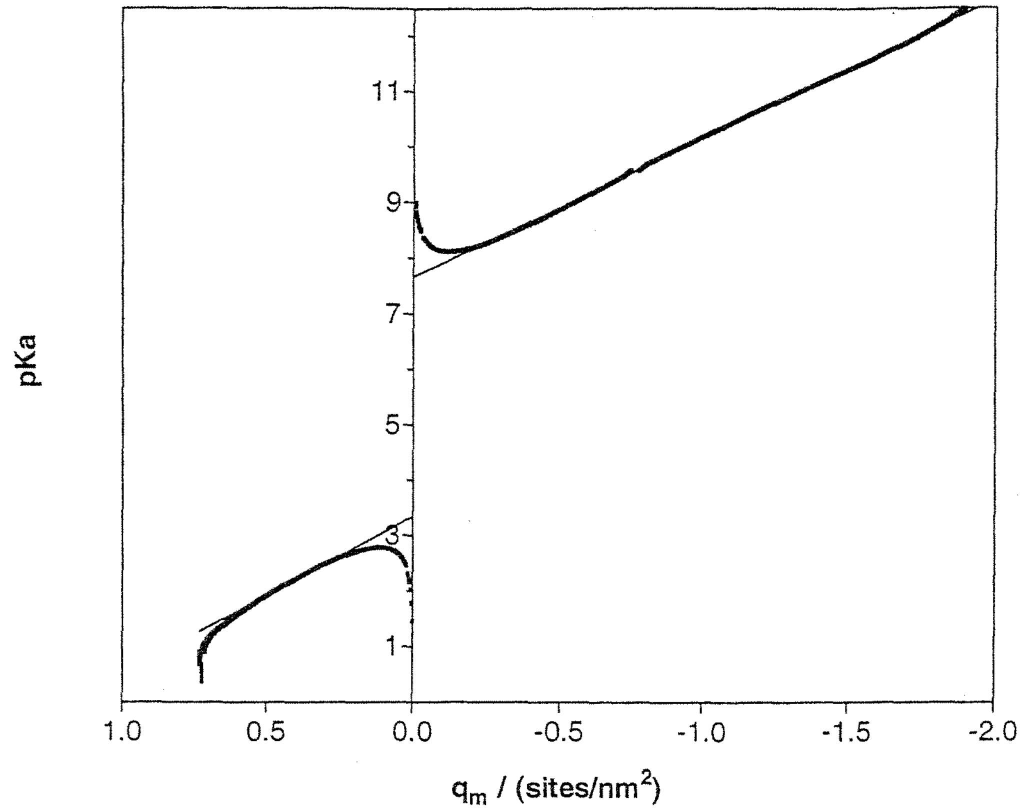

Figure 9: Analysis of P-25 titration curves according to a 2-pK$_a$ double-layer model.

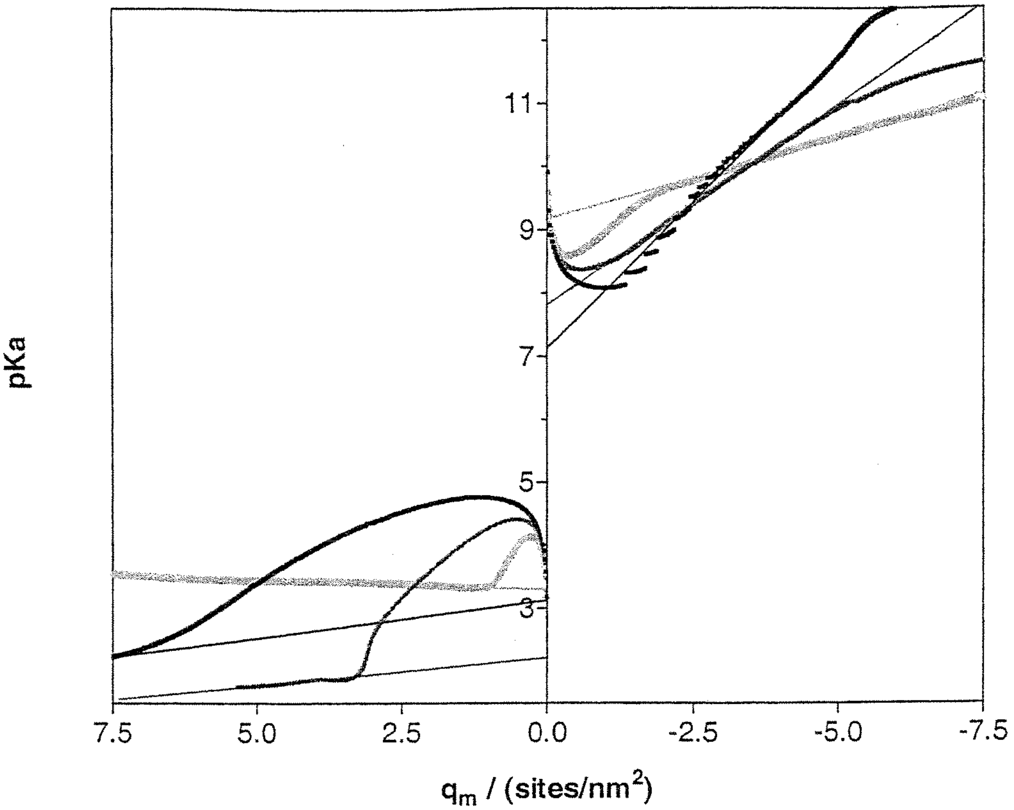

Figure 10: Analysis of Q particle titration curves in 1 M electrolyte (black), 0.1 M electrolyte (dark gray), and 0.01 M electrolyte (light gray), according to a 2-pK$_a$ double-layer model.

Chapter 7

Supplementary Investigations

Abstract

The surface photodynamics of TiO_2 photocatalysts are investigated by solid-state MAS NMR spectroscopy and by theoretical investigations. NMR spectra indicate the influence of paramagnetic species on the surface proton resonances, apparently due to electron trapping at TiOH structures at local surface defects. Force field calculations confirm previously reported vibrational frequency assignments for the same Ti(IV)O-H and Ti(III)O-H structures, and correctly predict the intensity increase upon electron trapping.

Introduction

The dramatic changes that occur on the surface of TiO_2 upon bandgap irradiation have been investigated in the previous chapters. Using the information available from the FTIR spectroscopy, the investigation was expanded to include solid-state Magic Angle Spinning Nuclear Magnetic Resonance (MAS NMR) spectroscopy. The magnetic resonance spin interaction of the ^1H nuclei bound to the surface of TiO_2 as TiO-H groups are highly influenced by the local electronic structure of the surface group. Although some structural characterization has been made using ESR, the structure of the site preceding the paramagnetic trapping remains unknown. We report a characterization of the potential surface trapping sites on TiO_2, and demonstrate their occupancy following irradiation.

Experimental

Commercial, polycrystalline TiO_2 (Degussa P-25, ~85% anatase, 15% rutile) was purified by sonication in deionized water and recovered by ultracentrifugation before being dried under vacuum. All samples were dehydrated at 350 °C under high vacuum for several hours, resulting in a pressure of about 1 μtorr. For a control experiment, the dry powders were then packed into 4 mm zirconia rotors in a glove box under a purified argon atmosphere and sealed before exposure to the lab atmosphere. Test samples were illuminated with UV radiation from a 1 kW Oriel Xe lamp for about 30 minutes under vacuum in a Pyrex Schlenk flask before packing in the rotor in the glove box. ^{1}H NMR spectra were taken with a Bruker AM 300 FT MAS Spectrometer operating at 300 MHz with a spin rate of 12 kHz.

Theoretical calculations were performed using a force-field model with charge and Morse potential terms. Using the Cerius^2 interface, a 8×8×8 unit cell lattice was built, and a single OH- group was placed in a central location on the (001) face. The model was then optimized my energy minimization according to the default charge parameters and the Morse potential parameters shown in Table 1. The minimized structure was then analyzed according to the normal mode vibrational frequencies associated with the surface titanol group. The Ti(IV)OH group was then reduced to Ti(III)OH, the structure was re-optimized, and the normal mode vibrations re-calculated. The theoretical data is compared to the measured IR data in Table 2.

Results and Discussion

The 1H NMR of the sample before dehydration shows a single sharp peak that is characteristic of water. The NMR of the sample with the dehydrated sample before irradiation indicates two distinct sharp proton resonances centered at 2.5 and 7.4 ppm

(Figure 1). Removing the proton-proton dipole coupling via CRAMPS experiments[1] do not resolve any fine structure within the bands. These data suggest that the broad peak widths are due to anisotropy of the chemical species on the surface, and not chemical exchange or dipole broadening.

Following irradiation, a broad resonance develops at 11.7 ppm with a corresponding intensity depletion of the sharp peak at 2.5 ppm (Figure 1). Also, the strongest resonance appears at 5.4 as opposed to 7.4 before UV treatment. The total intensity of the spectrum is much greater following irradiation, suggesting the sample was contaminated with atmospheric H_2O during the preparation for analysis. Rehydrating the surface without UV treatment does not reproduce these phenomena. Samples that remained well dehydrated did not show any changes.

The two peaks 2.5 and 7.4 ppm, which are prominent before irradiation, have been assigned to the proton resonances in Ti(IV)O-H structures on the surface of the TiO_2. The structure(s) that produce the resonance at ~2.5 ppm appear to be responsible for charge trapping, since they are most greatly affected by irradiation. Previously published data suggest that this resonance is due to surfacial impurities inherent to P-25.[2] ESR studies suggest that such irregularities on the surface act as electron traps.[3] The broad peak at 11.7 ppm, which develops after irradiation, is assigned as the Ti(III)O-H proton resonance. The broad linewidth is characteristic of a proton resonance near a paramagnetic center. The sharp band at 5.4 ppm following irradiation is most likely due to the remaining Ti(IV)O-H structures that are not capable of electron trapping.[4]

The theoretical investigation confirms the previous assignment of the electron trapping structure. Although the predicted vibrational frequencies are not directly comparable to the actual data[5] (Table 2), the observed changes upon reduction of the titanol structure are closely reproduced in theory. Demonstration of the frequency and intensity shift confirms our previous conclusion that electron trapping is restricted to a single type of surface titanol structure.[4] This is evident both in the dissapearance of a single, acidic Ti(IV)O-H band (3647 cm^{-1}), and the appearance of a single Ti(III)O-H band.

Acknowledgements

We offer our thanks to Sonjong Hwang for his assistance with the MAS NMR experiments. Thanks also to William A. Goddard III for graciously providing the processor time for the theoretical calculations, and to Qingsong Wang for his assistance with the force field model. This work was funded by the NSF and the Caltech Materials and Process Simulation Center.

References

---

[1] Brum, D.P., *Concepts in Magnetic Resonance*, 1990, 2, 213.

[2] Crocker, M.; Herold, R.H.M.; Wilson, A.E.; Mackay, M.; Emeis, C.A.; *Hoogendoorn, A.M. J. Chem. Soc. Faraday Trans.*, **1996**, 92, 2791.

[3] Nakaoka, Y.; Nosaka, Y., *J. Photochem. Photobiol. A: Chemistry,* **1997**, *110*, 299.

[4] Szczepankiewicz S.H.; Colussi A.J.; Hoffmann M.R. *J. Phys. Chem. B*, **2000**, *104*, 9842-9850.

[5] Taken from: Szczepankiewicz S.H.; Moss J.A.; Hoffmann M.R. "Electron Traps and The Stark Effect on Hydroxylated Titania Photocatalysts." Submitted for publication in *J. Phys. Chem. B.*

Morse Parameters	*Do (kcal/mol)*	*Ro (Ang)*	*Gamma*
Ti-Ti	0.5976	3.3725	14.1328
O-O	5.1939	3.7207	7.008
H-H	0		
Ti-O	17.3202	1.9123	9.5322
H-O	19.55	1.077	8.4394
H-Ti	0		

Table 1: The Morse parameters used in the force field model.

	actual		*theory*	
	E/cm-1	intensity	E/cm-1	intensity
normal	3647	0.187	3217	0.088
activate	3716	0.303	3281	0.114
change	69	162%	64	129%

Table 2: Actual and theoretical normal mode vibrations of the Ti(IV)O-H (normal) stretch and the Ti(III)O-H (activated) stretch.

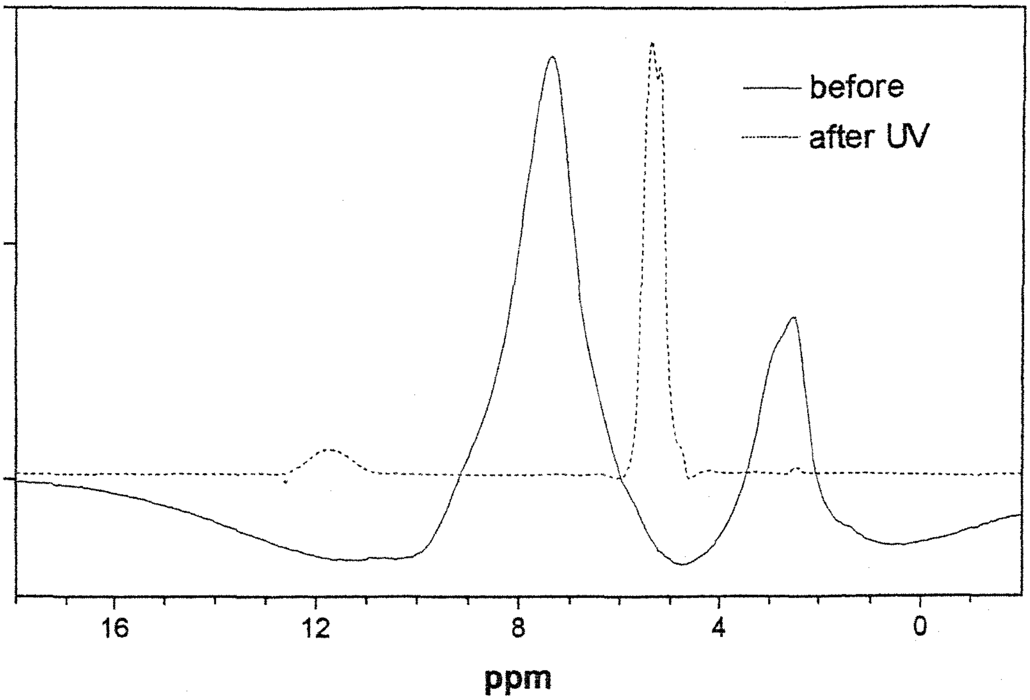

Figure 1: The ^1H MAS NMR spectra of P-25 TiO_2 before and after UV treatment under vacuum.

Chapter 8

Epilogue

In the preceding chapters, research was presented which helps elucidate the mechanism of electron trapping on the surface of TiO_2 photocatalysts. The evidence demonstrates that electron trapping on the surface is not an entirely random process. Localized deep electron trapping at a single type of surface TiOH group is observed through infrared spectroscopy, and corroborated with NMR spectroscopy and a theoretical investigation. The lifetimes of the free carriers can therefore be adjusted by specifically changing the characteristics of these trapping sites. Removing these electrons from the trap states by reducible species at the surface is an integral part of the photocatalytic mechanism.

This research has direct applications for the development of new photocatalysts. Although the prospect of a cheap, clean process for decontaminating polluted water and air is very attractive, the poor overall efficiency is a primary fundamental problem prohibiting the industrial scale implementation of photocatalytic processes. Moreover, the efficiency diminishes with a square-root dependence on photon flux at practical conversion rates, eliminating the possibility to compensate for the low efficiency with a more intense excitation source. No photocatalysts have been created that exceed this limitation.

Photocatalytic degradation of organic contaminants in water over illuminated titanium dioxide is limited by the single electron reduction of dioxygen.[1] The rate of this limiting process is restricted by the biphasic nature of the system. Although conduction band electrons of excited TiO_2 are energetic enough to drive this reduction, they must cross the crystal-solution interface. This barrier imposes both thermodynamic and kinetic restrictions on the electron transfer.

Deep electron traps at the surface of TiO_2 allow conduction band electrons to relax below the reduction potential of dioxygen, significantly slowing the reaction. Electrons in these deep traps will probably recombine with available holes since the electrons are thermodynamically depressed.[2] Electrons that avoid these deep traps are further restricted by their ability to cross the interface.[3] For this bimolecular reaction, both the electron and oxygen must meet at the interface. The probability for such an encounter to occur is vanishingly small unless the concentration of one or both species is high at the interface.

Dioxygen barely binds to pure titanium dioxide in the dark, superoxides appear only on irradiated TiO_2,[4] and the presence of surface defects is necessary to achieve a high photonic efficiency with unmodified catalyst.[5] This evidence suggests that dioxygen reacts only with electrons trapped at defects on the surface.[6] Trapped electrons must be immobilized long enough for free oxygen molecules to randomly encounter them. Since the solubility of oxygen in pure water is low, the average time required for such collisions to occur is relatively long (~0.4 ms).[*] The independence of photocatalytic quantum efficiency with respect to illumination intensity of pure TiO_2 at low photon fluxes demonstrates this limiting factor since the electron production rate is equal to or less than the electron transfer rate.[1,5] An electron trapped for this amount of time on the surface of

---

[*] For a 30 nm TiO_2 particle with a single electron on the surface in an oxygen saturated aqueous solution, and requiring collision within 0.2 nm radius.

TiO_2 is likely to encounter a photohole, resulting in recombination instead of electron transfer.[7]

It is known that the introduction of photocatalytic inhibitors such as phosphate likely interact with these active sites, enhancing the annihilation reaction. Using the results of this thesis as a basis for investigation, it is possible that different surface species may be found that specifically inhibit the annihilation reaction, and enhance the photocatalytic reactivity of the catalyst. This would allow a more efficient turnover of photons at low photon fluxes, and possibly extend the high efficiency regime to higher photon fluxes, resulting in higher overall conversion rates.

The donation of electron density by a ligand "L" to a Ti^{IV} site on the surface determines the potential of the reduction process responsible for electron trapping by destabilizing the Ti^{III} state, produced according to the electron trapping reaction,

$$-Ti^{IV}\text{-}L + e^-_{cb} \leftrightarrow -Ti^{III(-)}\text{-}L \qquad (1)$$

via like-charge d-d electron repulsion.[12] Strongly electron donating groups such as carboxylate ligands force the energy of the Ti^{III} states up into the conduction band, effectively removing the trap. Less electropositive ligands that only promote this potential near the conduction band edge may not remove the traps, but merely restrict their depth. This allows only shallow trapping of electrons on the TiO_2 surface, which aids photocatalysis by prohibiting bulk recombination processes, but maintains an effective redox potential for driving reductions. An appropriate surface modification that does not inhibit active sites, yet binds specifically to annihilation (deep trapping) sites, and also provides the necessary reduction potential of the surface state may serve to enhance the overall reactivity of the catalyst.

References

---

[1] Grela M.A.; Brusa M.A.; Colussi A.J. *Journal of Physical Chemistry B*, **1996**, *100*, 10986.

[2] Grela M.A.; Colussi A.J. *Journal of Physical Chemistry B*, **1997**, *101*, 16940.

[3] Koval C.A.; Howard J.N. *Chemical Reviews*, **1992**, *92*, 411.

[4] Noda H.; Oikawa K.; Kamada H. *Bull. Chem. Soc. Jpn.*, **1992**, *65*, 2505.
Boonstra A.H.; Mutsaers C.A.H.A *Journal of Physical Chemistry B*, **1975**, *79*, 1694.

[5] Gerischer H.; Heller A. *Journal of Physical Chemistry B*, **1991**, *95*, 5261.

[6] Nakaoka Y.; Nosaka *J. Photochem. Photobiol. A.*, **1997**, *110*, 299.
Howe R.F.; Gratzel M. *Journal of Physical Chemistry B*, **1985**, *89*, 4495.

[7] Gerischer H. *Electrochemica Acta*, **1995**, *40*, 1277.